Progress in Surface Science 96 (2021) 100613

Contents lists available at ScienceDirect

Progress in Surface Science

journal homepage: www.elsevier.com/locate/progsurf

Surface transfer doping of diamond: A review

Kevin G. Crawford [*,1], Isha Maini [1], David A. Macdonald, David A.J. Moran

School of Engineering, The University of Glasgow, UK

A B S T R A C T

Ultra-wide bandgap materials show great promise as a solution to some of the limitations of current state of the art semiconductor technology. Among these, diamond has exhibited great potential for use in high-power, high-temperature electronics, as well as sensing and quantum applications. Yet, significant challenges associated with impurity doping of the constrained diamond lattice remain a primary impediment towards the development of diamond-based electronic devices. An alternative approach, used with continued success to unlock the use of diamond for semiconductor applications, has been that of 'surface transfer doping' - a process by which intrinsically insulating diamond surfaces can be made semiconducting without the need for traditional impurity doping. Here, we present a review of progress in surface transfer doping of diamond, both a history and current outlook of this highly exploitable attribute.

1. Introduction

The carbon allotrope diamond possesses a remarkable amalgamation of properties, making it an 'extreme' material, highly appealing for a wide range of applications [1]. Diamond is well known for its position atop the Mohs scale of hardness, by which all other materials are measured [2]. It possesses an extremely high thermal conductivity of up to 22 W cm^{-1} K^{-1}, while also being a *bona fide* electrical insulator in its intrinsic state due to a wide bandgap of 5.5 eV [3–5]. This results in a high breakdown field of 13 MV/cm [5–7], with high typical intrinsic carrier mobilities of 1945 cm V^{-1} s^{-1} and 2285 cm V^{-1} s^{-1} reported for electrons and holes respectively [8]. Diamond owes its extreme properties to the carbon atom and the *diamond* structure of its crystalline lattice, for which is named after the material itself. Each carbon atom forms four sp^3-hybridised atomic orbitals, which overlap with adjacent atoms to form sigma (σ) bonds giving rise to a short C—C bond length of 0.154 nm and a high bond energy of 711 kJ/mol [4]. These rigid covalent bonds allow heat to be efficiently dispersed via lattice vibrations, which is the origin of diamond's extraordinary intrinsic thermal conductivity despite its large bandgap and electrically insulating behaviour. This combination of high thermal conductivity and electrical resistance is uncommon amongst other materials and highlights diamond's unique potential for high-power electronic applications.

Despite a low packing fraction, the relatively small mass of the carbon atom gives diamond the highest atomic density of any known terrestrial solid, making it extremely robust [4]. The strength of the relaxed C-C bond in this configuration also makes diamond chemically inert and hardened to the effects of irradiation [9,10]. Its large indirect bandgap imbues transparency from the far-infrared to the ultraviolet regimes, enabling various optical applications [11–13]. The inherent resilience of diamond lends it an advantage in harsh environments when compared to other materials. For instance, in the 1970s, large area natural diamonds were sourced by NASA to serve as observation windows in their Venus space probe, due to the highly corrosive atmosphere of the planet [14]. The low erosion yield of diamond makes it attractive for use as a window material and for coatings to the exterior of spacecraft [15]. Today, the advent of synthetic diamond using high-temperature, high-pressure (HPHT) or chemical-vapour deposition (CVD) growth techniques has

* Corresponding author.
E-mail address: Kevin.Crawford@glasgow.ac.uk (K.G. Crawford).
[1] Equally contributing authors.

https://doi.org/10.1016/j.progsurf.2021.100613

Available online 4 February 2021
0079-6816/© 2021 The Author(s). Published by Elsevier Ltd. This is an open access article under the CC BY-NC-ND license (http://creativecommons.org/licenses/by-nc-nd/4.0/).

Nomenclature

2DHG	two-dimensional hole gas
ε_r	relative permittivity
μ_e	electron mobility
μ_h	hole mobility
λ	thermal conductivity
Γ	centre of the Brillouin zone
χ	electron affinity
ρ_s	sheet carrier density
$\rho_{s,sat}$	sheet carrier density saturation
B_{FOM}	Baliga figure of merit
BH_{FOM}	Baliga high-frequency figure of merit
E_{max}	critical electric breakdown field
E_{ME}	mobility edge boundary energy
FOM	figure of merit
F-diamond	fluorine-terminated diamond
F-termination	fluorine termination
f_T	cut-off frequency
f_{max}	maximum oscillation frequency
H-diamond	hydrogen-terminated diamond
H-termination	hydrogen termination
HCA_{FOM}	Huang chip-area figure of merit
HD_{FOM}	Huang device performance figure of merit
HM_{FOM}	Huang material figure of merit
HT_{FOM}	Huang high-temperature figure of merit
L_g	gate length
L_{gd}	gate-drain length
L_{gs}	gate-source length
L_t	transfer length
MIGS	metal-induced gap states
NEA	negative electron affinity
O-diamond	oxygen-terminated diamond
O-termination	oxygen termination
PEA	positive electron affinity
QW	quantum well
Q_{gd}	gate-drain charge in a MOSFET
R_c	contact resistance
R_{on}	on-state resistance
R_q	root mean square deviation roughness
TMO	transition metal oxide
ν	frequency
V_B	breakdown voltage
V_{gs}	gate-source voltage
V_{ds}	drain-source voltage

enabled material production with controllable properties [1]. Fig. 1 shows a commercially available single crystal CVD diamond substrate obtained from Element Six, with a (1 0 0) surface orientation and surface devices fabricated by electron-beam lithography.

Due to its unique intrinsic properties, diamond has gained much attention as a robust electronic material for use in high-frequency and high-power electronics [5–7,16,17]. Various figures of merit (FOMs) are often used as an aid to compare the intrinsic potential of emerging material systems for various electronic applications (Table 1). One of the most commonly used FOMs is the Baliga figure of merit (B_{FOM}), alongside its high-frequency variant (BH_{FOM}) [18]. The B_{FOM} is a ratio between the square of the avalanche breakdown voltage (V_B^2) and the specific on-state resistance for a device ($R_{on,\,sp}$). In terms of fundamental material properties, it is often expressed as: $\varepsilon_r \mu_e E_{max}^3$, where E_{max} is the critical electric breakdown field, μ_e is the electron mobility and ε_r is the electric permittivity of the semiconductor. B_{FOM}'s cubic dependence on E_{max} discriminates in favour of high breakdown-field materials such as diamond. However, variations in E_{max} and μ_e with temperature and doping concentration make this advantage more contentious [19]. Furthermore, B_{FOM} assumes power losses are due to dissipation during a device's on-state operation, from current flow through the device's network of resistances. For this reason, B_{FOM} is more applicable to low frequency operation where conduction losses are dominant. The BH_{FOM} modifies this assumption by including the impact of switching losses due to the charging and discharging of the input capacitance;

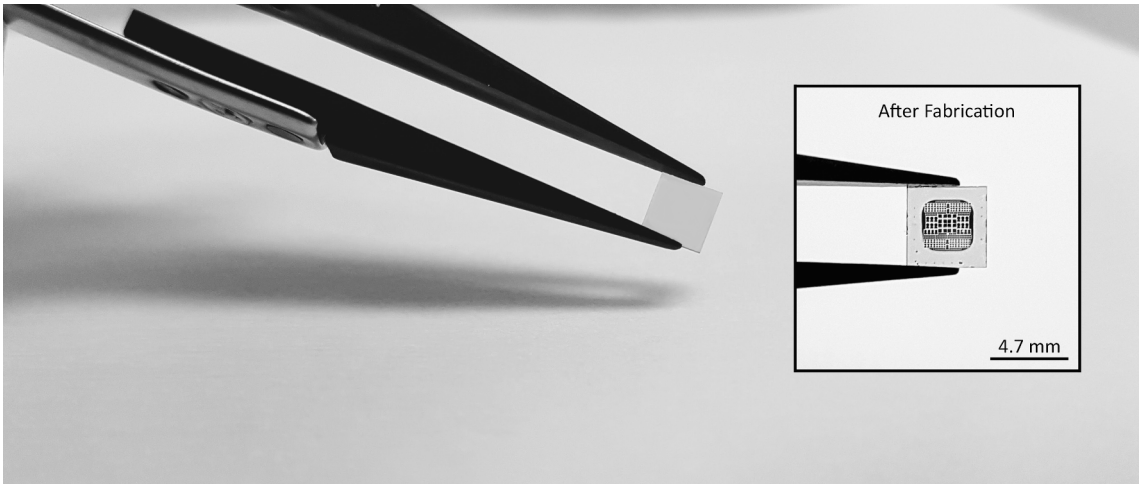

Fig. 1. Image of a 4.7 mm × 4.7 mm × 0.5 mm single crystal CVD (100) diamond substrate with devices fabricated using electron-beam lithography.

Table 1
Comparison of figures-of-merit for diamond compared with other semiconductors based on Baliga's and Huang's analysis [7,18,20]. HD_{FOM} excluded due to the wide variation between existing diamond switching devices.

	Si	SiC	GaN	Diamond
Baliga FOM ($\varepsilon_r \mu_e E_{max}^3$)	1	440	2950	4.73×10^5
Baliga High Frequency FOM ($\mu_e E_{max}^2$)	1	58	237	1.2×10^4
Huang Material FOM ($E_{max}\sqrt{\mu_e}$)	1	7.5	8.0	23.8
Huang Thermal FOM ($\lambda/\varepsilon_r E_{max}$)	1	0.6	0.1	1.7
Huang Chip-Area FOM ($\varepsilon_r \sqrt{\mu_e} E_{max}^2$)	1	58	192	3.9×10^3

resulting in an expression of power loss inversely proportional to $\mu_e E_{max}^2$, i.e. with a quadratic (and not cubic) dependence on E_{max}. Baliga's figures presented in Table 1 are adjusted to a relative scale, with silicon assigned a nominal value of 1.

Huang introduced additional figures of merit for material (HM_{FOM}), high-temperature (HT_{FOM}), chip-area (HCA_{FOM}) and device (HD_{FOM}) performance, which attempt to better capture the actual switching behaviour of different semiconductors [20]. HM_{FOM} indicates material suitability for high frequency applications and is expressed as $E_{max}\sqrt{\mu_e}$, which suggests a linear inverse dependence of power loss on E_{max}. HT_{FOM} utilises the expression: $\lambda/\varepsilon_r E_{max}$, where λ represents the material's thermal conductivity to predict temperature rise in a fixed-chip area device for a given material. This ratio is inversely proportional to thermal dissipation losses, and therefore a higher HT_{FOM} indicates a lower temperature rise (and lower overall power loss). The HCA_{FOM} allows for comparison of the relative chip-area of a device for equitable performance in different material systems; it is expressed as the product: $\varepsilon_r \sqrt{\mu_e} E_{max}^2$, an expression which is inversely proportional to the optimal chip-area of a device for a fixed on-state drain current density. Lastly, the HD_{FOM} aims to benchmark the performance of unipolar switching power devices using the square-root of the product of on-state resistance and gate-drain charge: $\sqrt{R_{on}.Q_{gd}}$. This expression is directly proportional to power loss (smaller is better) and is dependent on device parameters, not inherent to material properties. Huang's figures presented in Table 1 are also adjusted relative to silicon with a nominal value of 1.

As shown in Table 1, intrinsic (or unintentionally doped) diamond surpasses other established wide-bandgap semiconductors. However, these figures of merit have prompted some important criticism. Baliga's figures have been suggested to be poor predictors of actual device performance [17], primarily due to the use of total power-loss approximations which neglect the off-state power dissipation and switching loss at the drain-source node. The use of specific input capacitance to estimate the switching loss of the gate-drive circuitry and use of on-state current (rather than current density) for power loss calculations has given rise to further criticism [18]. Huang's figures have been criticised for oversimplifying switching behaviour, ignoring power-loss due to gate-switching, and instead using an expression proportional to the product of the gate-to-drain Miller charge and specific on-resistance. As justification for this, Huang argues that the charge-discharge cycling of the gate-to-drain charge dominates the switching loss for high voltage devices [20], emphasising that gate-charge waveforms provide an improved estimation of switching losses relative to Baliga's method [18].

As highlighted by the preceding discussion, such comparisons should be taken only as guidance to a material's relative potential, based purely on inherent properties. For example, fabricated diamond devices have yet to demonstrate carrier mobilities remotely close to intrinsic material measurements and the use of diamond as a semiconductor material has met with several challenges in its early stage development: primarily inherent to the material system itself. Strong σ-bonding between adjacent carbon atoms in the

diamond lattice makes substitutional doping extremely difficult.

Alternatively, surface transfer doping provides a promising route to achieving semiconducting properties in diamond by avoiding the innate limitations associated with traditional impurity doping. Here, we present a review of the surface transfer doping process in diamond, both a history of early discoveries and a detailed view of current developments. While the minutiae of surface transfer doping are still a topic of some debate, significant experimental advances in the recent decade alone have significantly improved our understanding of this highly exploitable attribute of diamond.

2. A history

For decades, researchers have attempted to access the highly desirable properties of diamond for various electronic device applications. As with the majority of semiconducting materials in use today, the crystal lattice of diamond must be 'doped' in some form to introduce a sufficiently high and stable density of mobile charge carriers. Attempts at establishing a mature doping process for diamond have met with mixed success. As with other wide bandgap semiconductors, achieving 'shallow' donors and 'deep-level' acceptors by impurity doping techniques with activation energies suitable for room temperature operation is exceedingly difficult in diamond. Boron quickly emerged as the most promising impurity acceptor to achieve *p*-type doping in diamond, despite a high activation energy of 0.37 eV [21,22], and has remained the 'dopant of choice' since the 1970s. Yet its relatively high ionization energy leads to degenerate levels of boron doping in diamond, turning the material semi-metallic and enabling variable hopping conduction [23,24]. By comparison, boron has an impurity activation energy that is an order of magnitude less in silicon (0.045 eV) [25].

There have been numerous studies on carrier mobility in single-crystal diamond [8,26–30]. Principally, these can be categorised as (1) measurements based on the optical excitation of intrinsic diamond, such as time-of-flight (TOF) and time-resolved cyclotron resonance (TRCR), (2) low-field Hall measurements performed on *n*-doped and *p*-doped diamond under thermal equilibrium, and (3) hole mobilities extracted from fabricated transistors. Measurements of room-temperature carrier mobility in *p*-type diamond range from 3 to 3800 $cm^2\,V^{-1}\,s^{-1}$ depending on substrate quality and doping density. However, work from the last decade has indicated hole mobility (μ_h) is typically around 2200 $cm^2\,V^{-1}\,s^{-1}$ for high-quality, intrinsic or lightly boron-doped diamond [8,31]. For boron-doped diamond, hole mobility has shown to decrease significantly as either dopant concentration or temperature increases [30–34]. The loss in mobility at higher temperatures is attributed to phonon-scattering mechanisms [27–37]. Near room-temperature, acoustic phonon scattering is the dominant mechanism, with μ_h decreasing as $T^{-1.5}$ for temperatures between 300 and 350 K [36,37]. At temperatures above 400 K, the hole mobility falls steeply as $T^{-2.5}$ to $T^{-3.66}$ due to additional scattering caused by optical phonons (Fig. 2) [6,27–35]. Neutral impurity scattering cannot be neglected in highly boron-doped diamond either. Due to its deep-level ionisation energy, most holes are localised to the acceptor level and therefore most of the impurities remain neutral [6,35–37]. The degradation of hole mobility with increasing carrier concentration and temperature lowers the appeal of boron-doped diamond as a substrate for high-temperature electronic applications.

Delta (δ) doping has been explored to alleviate the decline in mobility associated with increased dopant concentration by forming a thin, highly boron-doped ($[B] \geq 5 \times 10^{20}\ cm^{-3}$) layer between two intrinsic layers in diamond. It was proposed that the delocalisation of carriers from the ionized dopant atom due to quantum confinement-effects would reduce ionised impurity scattering and result in a

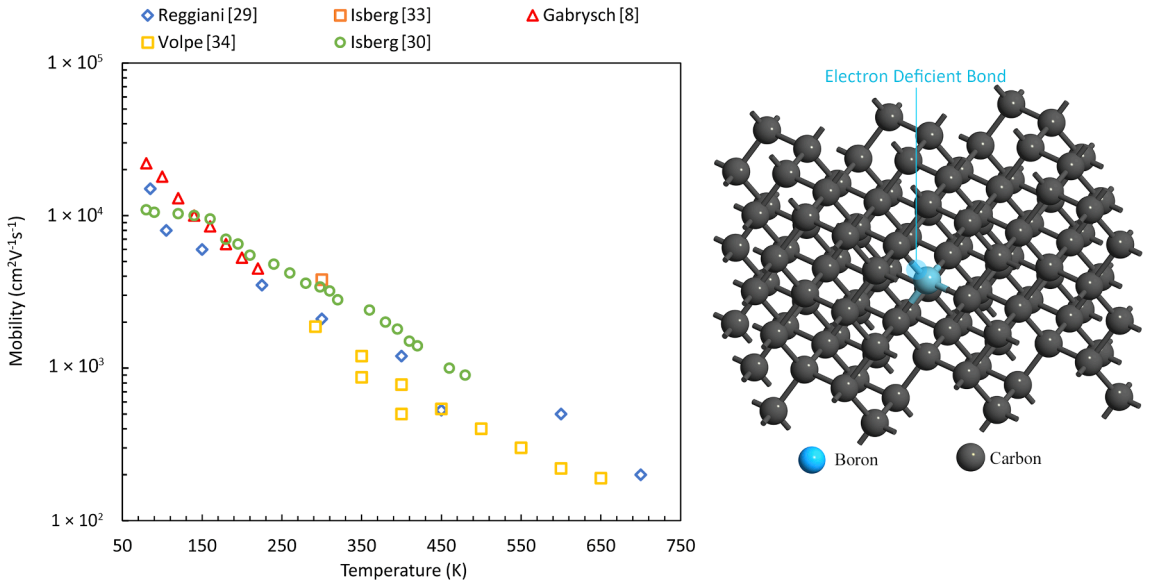

Fig. 2. Reported hole mobility in lightly boron-doped diamond with increasing temperature (left) [8,29,30,33,34] and representation of substitutional doping in boron-doped diamond (right), whereby the resulting electron-deficient bond within the crystal lattice generates a corresponding hole in the bandgap [6,21]. Image of diamond lattice generated using QuantumWise.

region with both a high carrier concentration and a high mobility [38]. However, attempts at achieving a true monolayer doping profile with significant mobility enhancement have met with limited success [38,39]. High energy boron doping techniques such as ion-implantation are also known to cause extensive damage to the diamond lattice, thereby degrading substrate quality and impeding device fabrication [40–44]. To avoid this, boron is typically incorporated during growth, however, heavy boron-doping during this phase induces inefficiencies in growth rate and soot formation. Balancing high levels of boron incorporation ($>10^{20}$ cm^{-3}) whilst maintaining desired crystallinity has remained challenging [6].

For *n*-type impurity doping of diamond, phosphorous remains the most common donor despite a high room temperature activation energy of 0.6 eV [43]. While phosphorous doped diamond thin films with donor concentrations as high as 6.8×10^{16} cm^{-3} have been produced, the activation energy is so large that carrier concentration at room temperature is limited to $\sim 10^{11}$ cm^{-3} [45]. Furthermore, while the carrier concentration increases to 10^{16} (at $\sim$ 1000 K) with increasing temperature, the Hall mobility drops as $\sim T^{-1.4}$ for temperatures up to 450 K and as $T^{-2.66}$ for temperatures exceeding 450 K, making both room temperature and high-temperature operation problematic [6]. More recently, with the detection of arsenic-bound excitons in diamond, a shallower dopant with an ionisation energy of 0.41 eV has been discovered [46]. However, arsenic incorporation in the growth phase is yet to be demonstrated. With limited progress towards the development of a mature *n*-type doping solution for diamond it was therefore expected that only unipolar device applications may become achievable, with bipolar devices requiring a significant breakthrough. For some, these intrinsic doping challenges led to a decline in interest towards the development of diamond for electronic applications, with effort re-focused on other wide bandgap materials such as GaN and SiC.

In 1989, a surface conductivity of 10^{-6} Ω^{-1} cm^{-1} was reported for hydrogen-terminated single crystal type IIa diamond (H-diamond), without any form of intentional impurity doping [47]. This value of conductivity is significantly higher than that typically measured for diamond without H-termination ($\sim 10^{-16}$ Ω^{-1} cm^{-1}) and, understandably, garnered significant interest which resulted in explicative experiments throughout the '90s. It was immediately clear that the termination of the diamond surface played a key role in the dramatically increased surface conductivity, yet unclear as to why. Initial theories proposed that hydrogen may diffuse into the diamond and contribute shallow acceptor states [48–50]. However, this was debunked by a team from Pennsylvania State University who demonstrated that removal of H-termination from the surface would completely reverse the increased surface conductivity [51]. In 1996, evidence of a hole accumulation layer below the H-diamond surface was reported [52]. Through X-ray photoelectron spectroscopy (XPS) and Kelvin probe measurements, they hypothesised electrons were being transferred from the diamond valence band into unknown acceptor states at the surface. Around the same time, Gi et al. demonstrated the electron transfer relied upon the atmosphere in which the H-terminated diamond was kept [53,54].

As the puzzle took shape, a vital experiment from Maier et al. in 2000 revealed several important aspects [55]. Under ultra-high vacuum (UHV), H-termination was removed from one half of a diamond sample by electron bombardment. This effectively removed conduction from that region of the surface, confirmed *in-situ* by two-probe measurement. Further annealing the sample *in-situ* at 410 °C also removed conductivity from the still H-terminated region. However, once the chamber was vented and the sample returned to an ambient air environment, the conductivity of the H-terminated half increased by 4 orders of magnitude within 20 min of exposure. Meanwhile, the region with removed H-termination remained highly insulating. This work empirically demonstrated the combined role of both H-termination and ambient air exposure in the increased surface conductivity, suggesting the presence of air borne species on the diamond surface behaved as the electron acceptor suggested earlier [52].

Years prior, in 1979, Himpsel et al. had observed that electrons excited by photons of energy $h\nu = 5.5$ eV ($\sim E_g$ for diamond) could emit from a H-terminated diamond surface [56]. This photo-excitation bias was much lower than concurrent theoretical predictions for the photoexcitation threshold of the diamond surface. Himpsel found that the H-diamond surface displayed a stable quantum yield that increased linearly from the photoexcitation threshold at $h\nu = 5.5$ eV to ~20% at 9 eV, further incrementing to ~40–70% for 13 eV $\leq h\nu \leq$ 35 eV. The secondary photoelectron energy distribution showed a dominant low-energy emission peak (FWHM $\sim$ 0.5 eV) at the conduction band minimum (CBM), which indicated a negative electron affinity (NEA) surface. A true NEA surface is a rare phenomenon and implies that the vacuum level at the surface lies below the conduction band minimum. The NEA enables thermodynamically spontaneous emission of electrons from the H-diamond surface, in a fashion similar to that of a cold-cathode.

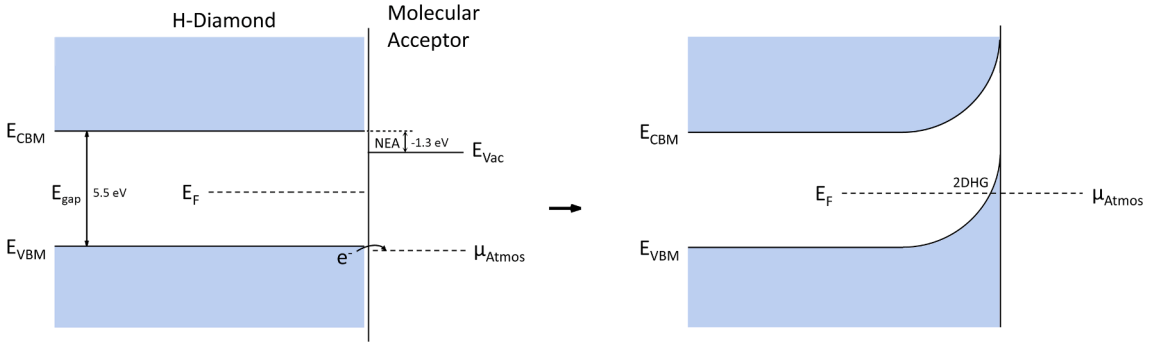

Fig. 3. Energy band diagram illustrating the formation of a two-dimensional hole gas in hydrogen-terminated diamond when exposed to ambient air. μ_{Atmos} represents the electrochemical potential of an adsorbed atmospheric layer containing hydronium cations, resulting in thermodynamically favourable electron transfer and upward band bending.

Drawing from the known NEA attribute of H-terminated diamond, Maier et al. proposed that an adsorbed aqueous adlayer at the diamond surface, containing solvated hydronium cations (i.e. a H_3O^+/H_2 redox couple), acted as the active surface acceptor species responsible for the hole-accumulation layer [55]. To understand Maier's proposal, consider Fig. 3 which illustrates the interface between hydronium cations and the H-diamond surface. The electrochemical potential (i.e. Fermi level of solvated ions in an atmospherically occurring layer) of hydronium cations is $\mu_{Atmos} = 4.4$ eV, which is 0.2 eV lower than the ionization potential (IP) for H-diamond (IP = 4.2 eV) [42,57]. When in contact, thermodynamically favourable electron transfer should occur from the H-diamond surface to hydronium cations, driven by the redox reaction $2H_3O^+ + 2e^- = H_2 + 2H_2O$ [58]. This charge-transfer would continue until the Fermi level of the diamond aligns with the Fermi level of the surface acceptors, causing upward band bending in the equilibration process, as seen in Fig. 3. A similar model was proposed in earlier experimental work by Gi et al., who exposed the H-diamond surface to various hydronium (H_3O^+) containing acidic gases (HCl, HNO_3, H_2SO_4) and concluded that the ionisation of acids in an adsorbed water-vapour adlayer pulled electrons from the surface atoms, thereby generating a hole-layer [53,54]. However, Gi's proposal was markedly distinct insofar as water-vapour alone was found insufficient to induce conductivity.

While Maier's concept of a transfer doping mechanism is convincing, later experimental work by Foord et al. in 2002 [59], Riedel et al. in 2004 [60], Chakrapani et al. in 2005/2007 [61,62], Kubovic et al. in 2010 [63,64], and Sato et al. in 2012 [65] has proposed that oxygen-ion acceptor species may be responsible for the observed conductivity at the H-diamond surface in atmosphere. Both Gi et al. [53,54] and Foord et al. [59] found the conductivity for freshly terminated H-diamond surfaces barely increased (from its insulating characteristic) when exclusively exposed to water-vapor or a range of common atmospheric gases alone. However, Foord noted a dramatic improvement in conductivity when the sample was first exposed to water-vapor, and then exposed to another gas (including oxygen, formic acid and carbon-dioxide). As early as 1999, Gi et al. speculated on the role of air-borne, water-solvated NO_2 in carrier generation for H-diamond, a possibility discussed further in Section 4 in the modern context [54]. Collectively, these experiments suggest that the "wetting layer" merely mediates the electron transfer to adsorbates but does not itself act as the primary

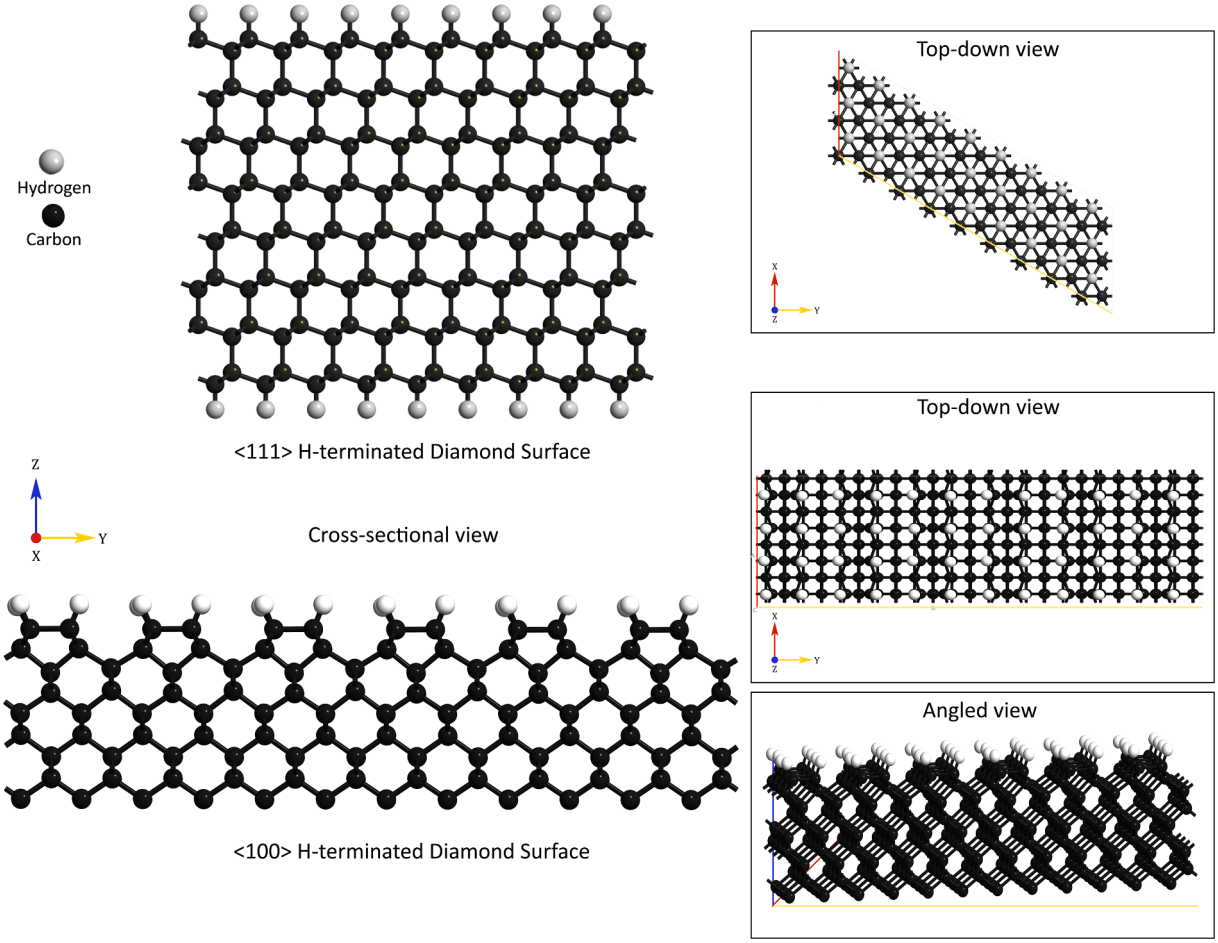

Fig. 4. Surface constructions of the C(1 0 0) 2 × 1:H (bottom) and C(1 1 1) 1 × 1:H (top) crystal planes in diamond, illustrated from different perspectives. The unterminated C(1 0 0) facet has two dangling bonds per surface atom resulting in a C(1 0 0) 2x1:H surface construction [70–80]. Exposure of the C(1 1 1) surface to atomic hydrogen can result in an ideal hydrogen-terminated truncated bulk configuration of C(1 1 1) 1 × 1:H. The C—H bond density at the C(1 1 1) surface is reported to be 1.4 times the bond density of the (1 0 0) surface [100]. Images created in QuantumWise.

acceptor species.

From these early experiments, models for the surface transfer doping mechanism of diamond began to take shape. The possibility of a thin, surface-bound *p*-channel has enabled a significant expansion of possibilities for diamond electronics and bolstered research interest into the exploitation of diamond as a semiconducting material.

3. The role of surface termination

The atomic configuration of an exposed diamond surface is most commonly of the (1 0 0) and (1 1 1) orientations, due to preferential cleaving along the crystal plane and growth conditions [66–68]. However, a (1 1 1) surface can be difficult to achieve for diamond grown by CVD as the nature of the growth process favours the (1 0 0) facet. As such, the majority of reported work regarding the diamond surface for electronic applications has been on the (1 0 0) plane.

As shown in Fig. 4, the bare C(1 1 1) surface has one dangling bond per surface atom; the clean, non-terminated (1 1 1) surface is known to reconstruct in 2 × 1 π-bonded "Pandey" chains, reducing the dangling bond density [69–72]. Termination of the C(1 1 1) surface with atomic hydrogen results in an ideal hydrogen-terminated truncated bulk configuration of C(1 1 1) 1 × 1:H. The C(1 0 0) facet instead has two dangling bonds per surface atom, with the bare surface having a 2 × 1 symmetry structured in π-bonded dimer rows. The high atomic density of the diamond lattice (with a surface atom density of 1.6×10^{15} cm^{-2}, as opposed to 6.8×10^{14} cm^{-2} for silicon) forbids hydrogen atoms from terminating both these dangling bonds due to steric hindrances. Instead, neighbouring surface carbon atoms form dimers with one another, leaving one dangling bond per surface atom available for termination. This results in a C (1 0 0) 2 × 1:H surface when saturated with hydrogen [70–80].

The structure of the hydrogenated C(1 0 0) diamond surface was debated throughout the '90s. While energetically the ideal termination would entail a 1 × 1:2H surface, in this configuration the hydrogen atoms terminating adjacent dangling bonds would be closer than in a hydrogen molecule [75–78]. The resultant steric interaction between hydrogen atoms would cause straining and distortion of the crystal lattice. The monohydride dimer (2 × 1:H) alleviates this repulsion by reorienting the surface carbon atoms to minimise the surface energy. However, early theoretical and experimental work on the C(1 0 0) surface showed varied results. In 1983, Lurie and Wilson became the first to directly observe the 2 × 1 reconstruction of the C(1 0 0) diamond surface using low-energy electron diffraction (LEED) after heating a sample to >1300 K [81,82]. In 1990, Hamza et al. correlated electron-stimulated desorption time-of-flight (ESD-TOF) measurements with LEED patterns for initially C(1 0 0) 1 × 1:2H terminated diamond, and observed that as annealing temperatures were ramped beyond 1240 K, half-order LEED spots indicating 2 × 1 reconstruction began to appear and increased in intensity up to 1534 K [83]. This was erroneously interpreted to imply that with increasing temperature (and therefore hydrogen desorption) the C(1 0 0) 1 × 1:2H surface morphs into the 2 × 1:H symmetric dimer. In a mirrored experiment conducted in 1992, the effect of dosing clean C(1 0 0) 2 × 1 surfaces with atomic hydrogen was investigated by Thomas et al. using LEED patterns and temperature programmed desorption (TPD) [84]. It was found that atomic dosing of hydrogen was an inefficient way to alter the surface reconstruction, and the 2 × 1:H pattern was maintained even at hydrogen doses equivalent to ~ 100 monolayers of H-atoms. This suggested that the monohydride terminated dimer (2 × 1:H) was more stable than the dihydride 1 × 1:2H configuration for the (1 0 0) facet. However, earlier results from Marsh & Farnsworth in 1964 [85], and Pate et al. [86] & Derry et al. in 1986 [87] had observed a 1 × 1 pattern, contradicting this. More definitive data emerged in 1993 when Aizawa et al. used high-resolution electron energy loss spectroscopy (HREELS) on homoepitaxial CVD diamond and showed a 2 × 1 pattern for (1 0 0) diamond [88]. Aizawa et al. further concluded that (1 1 1) and (1 0 0) were respectively trihydride and monohydride terminated [88]. A series of HREELS studies from the U.S. Naval Research Laboratory concluded that monohydride terminated dimer row reconstruction is the most stable configuration for the hydrogenated C(1 0 0) surface [80,89]. While in contradiction to some earlier work, a consensus emerged supported concurrently by theoretical work [75–79,90] and upheld to-date by experimental studies [90,91–94]. It is now generally accepted that the C(1 0 0) 2 × 1:H surface is the most stable hydrogenated (1 0 0) configuration observed experimentally [70–80]. From the discussion above, it is also evident that the preferred chemical moiety of H-termination and surface reconstruction is crystal-face specific, owing to the difference in steric interactions between hydrogen atoms for different surface reconstructions [88,95,96].

When the diamond surface is terminated with a non-carbon species, a dipole is formed due to the difference in electronegativity between the carbon atom and the terminating atom. On termination with the two most commonly studied species, oxygen and hydrogen, the total surface energy is further lowered [73]. As discussed in Section 2, H-termination was found to play a critical role in the formation of diamond surface conductivity. Himpsel et al. reported increased electron emission per adsorbed photon for H-terminated diamond and attributed this effect to NEA of the surface, generated by the electronegativity difference of the C—H bond [56]. The polar covalent character of the $C^{\delta-}$—$H^{\delta+}$ bond has an associated potential drop perpendicular to the diamond surface, with an electric field extending along the C—H bond length. As per photoelectron yield and XPS measurements by Cui et al., the vacuum level at the surface of a clean reconstructed C(1 1 1) 2 × 1 diamond surface lies 0.38 eV above the CBM [42]. For the C(1 1 1) 1 × 1:H (and C(1 0 0) 2 × 1:H) surface, the potential drop across the C—H bond pushes the surface vacuum level down by 1.65 eV, which results in a surface with a NEA of $\sim\chi = -1.3$ eV [42,57,59,72,97–99]. This results in a valence band maximum (VBM) situated 4.2 eV below the vacuum level (i.e. ionization potential, IP = 4.2 eV). The IP of 4.2 eV for H-diamond is lower than most semiconductors and is made possible by the already low electron affinity (EA) of intrinsic diamond. Silicon, for example, has an IP of ~5 eV despite having a much smaller bandgap than diamond (1.1 eV).

Cui et al. constructed a band-diagram, similar to that shown in Fig. 5a, using XPS measurements of the C(1 1 1) 1 × 1:H surface [42]. Note that the band diagram shows downward band bending at the surface, since it represents the energetics of H-diamond in UHV wherein no surface adsorbates exist to enable charge transfer. As described in earlier models, upward band bending is observed at the

H-diamond surface when exposed to atmospheric adsorbates, making the environment a crucial determinant of the surface energetics for H-diamond [55]. Magnitude of the NEA is posited to vary depending on the surface orientation, with the (1 1 0) surface being attributed a NEA as high as $\chi = -1.8$ eV by some calculations [100]. The NEA of a H-terminated diamond surface was determined independently by (chronologically); Eimori et al. [101] using ultraviolet photoemission spectroscopy (UPS), by Takeuchi et al. [102] using total photo-yield spectroscopy (TPYS), by Cui et al. [42] using TPYS and XPS, by Maier et al. [57] using XPS and by Diederich et al. [103] using XPS and UPS, among others. Its magnitude is consistently quoted in literature as 1.1–1.3 eV. Since the potential drop is approximately linear along the C—H bond length, electrons associated with the terminal carbon still experience a small energetic barrier while escaping the bulk diamond, which is illustrated along with the locally variant crystal potential for the C(1 0 0) 2 × 1:H surface in Fig. 5b. However, given that the width of this barrier is under 0.5 Å, it is easily overcome by quantum mechanical tunnelling [56].

Several methods of achieving hydrogenation of diamond surfaces have been reported. As early as 1873, a technique using olive oil and diamond grit was developed to polish the diamond surface [104]. The olive oil reportedly also acts as a source of hydrogen, and partially H-terminated diamond has been achieved using this method [86,87,105]. Plasma-enhanced CVD (PECVD) diamond is typically H-terminated as-grown due to the presence of hydrogen radicals in the growth chamber which preserve the sp^3 phase of carbon [106–109]. Today, optimised iterations of the microwave PCVD (MPCVD) methods developed by Kamo et al. are widely used to manufacture electronic grade CVD diamond which is H-terminated as-grown [110]. The optimal ratio of carbon, hydrogen and oxygen in the growth chamber has been discussed using a three-component diagram that defines ideal phases for low-pressure diamond synthesis [111].

Ex-situ microwave plasma H-termination has become standard in diamond electronics research, whereby a typically oxygen-terminated (O-terminated) surface is exposed to a high-power hydrogen plasma at elevated temperatures (typically 600–800 °C). This process often roughens the surface to varied degrees dependant on various factors such as exposure time, plasma power density, crystal quality and polishing [112–114]. The hydrogen plasma is well known to attack defect sites in particular, likely due to preferential etching of non sp^3 bonded carbon [115]. By carefully tailoring plasma conditions, a smoothing effect has also been reported [116].

Thermal hydrogenation is a potentially useful alternative to plasma exposure and has shown some success [85,117]. This approach uses hot-filament assisted dosing of atomic hydrogen to obtain H-diamond substrates. In 1986, Pate et al. identified the potential benefit of using atomic hydrogen -and not molecular hydrogen- to achieve good termination [86]. Under UHV, they generated atomic hydrogen using a heated tungsten filament (~1800 °C) placed proximal to a reconstructed (2 × 1) diamond surface. The surface was then characterised using photo-stimulated ion desorption (PSID) and HREELS, which showed that surfaces exposed to atomic hydrogen (but not molecular hydrogen) exhibited H-termination.

In contrast to H-termination, an O-terminated diamond surface results in a positive electron affinity (PEA) reported to be around $\chi = +1.7$ eV [57]. This is due to a reversed surface dipole $C^{\delta+}$—$O^{\delta-}$, whereby the electronegativity of oxygen is greater than carbon. Magnitudes for the PEA of the O-terminated surface have been reported to be as high as +2.14 eV [118,119]. The oxygen chemistry on low-Miller index C(1 0 0) diamond surfaces is complicated due to the coexistence of carbonyl, hydroxyl, peroxide, epoxide and ether groups. Unlike H-diamond, terminating chemical moieties have not been attributed to specific crystal faces for O-diamond, although as explained below, low-index surface sites seem to preferentially form ether groups. In a study using HREELS and Auger electron

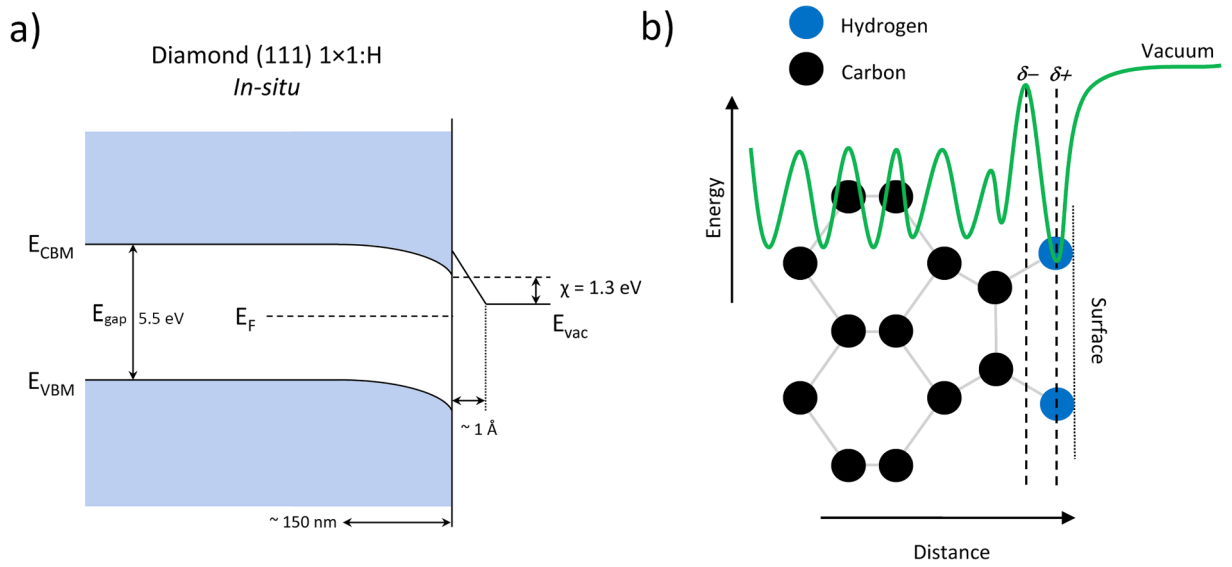

Fig. 5. a) Band diagram illustrating the downward band bending of hydrogen-terminated diamond in ultra-high vacuum, wherein no surface species are present to enable charge transfer b) Illustration of the dipole formed at the surface of (1 0 0) hydrogen-terminated diamond, generated by the difference in electronegativity between carbon and hydrogen [56].

spectroscopy (AES) analysis, Pehrsson et al. found that the distribution of terminating oxygen species varies depending on the oxidation conditions, with ether groups dominating unheated substrates at saturation oxygen coverages [91]. In a follow-up study, the impact of increasing substrate temperature, for temperatures (T) such that 24 °C ≤ T ≤ 670 °C, was investigated [92]. They found that oxidation at elevated temperatures increased the carbonyl to ether ratio and subsequently proposed a possible mechanism by which oxygen at the step edges of a roughened surface could assist in this conversion. The stability of carbonyl termination was further supported by [75]. Contrary to these findings, the preferential coverage of hydroxyl or ether groups on (1 0 0) substrates was predicted by prior molecular-dynamics studies [73,120]. However, at elevated temperatures, the accelerated adsorption and desorption of CO and CO_2 roughens the diamond surface, leaving a defect-dominated surface with a distinct chemistry from the unheated (1 0 0) surface. Pehrsson et al. contended that roughened surfaces have increased instance of reactive surface-sites and a decreased density of ether-bonding low-Miller index sites, which explains their unusually higher carbonyl fraction [92]. For studies conducted on atomically smooth C(1 0 0) surfaces, hydroxyl and ether groups dominated O-termination moieties, with marked improvements in interfacial O-coverage [93,94,121]. As fresh data emerges, more precise descriptions of the species rich O-diamond surface are continually being formulated.

This wide range of terminating moieties, variant with temperature and local roughness, leads to interesting inhomogeneities in the local EA for O-diamond. Furthermore, there exists a discrepancy between theoretical [73,122] and experimental [93,94,97] results for the EA of an O-terminated surface. Theoretical models for the EA of ether or carbonyl terminated diamond surfaces have predicted twice the experimentally established values of $\chi \sim +1.7$ eV, while for hydroxyl terminations a near-zero EA or NEA (i.e. $\chi \leq 0$) was predicted. Electron affinities, as measured by photoelectron spectroscopy, are therefore likely to be averaged values, which account for the impact of inhomogeneous surface termination due to patches of ether, carbonyl and hydroxyl moieties [94,121]. This results in some interesting effects, such as the inhomogeneity of Schottky barrier heights on O-diamond. As reported by Muret et al., the chemical evolution of the surface due to annealing (at T ≥ 350 °C) caused the ordinarily Fermi-level pinned O-diamond surface to undergo a large reduction in both barrier inhomogeneities and the magnitude of the barrier height [94]. This was later supported by other experimental work [121].

Unlike H-diamond, O-diamond is insulating in both vacuum and air, implying that charge transfer at the surface is not thermodynamically spontaneous. The change in conductivity amid terminations has been widely reported in literature [53–55,57,59,60,97,98,123]. *Ab-initio* density-functional studies (DFT) of C(1 0 0) diamond surfaces provide a theoretical basis for the insulating characteristic of O-terminated diamond [73,75–77,122]. For instance, in simulated interactions between H-diamond and a surface-physiosorbed CO_3H molecule, the density of states (DOS) for the H-diamond surface was significantly altered by the adsorbate molecule, whereas DOS for the O-terminated surface remained mostly unchanged [74]. In H-diamond with physiosorbed CO_3H, shallow acceptor states at ~0.4 eV above the VBM appear. Liu et al. remarked that these states arise as a result of the interaction between the C—H σ-bond and non-bonded O 2p orbitals of the CO_3H molecule [74]. Notably, these acceptor states were absent for the O-terminated diamond surface with physiosorbed CO_3H; showing the surface adsorbate had no influence on the surface conductivity of the oxygenated diamond film. Other density-functional studies have also reported the lack of electron transfer between O-terminated diamond and compositionally variant atmospheric adlayers, underpinning its highly insulating behaviour.

Diverse methods of oxidation for diamond surfaces have been reported, including thermal oxidation [124,125], hot-filament cracking [91,92], UV-ozone treatment [60,121,126,127], plasma exposure [119,127,128], chemical oxidation [116,121,127,129,130] and anodic electrochemical polarisation [127,131]. Comparative studies have shown that both the oxygen coverage (%) and its functional moiety are strongly dependent on the oxidation process used [121,127,129,132,133]. Generally, wet chemical oxidation methods have produced the highest surface oxygen concentrations at around ~10.2%. However, electrochemical oxidation has been shown to induce exceptionally high oxygen coverage (≥18%) [132].

Various other surface terminations have been explored on the diamond surface, such as fluorine termination (F-termination) and combinations of oxygen with light metals Li, Na, Mg, K and Cs [134]. Most notably, O'Donnell et al. predicted an oxygen-lithium terminated surface would yield a large NEA of 3.9 eV using DFT [135]. It was also proposed that the surface incorporation of light alkali metals such as Li and Mg onto the O-terminated surface would break C—O—C (ether) bonds in favour of stable C—O—X complexes (where X is either Mg or Li) [136]. The local potential environment induced by the Mg/Li adsorbate was hypothesised to induce a strong surface dipole, causing negative charge accumulation around the C—O orbitals and leaving a fractional positive charge at the oxygen-alkali site, thereby generating a NEA surface. Photoelectron yield and XPS studies have complemented O'Donnell's theoretical work, demonstrating stable NEA surfaces for magnesium and lithium-adsorbed O-diamond [128,137]. Indeed, the magnesium-adsorbed O-diamond surface boasts the highest NEA measured to date at $\chi = -2.01$ eV, significantly higher than the NEA of a H-terminated surface.

A large PEA of 2.56 eV has been reported for a plasma fluorinated diamond surface [138]. Other attempts at fluorinating diamond used atomic fluorine or molecular F_2 in its gaseous phase [139–141]. Approaches using fluorine-containing plasmas have achieved success with CF_4 [142–147], XeF_2 [138,148], CHF_3 and SF_6 [149,150]. Wet-chemical fluorination techniques have also been reported to result in a high degree of surface coverage [151]. *Ab-initio* studies of the F-diamond surface have indicated that the C—F bond has ionic characteristics which produce a very strong and stable bonding configuration [152,153]. From quantum mechanical simulations and LEED patterns, the C(1 1 1) 1 × 1:F, C(1 1 1) 2 × 1:F and C(1 0 0) 2 × 1:F surface constructions have all demonstrated good stability [139,140].

In addition to electronic properties, changes in surface-termination can also drastically alter tribological and electrochemical parameters. Contact angle measurements are a popular technique to assess the hydrophobicity of a surface [154]. Essentially, the higher the contact angle the more hydrophobic the surface is, as water droplets tend to aggregate more closely. The mean contact angle is reported as 47.2° ± 4° for O-diamond, 81.3° ± 3° for H-diamond and 103° ± 1.1° for F-terminated diamond surfaces [154]. The high

hydrophobicity of the F-diamond surface makes it difficult for water-solvated molecules to adhere. This enhances its chemical inertness and results in favourable tribological properties [143,144,155,156]. Furthermore, the high charge-density at the F-diamond surface is postulated to cause an electrostatic screening effect for adsorbed molecules [153], which may explain the wide redox potential windows observed for fluorinated boron-doped diamond electrodes relative to their hydrogenated counterparts [143,155,156]. The combination of chemical inertness, favourable tribological properties and a wide redox potential window have made fluorinated diamond attractive as an electrode material, although wider potential for electronic applications is yet untapped.

From the above discussion, the highly complex nature of diamond surfaces is apparent when viewed from a topological and electrochemical perspective. Transfer doping is an intimately surface-bound process, whereby seemingly minute variations in surface conditions will drastically alter the electronic and chemical properties of diamond.

4. Electron acceptor materials on hydrogen-terminated diamond

Many reported works have attempted to replicate the diamond surface transfer doping effect observed under atmospheric conditions, using engineered materials, lending us a greater understanding of the transfer doping process while also demonstrating the potential for greatly enhanced results in both conductivity and stability. The following section will discuss these efforts, organised as I. Molecular Species and II. Metal-Oxides. This is not to suggest that surface transfer doping of diamond can only be achieved by these two mediums. Rather, the majority of reported electron acceptor materials on H-diamond, to-date, can be described in this way.

4.1. Molecular species

A compilation of reported empirical conductivities for various molecular species on diamond is shown in Fig. 6. While by no means exhaustive, each reported alternative transfer doping species to-date is represented, to the best of our knowledge. For comparison, we have also included 13 points from our own data for air-induced doping taken from CVD (100) single crystal H-diamond samples exposed to atmosphere only.

Doping by atmospheric molecules can be highly sporadic as seen in Fig. 6, with mobilities ranging from 20 to 100 $cm^2.V^{-1}S^{-1}$ and typical carrier densities from $1 \times 10^{12} - 1 \times 10^{13}$ cm^{-2} [157,158]. This is likely due to multiple, difficult to control variables such as diamond surface morphology, hydrogen coverage, contamination, the composition of the spontaneously occurring atmospheric adsorbates, as well as variation in substrate composition and quality. While values for air-doped H-diamond vary, 2D carrier densities are seldom seen to surpass $\sim 1 \times 10^{13}$ cm^{-2}.

The fullerene molecule C_{60} and its fluorinated variants ($C_{60}F_x$,x = 18, 36, 48) were some of the first shown to be effective electron acceptors on H-diamond, due to their highly oxidising nature resulting in a high EA. Carrier concentrations in H-diamond generated from the deposition of fullerenes have been comparable to that of air exposure [98,159,160]. Strobel et al. deposited C_{60} onto both H-terminated and O-terminated diamond to demonstrate no conductivity increase would be observed without H-termination. Other molecules capable of inducing surface transfer doping have since been reported, including tetracyanoquinodimethane (F4-TCNQ) [161]. For the fullerenes shown in Fig. 6 i.e. TNCQ and its fluorinated variants, a mobility of 70 $cm^2\ V^{-1}\ S^{-1}$ was assumed by Qi et al. in

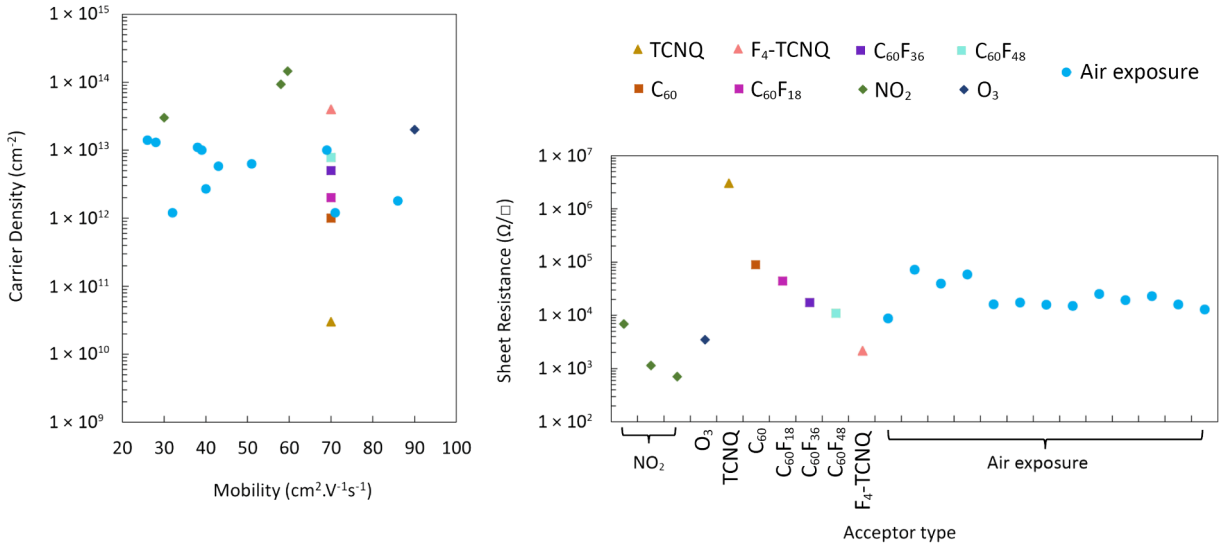

Fig. 6. Compilation of carrier transport values reported in literature for different molecular species found to induce transfer doping of hydrogen-terminated diamond [65,118,160,162,167]. Values for carrier density, mobility and sheet resistance were extracted by Hall measurement, with the exception of TNCQ and its fluorinated variants. For these, a mobility of 70 $cm^2\ V^{-1}\ S^{-1}$ was assumed by Qi et al. in order to estimate carrier densities from two-probe conductivity measurements [161].

order to estimate carrier densities from two-probe conductivity measurements [161]. As such, these values were reported with a large margin of error yet remain comparable relative to each other in demonstrating potential as transfer dopants.

As mentioned in Section 2, early theories regarding atmospheric transfer doping species speculated that hydronium cations arising from atmospheric water vapour were the primary air-borne surface acceptor species. Later work demonstrated the role of oxygen-ion acceptors and posited that the water adlayer only acted to mediate electron transfer. However, this has since been disputed by studies which discounted the effect of H_2O entirely and found that high relative humidity in air may in fact decrease induced surface conductivity [64]. Riedel et al. were among the first to report on the enhancement in surface conductivity of H-diamond upon ozone-exposure [60]. They established that the "re-activation" of annealed samples (at 250 °C $\leq$ T $\leq$ 750 °C) by ozone-exposure was necessary to observe surface conductivity. Several models were proposed to explain this: given that the oxidisation of the surface was below the detectable limits of XPS, it was assumed that less than $\leq$1% of the surface was O-terminated due to ozone exposure. While this is not enough to affect the energetics of charge transfer directly, i.e. 0.01 monolayer oxygen coverage does not significantly impact the ionisation potential of diamond, the ozone centres may act via a catalytic mechanism to speed up the kinetics of the electron transfer between the diamond surface and the ambient environment. A model was proposed whereby the ozone was posited to create localised bonding configurations that remove or lower the activation barriers for electron exchange and thereby assist in reintroducing the post-anneal surface conductivity [60].

The lowest sheet resistance reported to-date for an H-diamond surface is 719 Ω/□, by Sato et al. in 2013 [162]. This was achieved by exposing the H-diamond surface to highly concentrated NO_2, resulting in carrier densities up to 1.5×10^{14} cm^{-2}. This experiment followed earlier work by Gi et al. [53,54], Hirama et al. [163], Kubovic et al. [63,64], and Kasu et al. [164] who all showed significant NO_2-induced surface conductivity in H-diamond. Sato's proposal [65,162] coincided with a detailed study by Takagi et al. [100] in which various air-borne species were investigated to determine their transfer doping capability, based on first-principles calculations and experimental measurements. H-terminated diamond exposed to NO_2, O_3, NO and SO_2 was shown empirically to exhibit sub-surface conductivity, whereas exposure to N_2O, CO_2 and N_2 had little or no effect in increasing conductivity. This result was compared with the electronic structure of each isolated molecule, which revealed that those with lowest unoccupied molecular orbitals (LUMO) positioned at or below the H-terminated diamond VBM would induce surface transfer doping. Soon after, Kubovic et al. [63] corroborated Takagi's findings by exposing the H-diamond surface to 1–5 ppm O_3, NO_2, NO and SO_2; among these, they found that exposure to O_3 resulted in the largest increase in carrier concentration and also exhibited good stability over time. However, it should be noted that only 5 ppm NO_2 gas was used by Kubovic [63] in the preceding study, compared with 20,000 ppm NO_2 used by Sato [162]. Using XPS spectra of O_3 adsorbed H-diamond, Kubovic showed that the presence of ozone resulted in upward band bending, similar to a NO_2 exposed H-diamond surface, and measured a 2D hole concentration of 7×10^{13} cm^{-2} after 1 h of exposure to 1 ppm O_3 [63]. This was in-line with quantum mechanical studies by Petrini & Larsson which found a combination of oxonium ions (H_3O^+) and ozone (O_3) solvated in the water adlayer on H-diamond predicted sheet carrier densities of ~10^{13} cm^{-2} [75].

The sensitivity of transfer doping to surface conditions is further emphasized by the apparent dependence of the sheet carrier density (ρ_s) on the surface orientation. Hirama et al. noted the saturation carrier density ($\rho_{s,sat}$) appeared to be proportional to the C—H bond-density and proposed that this was due to negatively-charged adsorbates accumulating at the partially positive $H^{\delta+}$ pole, thereby inducing hole-accumulation in the near-surface diamond to maintain charge neutrality [165]. Since the C—H bond density depends on the surface orientation, Hirama et al. used this model to explain why (1 1 1) surfaces with a C—H bond density of 1.82×10^{15} cm^{-2} exhibited half the sheet resistance and twice the $\rho_{s,sat}$ of a (1 0 0) surface, which has a lower bond density of 1.58×10^{15} cm^{-2} [165]. Sato et al. noted the same trend, i.e. that $\rho_{s,sat}$ increased with higher C—H bond density, showing a dependence on surface orientation [65,162]. First principles computation by Takagi et al. demonstrated that the VBM for a (1 1 0) surface is closest to vacuum level (lowest IP), followed by (1 1 1) surfaces, and finally (1 0 0) surfaces. This follows from the fact that the C—H bond density for the (1 1 0) surface is 1.4 times that of the (1 0 0) surface and 1.2 times the (1 1 1) surface [100]. Sato et al. proposed that the higher valence-band edge for the (1 1 0) surface increases the energy deficit from the VBM to the LUMO of the adsorbate molecule, thereby causing steeper upward band bending and increased sheet hole density [162]. Kawarada et al. have also noted this difference in sheet hole density, finding the hole density of (1 1 1) and (1 1 0) surfaces was 30–50% higher than that of the (1 0 0) surface [166].

Geis et al. concluded a study in 2018 which examined the nature of NO_2 induced transfer doping on H-diamond [167]. Characterising diamond powder exposed to hydrogen plasma and subsequently NO_2, they found no evidence of NO_2^- on the diamond surface by means of infrared adsorption. Rather, NO_3^- was abundantly present. From this they hypothesised a more complex interaction by which NO_2 radicals form N_2O_4, which in turn produces $NO_3^- + NO$ with the aid of an electron transferred from the H-diamond surface. The generated NO_3^- remains at the surface and maintains corresponding holes within the diamond. While stable in a dry N_2 environment, the NO_3^- concentration was found to reduce once exposed to ambient air and thus the increased surface conductivity of the diamond was lost. This, naturally, poses the question of whether suitable encapsulation of the surface after NO_2 exposure can maintain surface conductivity. Such an approach has met with success, as will be discussed in the next section [168]. Additionally, Geis et al. also noted the suppression of C—H optical absorption spectral features after NO_2 exposure, indicating that between 25 and 75 % of H-atoms from the H-terminated diamond surface are removed by exposure to NO_2 [167]. They proposed that the underlying mechanism for this may involve the breaking of the C—H bond to form HNO_2, however the implications of possible H-removal from the surface remains unclear.

4.2. Metal-oxides

To improve stability of H-diamond surface conductivity, many solid encapsulation materials have been explored. Of these, metal-oxides have been most prevalent. A compilation of reported H-diamond conductivities when transfer-doped by various metal oxides is

shown in Fig. 7. Select transition metal oxides (TMOs) in particular have demonstrated to be effective transfer dopants of H-diamond due to their high EA. In 2013, Russell et al. reported on molybdenum trioxide (MoO_3) induced transfer doping, which boosted carrier concentration of the diamond 2D hole gas (2DHG) by an order of magnitude [169]. This increase was systematically confirmed by Hall measurement and photoemission spectroscopy, revealing a clear charge separation across the diamond/MoO_3 interface and saturating beyond 1.6 nm of deposited oxide. The band bending mechanism proposed to explain the 2DHG formation by a high EA material is illustrated in Fig. 8. With a suitably high EA, the surface electron acceptor CBM sits below the VBM of H-diamond. As the Fermi levels align, upwards band bending results in the formation of a 2DHG below the diamond surface. It is therefore expected that carrier concentration may scale with the relative magnitude of the surface acceptors' EA. In 2014, Tordjman et al. also reported on MoO_3 induced transfer doping of H-diamond, with carrier densities up to $\sim 1 \times 10^{14}$ cm^{-2} and proposed the same band bending mechanism driven by the large EA of MoO_3 [170].

This work was soon followed by several other studies involving vanadium pentoxide (V_2O_5) [171,172], tungsten trioxide (WO_3) [171,173], rhenium trioxide (ReO_3) [173], niobium pentoxide (Nb_2O_5) [171] and chromium trioxide (CrO_3) [174]. Some of the lowest sheet resistances reported to-date have been demonstrated by MoO_3, V_2O_5 and WO_3 with carrier densities in excess of 1×10^{14} cm^{-2} [170,171,173]. High-temperature stability has also been shown for V_2O_5 and MoO_3 up to 300 °C [157], and ReO_3 up to 400 °C [173]. TMOs therefore arguably present a more attractive electron acceptor solution compared to molecular species such as C_{60} or NO_2, due to their greater stability across a wider temperature range and the reliably high carrier concentrations they generate, driven by a solid material with controllable properties. Despite this, the high EA of some TMO materials has shown to be sensitive to environmental conditions, due to their hygroscopic nature [175]. Tordjman et al. likewise commented on the importance of MoO_3 oxidation in preserving its high EA for maximising charge transfer [170]. Encapsulation and hence passivation of some of these materials using more inert dielectric layers has demonstrated a route to preserve both atmospheric and thermal stability, however [157]. Similarly, thermal desorption of atmospheric adsorbates from the diamond surface prior to TMO deposition has been shown to improve stability over time [157]. A simulation study of MoO_3 and V_2O_5 induced H-diamond transfer doping was reported by McGhee et al., using DFT [176]. Their theoretical results showed a clear shift in the VBM of H-diamond interfaced with either MoO_3 or V_2O_5, driven by electron transfer between the diamond and surface bound material. In particular, they highlight the importance of the metal-oxide's oxygen incorporation, proposing the majority of transferred charge migrates to oxygen atoms within the TMO.

The use of a solid electron acceptor medium to induce a 2DHG below the H-diamond surface, such as MoO_3, poses the question of possible parallel conduction through the oxide layer as a result of transferred electrons from the diamond valence band. The assumption has been that the oxide, reported to be highly insulating, does not possess a coherent band structure capable of supporting carrier transport [169,170,172,177]. The resulting Hall coefficient and positive polarity of the Hall voltage from empirical measurements suggests this to be the case. However, the effect of much larger electric field strengths (such as in power devices) on the oxide's donated electrons is yet to be reported. As will be discussed further in Section 6, some early H-diamond electronic devices fabricated with TMO materials have not yet shown this to be an issue [177,178].

Metal oxides such as MoO_3 are known to be highly oxidising and could possibly result in additional chemical interactions with the diamond C—H surface. The relatively simplified charge transfer model shown in Fig. 8 assumes no chemical reaction between the H-terminated diamond and the overlaying metal-oxide, and therefore may need additional consideration. Some reports have suggested that, much like NO_2-doped diamond, oxygen atoms in metal-oxides may participate in a complex interaction with the H-diamond surface to induce surface conductivity [16,179–181]. Along with earlier data from Riedel et al. [60], which was discussed in the previous section, work by Oing et al. has suggested that H-diamond surface conductivity may benefit from a small proportion of O-termination (<2.2%) [180]. The formation of intermediate C—O—H complexes and the importance of their role in inducing surface

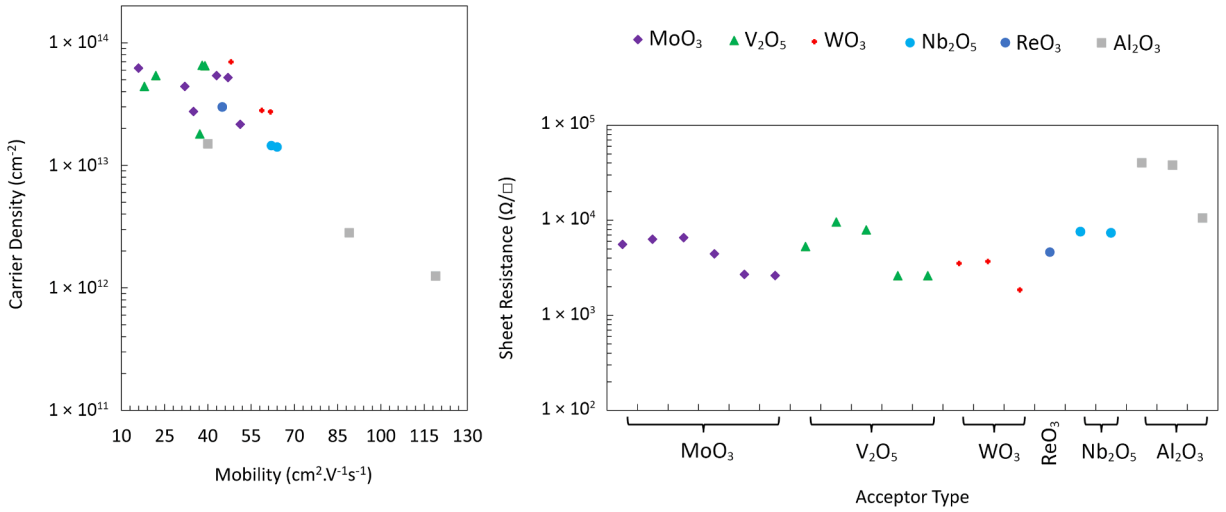

Fig. 7. Compilation of carrier transport values reported in literature for different solid oxide materials found to induce transfer doping of hydrogen-terminated diamond [114,157,169,171,172,173,185]. Values for carrier density, mobility and sheet resistance were extracted by Hall measurement.

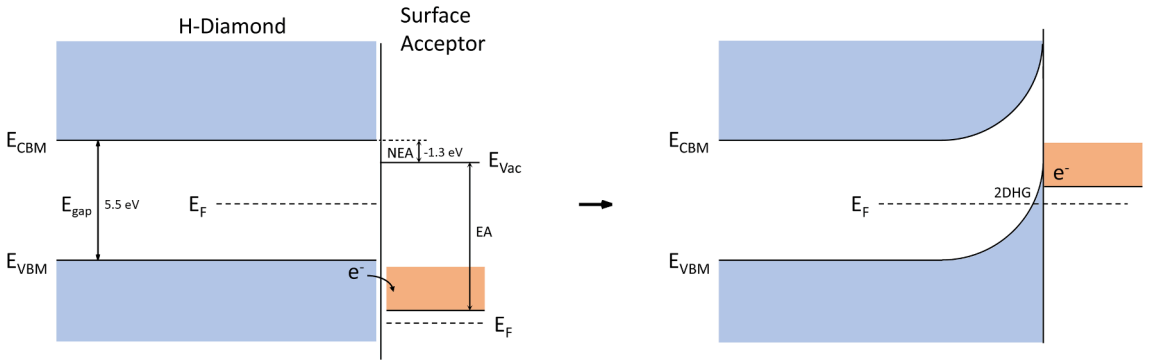

Fig. 8. Energy band diagram illustrating the formation of a two-dimensional hole gas in hydrogen-terminated diamond when in contact with a high electron affinity material. Driven by the relative electron affinity of the surface acceptor, thermodynamically favourable charge transfer to the surface material results in upward band bending.

conductivity has been speculated. This calls into question the completeness of the classical surface transfer doping model which postulates a semiconductor-insulator material matrix that interacts electronically, but not chemically. Nonetheless, the strong relationship between the induced sheet carrier density and the magnitude of the difference between the diamond bandgap and the EA of deposited metal-oxide has experimentally suggested the standard transfer doping model still holds [171]. TMOs such as V_2O_5 and WO_3 are also electrochromic, adapting their optical properties in the presence of high electric fields [182]. It remains to be seen whether this property will be detrimental to electronic applications, yet preliminary evidence from field effect transistor (FET) devices fabricated with V_2O_5 suggest this may not be an issue at lower field strengths [177,183].

Prior to the work on high EA TMOs, in 2012 Hiraiwa et al. reported on use of Al_2O_3 as a means to encapsulate and stabilise surface conductivity in H-diamond [184]. This was reportedly achieved by incorporating H_2O as an oxidant to the atomic layer deposition (ALD) process of Al_2O_3. A follow-up paper showed excellent thermal stability using the same technique, while maintaining comparable carrier densities to that typically observed for air-induced doping of H-diamond [185]. Al_2O_3 has also been proposed to encapsulate H-diamond post-exposure to NO_2. In this approach, the diamond 2DHG is initially generated *in-situ* by exposure to NO_2 and then stabilised before exposure to atmosphere by encapsulation with a layer of ALD Al_2O_3. Both approaches to Al_2O_3 encapsulation have demonstrated excellent thermal and ambient stability [184,185]. Additionally, Al_2O_3 is an established surface dielectric material with the potential to withstand the high electric fields generated in high-power devices.

Al_2O_3 itself does not possess a particularly high EA, however, as illustrated in Fig. 9, wherein a comparison of the CBM for TMO materials in relation to the diamond bandgap is presented. High EA TMO materials have their CBM positioned well below the VBM of H-diamond as required by the transfer doping model to instigate charge transfer from the diamond valence band. Yet, Al_2O_3 appears capable of initiating transfer doping of H-diamond without the intentional introduction of species to the diamond:oxide interface (such as NO_2 or H_2O) [171]. As such, the mechanism by which Al_2O_3 acts to induce surface conductivity in H-diamond has been somewhat debated. Possible explanations include charged defect sites within the Al_2O_3 acting as acceptor states or potentially an effect of the precursors involved in the ALD of Al_2O_3 [186].

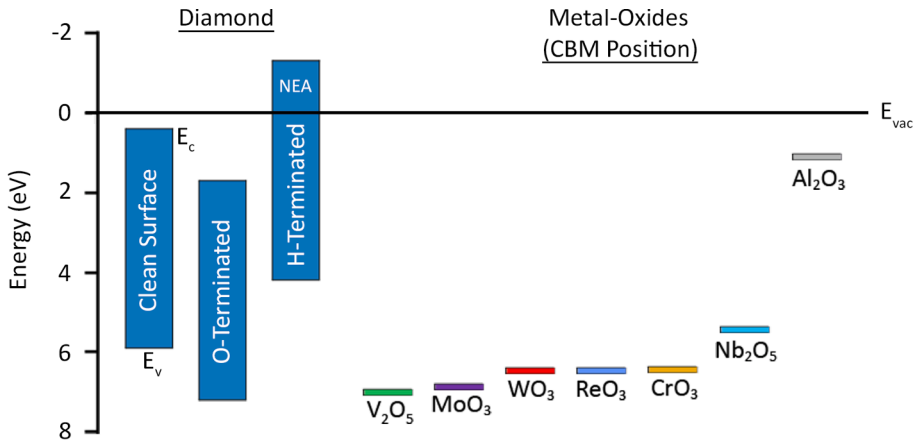

Fig. 9. Electron affinities of various metal-oxides relative to the bandgap of diamond [169,171,172–174]. On the left: hydrogen-terminated, oxygen-terminated and the 'clean' non-terminated diamond bandgaps are represented. On the right: the conduction band minima of various metal-oxides relative to vacuum energy. All oxides shown, apart from Al_2O_3, have their conduction band minima positioned energetically below the valence band maxima of hydrogen-terminated diamond.

As demonstrated by Kawarada et al. [166] and later supported by Yang et al. [187], air-exposure is not critical to achieving conductivity in H-diamond with an Al_2O_3 overlayer. This suggests that Al_2O_3 can play a role in the charge-transfer mechanism in addition to merely encapsulating molecular acceptor species on the H-diamond surface. However, hydrogen plasma exposure post-Al_2O_3 deposition was necessary in one study to induce charge transfer [187]. Several models have been proposed to explain this. Kawarada et al. commented on the large valence band off-set between H-diamond and Al_2O_3, proposing that unoccupied levels within the bandgap of Al_2O_3 may exist below the valence band edge of H-diamond [188]. This concept is illustrated in Fig. 10, and possible candidates for these states are described here [189]. Ren et al. reported XPS measurements for H-diamond encapsulated with ALD grown Al_2O_3 [190]. A large band off-set of 3.3 eV was observed, while the O/Al ratio of the Al_2O_3 film suggested the presence of interstitial oxygen and aluminium vacancy defects which may act as electron acceptors below the H-diamond VBM. To the best of our knowledge, Al_2O_3 transfer doping of diamond has been almost entirely demonstrated by ALD grown films. Verona et al. reported transfer doping of H-diamond using Al_2O_3 deposited by electron-beam evaporation [171]. However, they observed sheet resistances several times greater (~40 kΩ/□) than that reported for H-diamond with ALD Al_2O_3 [185].

Expository work conducted by Yang et al. utilised *in-situ* XPS to elucidate the nature of defects in Al_2O_3 and proposed an "interface model" to explain the observed results [187]. They reported that the surface conductivity and upward band bending of air-exposed H-diamond was initially reduced upon deposition of a ~2 nm Al_2O_3 layer by plasma-enhanced ALD (PEALD). In prior studies, it was demonstrated that the oxygen plasma used during the PEALD process may introduce a concentration of defects or interstitial oxygen atoms which act as electron acceptors (traps) in the near-interface oxide layer [191,192]. Purportedly, these defects result in a negative charge layer proximal to the H-diamond:oxide interface, and thereby induce positive charge compensating ionised impurities in the interface layer. The resultant dipole leads to an upward energy shift across the diamond:oxide interface, and consequently downward band bending was observed at the H-diamond surface (i.e. a higher C1s binding energy). Annealing the samples to 500 °C post-deposition reduced the observed band-shift, which could be explained by the thermal diffusion and desorption of oxygen-induced defect sites. After deposition of the ~2 nm PEALD of Al_2O_3, the samples were exposed to a hydrogen plasma at 500 °C. The hydrogen plasma was shown to modify the interface layer and restore the upward band bending and surface hole accumulation. Evidently, the effect of hydrogen plasma exposure was diametrically opposed to the effect of oxygen plasma exposure. It was therefore proposed that the hydrogen plasma introduced donor-like defects in the near-interface oxide layer, i.e. defects of the opposing polarity to the oxygen plasma. The accumulation of these positively ionised impurities in the near-interface oxide induces compensatory negative charges in the interface layer, thereby restoring the upward band bending. Notably, this configuration of H-diamond/thin-Al_2O_3 was found to be stable during a 500 °C anneal. Yang et al. subsequently proceeded with a second Al_2O_3 PEALD process and noted that once again the donor-like defects introduced in prior steps by the hydrogen plasma were removed and replaced by acceptor-like defects as a result of oxygen plasma exposure, mimicking what was previously observed [187]. The negatively ionized impurities in the interface layer were also replaced by positively charged ions. This was demonstrated by a 1.2 eV shift of the Al 2p core levels towards a lower binding energy. Intuitively, this should be accompanied by a complementary shift of the C1s levels to a higher binding energy (indicating downward band bending at the H-surface), yet this was not observed. Presumably the pre-existing Al_2O_3 overlayer prevented the necessary interface modifications, and charge accumulation was minimally affected by the oxygen plasma in subsequent PEALD cycles.

In a computational study, Wu et al. modelled the electronic properties of various possible interface types between overlaying Al_2O_3/C (1 0 0) surfaces, i.e. depending on whether Al or O interact with the diamond lattice at the heterointerface [193]. Calculated DOS showed 2DHG behaviour appearing at the C—Al interface with a hole density of 10^{13} cm^{-2}, which agrees well with experimental results. This is distinct from the "interface model" proposed by Yang et al.[187]: instead of the electric field-effect induced by defect sites, the formation of hybridized bonding states between the C 2p and Al 3p orbitals was suggested. These hybridized bonding states lie below the valence band of the H-terminated diamond surface, with a large valence band offset of 4.2 eV for the C:H—Al interface. Surface conductivity was therefore attributed to electron transfer from the diamond valence band to these hybridized states. Given that the C—Al bond is ½ an electron deficient, the C—Al bond is unsaturated and may accept transferred electrons.

Geis et al. reported a low sheet resistance of 1.5 kΩ/□ for H-diamond coated with a mixed metal-oxide, proposing a charge transfer model driven by the acidic properties of the metal-oxide and density of surface states acting as electron traps [179]. Experimentally

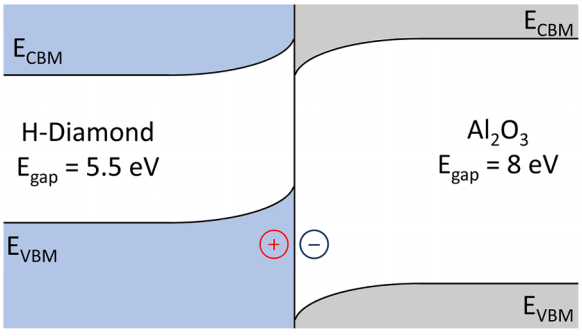

Fig. 10. Illustration of band off-set between hydrogen-terminated diamond and ALD Al_2O_3 showing point defects within the oxide bandgap initiating charge accumulation, proposed to explain the formation of a two-dimensional hole gas within hydrogen-terminated diamond [188].

they produced three H-diamond substrates, of which two were coated with ALD grown Al_2O_3-SiO_2. All three samples exhibited a sheet resistance of ~6 kΩ/□ or lower. The air-exposed sample (without Al_2O_3-SiO_2 deposition) had the highest and most unstable sheet resistance above 6 kΩ/□. Of the Al_2O_3-SiO_2 coated samples, one was stored in dry N_2 for 2.6 days, during which time it showed a stable resistance of ~5 kΩ/□, which then decreased to 3.5 kΩ/□ upon air-exposure. The other sample was air-exposed immediately after Al_2O_3-SiO_2 deposition and showed a dramatic drop in sheet resistivity from 3.5 kΩ/□ to 1.5 kΩ/□ after 20 min of ambient air exposure. Although a reaction pathway exists for Al_2O_3-SiO_2 to induce surface conductivity in H-diamond despite the absence of air-exposure, it was proposed that the catalytic effect of oxygen (in air) enhanced the electromotive potential of Al_2O_3-SiO_2 to 6.45 eV and thereby generated a significantly lower diamond sheet resistance [194,195].

While neither SiO_2 nor Al_2O_3 are strong acids or have a high density of surface states that may act as electron traps, the Al_2O_3-SiO_3 complex is a strong acid with a high surface state density. In quantum chemical computations, Kawakami et al. established that the $SiOH_2$ site acts as a Bronsted acid (H + donor), dissociating via the reaction pathway: $SiOH_2 \rightarrow SiOH + H^+$ [196]. In the dielectric complex, Al atoms can displace Si atoms in the SiO_2 lattice, occupying a tetrahedral site surrounded by four O-atoms. Ordinarily, Al only has three valence electrons but can acquire an extra electron (acting as an electron-accepting Lewis acid) when in this configuration. Evidently, the proposed transfer doping mechanism in this case is markedly different from the induced-defects model for ALD Al_2O_3, wherein oxygen exposure negatively impacted surface conductivity.

The transfer doping models presented in this section can be broadly categorised as: (a) the classical transfer doping model which assumes non-bonding diamond/metal-oxide interfaces where charge-transfer is simply a consequence of favourable band-energetics, (b) models which propose that the electric field-effect of charged interface states shifts the valence band of diamond, resulting in hole accumulation at the valence-band edge, and (c) models which suggest the formation of hybridised bonding orbitals between the diamond surface and overlaying materials. The role of surface species is crucial in all three models, however, at present it is difficult to describe a single electron exchange mechanism which explains all experimental and theoretical observations comprehensively. That multiple distinct mechanisms of electron exchange may exist, is certainly possible.

5. Electronic properties

Once established, the 2DHG of transfer-doped H-diamond is in itself a fascinating and important area of inquiry. The following section discusses observed carrier transport behaviour in transfer-doped H-diamond, as well as the distinct, yet important, aspect of forming external electrical contact to the then established sub-surface conductive channel.

5.1. Carrier transport

High hole and electron mobilities have previously been reported for intrinsic bulk diamond, by TOF measurement [26–28]. Yet, mobility values for surface transfer-doped H-diamond have seldom exceeded 300 $cm^2 V^{-1} S^{-1}$ and have been reported as low as 3 $cm^2 V^{-1} S^{-1}$ [197]. The observed mobility values tend to have a strong correlation with carrier concentration, suggesting a dominant inverse relationship between the two. This trend can be seen in Fig. 7, as mobility tends to decrease when carrier density increases. As part of the classical surface transfer doping process, the holes generated within diamond by electrons departing to energy states provided by a surface acceptor material is expected to form a 2DHG in close proximity to the interface, confined by the balanced presence of corresponding charge in the acceptor material [198]. Studies into the nature of this 2DHG and properties of the carrier transport has been an evolving topic.

Nebel et al. reported on low temperature Hall measurements (70–200 K) for air-doped H-diamond layers and showed evidence of a narrow hole accumulation layer at the valence band edge [199]. On the basis of Kelvin force and Hall effect measurements, they concluded that surface conduction was “disorder dominated”, with a high density of surface states and scattering sites that resulted in short-range potential fluctuations [35]. The origin of this disorder was attributed to imperfect H-termination and high surface roughness. They also observed “carrier freeze-out” at temperatures below 70 K; a phenomenon which occurs when the sheet carrier density collapses below a critical temperature. This bolstered the idea that holes in H-diamond were confined to localised states which exist at energies near the valence-band minima, akin to the Anderson-Mott mobility edge model.

The Anderson model [200], later modified by Mott [201–203], predicts a thermal activation barrier to conductivity due to microscopic inhomogeneities in the surface potential inducing carrier localisation. As one may intuit, the effect of random surface potential variations is to smear the energetic continuum of the valence and conduction band edges, leaving localised low-energy states and delocalised higher energy states. Mott introduced the concept of a “mobility edge”, i.e. a boundary energy E_{ME}, above which the wavefunctions of the carriers span the extent of the quantum well, propagating freely. Below E_{ME}, carriers move sluggishly between localised states through phonon-assisted tunneling – a mechanism known as variable-range hopping, which causes a strong temperature-conductivity dependence as the generation of phonons increases. Above a critical temperature (i.e. when the Fermi-level $E_F \geq E_{ME}$), holes acquire sufficient thermal energy to excite into delocalised states which span across the 2D-quantum well, thereby establishing metallic conduction. The model therefore predicts a thermally activated conductivity (measured in Ω^{-1} cm^{-1}) mechanism, with the critical thermal activation energy decreasing as the carrier concentration increases: a trend corroborated by the results of Nebel’s study [199]. Furthermore, carrier concentration was predicted to be thermally activated as well, which was used to explain why the sheet carrier densities of the samples fell sharply when below a temperature of 70 K, as holes became confined to localised states below a critical temperature. Weak temperature dependent decline in mobility was observed for intermediate temperatures between 200 K and 330 K, attributed to mechanisms such as phonon-induced, impurity and surface roughness scattering. However, mobility was not considered to be thermally activated.

A study by J. Garrido et al. reconsidered the mobility-edge model [204]. In contrast to Nebel's results [199], they observed no carrier freeze-out down to temperatures as low as 30 K. Additionally, they observed that while carrier concentration was not thermally activated in their samples, both conductivity and mobility exhibited thermal-activation. This was in contrast to predictions from the Anderson-Mott model [200–203]. They instead adopted a "percolation theory" model pioneered by Arnold [205–207], who proposed the coexistence of metallic and thermally-activated conduction over a multitude of carrier concentrations, instead of a strict transition from one to the other across the mobility-edge as assumed by the Anderson-Mott model. Arnold's percolation model proposed that carrier transport in a strongly localised system is a "combination of percolation around, scattering from, and thermal emission over random potential barriers" [205–207]. Long-range potential fluctuations (due to the accumulation of charged adsorbates at the surface) induce a macroscopically inhomogeneous transport channel, wherein the position of the Fermi level E_F varies from $E_F \geq E_{ME}$ (in metallic regions) to $E_F < E_{ME}$ (in insulating regions). Within this paradigm, it becomes erroneous to describe the energy of the 2D system as being above or below a fixed mobility-edge, since it can simultaneously be both in different regions. At low carrier concentrations, the metallic-like regions are isolated from each other by insulating regions, and conduction occurs by thermal activation of carriers over the potential barriers that separate these regions. This explained why conductivity at low carrier concentrations appears to be thermally activated. As the carrier concentration increases, the metallic regions become larger and the potential barriers begin to shrink. The "percolation threshold" for a 2D system occurs when the fraction of the metallic regions equals the fraction of the insulating region (ε). At this threshold, continuous percolation pathways are established between the metallic regions, circumventing the potential barriers. As per Arnold [205–207], for materials with a high carrier concentration ($\varepsilon \leq 0.5$), at low temperatures conductivity saturates to a value independent of temperature, relying entirely on percolation paths. This deviates from the exponentially thermally activated behaviour observed for low carrier concentrations. At very high carrier concentrations ($\varepsilon \ll 0.5$), the metallic regions envelope most of the surface and conduction ideally becomes entirely temperature independent.

Differing from Arnold's original model, Garrido et al. proposed that at low temperatures and carrier concentrations, variable-range hopping becomes the dominant conduction mechanism: i.e. the conductivity and mobility do not appear to saturate to a constant minimum value but continue to fall as $T^{-1/3}$ [204]. Therefore, Garrido's percolation model predicts the following behaviours: (i) as the carrier concentration decreases, thermally-activated mechanisms become dominant with an exponential temperature dependence for conductivity and mobility at low temperatures, (ii) above the percolation threshold ($\varepsilon \leq 0.5$, high carrier concentration) conductivity and mobility show decreased temperature dependence and transport occurs primarily through conductive percolation channels, however, (iii) below the percolation threshold and at low temperatures, phonon assisted variable-range hopping prevails.

As with any semiconducting material, the mobility of majority carriers in diamond is influenced by their effective mass, which makes the band-structure of diamond important to a complete analysis. From *ab-initio* calculations [35,208] and confirmatory cyclotron resonance experiments [28], we know that the three uppermost valence bands in diamond have their maxima at the Γ point of the Brillouin zone. The two upper bands, named the heavy-hole and light-hole bands, are degenerate at the Γ point, while the split-off band is located 6 meV below them. The small energy difference between the two-fold degenerate heavy hole & light hole bands and the split-off band is unique to diamond, with much larger values being observed for other semiconductors [35]. This implies that the hole population in the split-off band is more probable for diamond than other semiconductors [35]. For temperatures >70 K, the ambient thermal energy is sufficient to allow for carriers to move freely between these bands, and all three bands can be considered degenerate at the Γ point, however for low temperatures the distinction becomes important. Using a Schrödinger-Poisson solver, Peterson et al. [35] treated all three bands separately to conduct an in-depth analysis of mobility limiting mechanisms for holes in H-diamond and found that their results agreed broadly with Garrido et al. [204].

Peterson et al. [35] proposed a similar percolation framework, whereby they hypothesized that holes in the 2D well percolate around long-range potential fluctuations induced by (i) negatively charged surface acceptors and (ii) 'C—H disorder', defined later in the text. A key observation from this study was that despite similar sheet carrier densities, samples may exhibit dissimilar behaviour with regards to their conductivities and mobilities. For instance, two of the samples utilised in the study (labelled as A and C) showed very similar carrier densities ($\sim 5 \times 10^{12}$ cm^{-2}), however exhibited drastically different thermal-activation energies for conductivity and mobility, with sample C showing a much higher activation threshold. By considering the fact that pre-Al_2O_3 encapsulation, sample A had a four-fold higher carrier density than sample C, in conjunction with the corollary that sheet carrier density is proportional to the C—H bond density, it appears that sample C has a much lower C—H dipole density than sample A. Under the percolation framework, this implies that holes would have to percolate around a higher density of insulating regions in sample C compared with sample A ($\varepsilon_C > \varepsilon_A$), thereby causing sample C to have a higher thermal activation energy despite a similar sheet carrier density. According to Peterson et al. [35], myriad variations in surface morphology may contribute to local variations in surface potential and introduce additional scattering mechanisms; these include non-homogenous distributions of surface acceptors due to inconsistencies in H-termination, erratic termination moieties and variations in surface reconstruction. Cumulatively, Peterson et al. have referenced to these effects as 'C—H disorder', however their exact impact on mobility remains to be explored [35].

Peterson et al. also commented on the impact of separation between the surface acceptors and the induced carrier density, finding an exponential dependence of the surface impurity scattering rate on the separation distance [35]. A theoretical study of the 2DHG has proposed surface impurity scattering to be the dominant mobility limiting mechanism [209], a conclusion also supported by [35,114,210–212]. This suggests it may be possible to boost mobility significantly by increasing the separation between the 2DHG and negative charge at the surface. Such a separation could potentially lead to a loss in carrier density, however.

Surface transfer doping of diamond with air exposure has made variable temperature measurements challenging, due to the ease with which atmospheric molecules on the diamond surface can be disrupted. Demonstrations of solid surface electron acceptor mediums such as TMOs and Al_2O_3 have enabled further investigation of electronic properties across a wide temperature range. Xing et al. reported a weak temperature dependence for both MoO_3 and V_2O_5 doped diamond, observing 2D Fermionic liquid behaviour down to

250 mK [213,214]. Between 20 K and 300 K, both carrier density and sheet resistance as extracted from Hall bar measurements remained relatively constant, showing little evidence of carrier "freeze-out". This is consistent with aforementioned results from Garrido et al. [204] and Peterson et al. [35], however conflicts with work from Nebel et al. [199]. From a transfer doping perspective, the absence of thermal dependence on the generation of carriers in TMO transfer-doped diamond would be expected, as activation energy is not a component of the proposed interfacial electron exchange model (Fig. 8). The same should hold for elevated temperatures at which, due to diamond's ultra-wide bandgap, the influence of additional thermally activated carriers for a transfer-doped system with no intentional impurity doping will be minimal. This relative temperature insensitivity further enhances the appeal of transfer-doped diamond as a semiconductor for robust electronic applications. These effects can be observed in [157], where sheet resistance for MoO_3 and V_2O_5 doped H-diamond under low vacuum remained relatively stable up to 573 K, suggesting a somewhat temperature agnostic doping system. Tordjman et al. reported an increase in mobility at temperatures up to 700 K for ReO_3 doped H-diamond, resulting in a significant conductivity increase while carrier density remained mostly stable [173]. Improved carrier mobility at elevated temperatures is highly uncommon for semiconductors due to phonon scattering. Tordjman et al. suggested a transition in the crystalline structure of ReO_3 at high temperatures may result in the formation of an emerging 3-dimensional channel with reduced screening from the diamond:TMO interface, contributing to the high-temperature mobility enhancement [173].

Effects of surface roughness on carrier transport were investigated by Wade et al., who reported an increased carrier concentration for rougher H-diamond surfaces when exposed to NO_2, measured for surfaces ranging from 5 nm to 450 nm root mean square deviation roughness (R_q) [215]. While increased surface area would intuitively suggest increased charge transfer per lateral unit area, their results suggest the increased area would not account for the increased carrier concentration seen. Instead, they propose steps and/or ridges in the topology of the diamond surface offer ideal reactive sites for NO_2 molecules to initiate charge transfer. A general trend of reduced sheet resistance for rougher H-diamond surfaces has also been reported by Crawford et al. [114]. This study of carrier transport for nominally identical etched diamond surfaces, exposed to varied hydrogen plasma power densities, observed lower sheet resistance for rougher surfaces ($R_q = 1.6$ nm) when compared to smoother surfaces ($R_q = 0.3$ nm), transfer-doped by MoO_3. However, in this case the improved conductivity appeared to be due to increased mobility. It was therefore speculated that this may have been due to removal of defect sites on the diamond surface, improved hydrogen coverage or perhaps increased average separation between the 2DHG and negative surface charge.

As iterated in the preceding discussion, improvements in substrate quality have allowed for low disorder diamond surfaces wherein metallic conduction prevails over hopping between localised states, even at very low temperatures. The quasi two-dimensional nature of the hole-accumulation layer in transfer-doped diamond is increasingly supported by literature, with low disorder surfaces allowing for the direct observation of extended 2D states and phase coherent quantum transport phenomena [216–218]. Early indications of 2D confinement came from electron field emission measurements on conductive, air-exposed H-diamond which showed discrete jumps in the emitted current density with increasing extraction electric field [219,220]. The stepwise emission current indicated that a 2D nanoscale quantum well with discrete energy levels exists in near-surface H-diamond; Gan et al. were able to reproduce the emission current profiles for air-exposed H-diamond samples computationally by assuming a triangular quantum well with a width of 4.9 nm and a depth of 115 meV, which is comparable to predictions using the Nernst equation [58,219]. Using self-consistent Poisson-

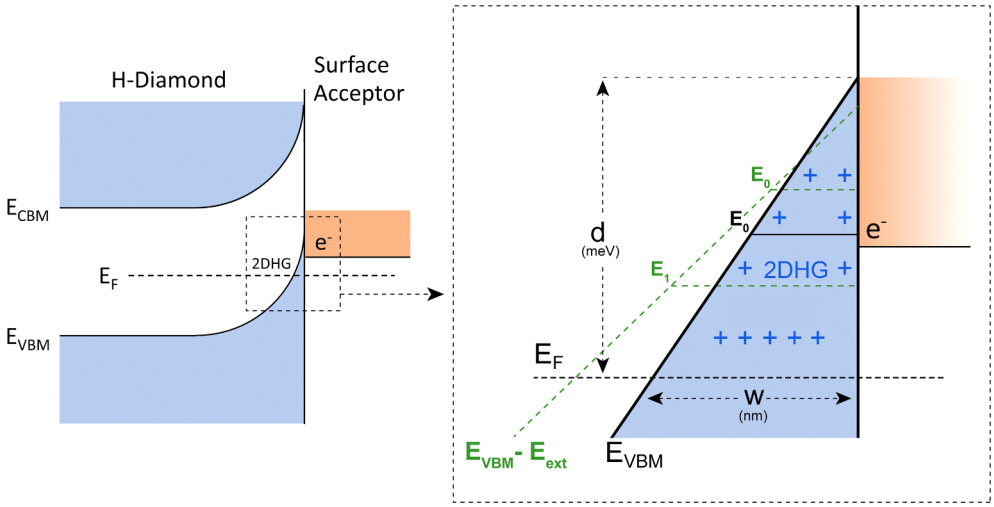

Fig. 11. Schematic of the asymmetrical triangular quantum well (QW) with discretized energy levels (E_0-E_1) formed at the surface of hydrogen-terminated diamond. The depth (d) and the width (w) of the QW have been reported to be between 100 and 300 meV and 1–5 nm for air-doped hydrogen-terminated diamond, with a hole sheet carrier density between 10^{12}–10^{13} cm^{-2} [58,216–221,225]. As the carrier density increases, the confining potential becomes sharper, leading to a narrower and deeper QW. The green dashed line shows the effect that an external electrical field, perpendicular to the surface, has on the shape of the QW. Without an applied field, the QW contains one discretized energy level represented as E_0. As the QW widens under the influence of an external field, it accommodates more levels [219]. (For interpretation of the references to colour in this figure legend, the reader is referred to the web version of this article.)

Schrödinger calculations in conjunction with Kelvin-probe and Hall effect measurements, Nebel et al. have also modelled a triangular potential well with a depth of 237 meV and a width of 2.7 nm [221].

The two-dimensional carrier confinement in diamond also leads to interesting spin properties for the holes. Generally, spin-orbit interactions in solids can be classified as symmetry independent and symmetry dependent. Symmetry independent spin-orbit interactions stem from intrinsic atomic orbitals, and scale with the atomic number of an element [222]; consequently, carbon has small intrinsic spin-orbit splitting – in fact, the smallest among all elements, next to boron. On the other hand, symmetry-dependent spin orbit coupling in semiconductors is driven primarily by two contributions: (i) the Dresselhaus effect [223] caused by inversion asymmetry in the crystal lattice or (ii) the Rashba effect [224] caused by the asymmetry imposed by an electric field perpendicular to the surface. For H-diamond, the Dresselhaus effect is small given the inherent inversion symmetry of the bulk crystal lattice, which is broken only at the surface. Conversely, the Rashba effect in H-diamond is much more pronounced; electron acceptors at the surface generate a strong electric field perpendicular to the plane of the 2D hole-accumulation layer, which creates a highly asymmetrical (and approximately triangular) confining potential, as illustrated in Fig. 11. This electric field is extremely strong ($>3.4 \times 10^6$ V/cm) for high hole densities ($\rho > 10^{13}$ cm^{-2}) and confines carriers to within a few nanometres of the surface [216,217,219,221,225]. It has therefore been proposed that the Rashba effect is the dominant mechanism in H-diamond which drives the spin-orbit interaction [216,217,225]. Magnetoresistance data offers important insight into the spin-orbit interaction strength of the diamond 2DHG and indicates whether holes experience weak localisation or weak antilocalisation effects. Quantum systems with strong spin-orbit coupling exhibit weak antilocalisation, a phase coherent backscattering mechanism which results in a positive correction to the Drude conductivity (i.e. lower net resistivity) [226]. Low-temperature magnetoresistance measurements by Akhghar et al. reported weak antilocalisation in transfer-doped diamond, which manifests as a cusp in the magnetoresistance curves at zero-applied magnetic fields ($B = 0$) and is a characteristic signature of strong spin-orbit coupling [216,225]. The spin-orbit splitting was subsequently deduced from the Drude correction to conductivity, in an approach outlined by Winkler et al. [227]. Furthermore, using an electrostatic gate with an ionic-liquid dielectric architecture, Akhghar et al. attempted to apply gated control to the spin-orbit interaction in the H-diamond 2DHG by modulating the hole concentration and therefore the magnitude of the confining potential [216]. They found that the spin-orbit splitting was tuneable over a five-fold dynamic range from 4.6 to 24.5 meV by linearly varying the sheet hole density [216]. These values for spin-orbit splitting are higher than those reported thus far for 2D hole systems in other semiconductors [228,229]. In 2020, Xing et al. [230] also demonstrated control over the spin-orbit splitting in H-diamond using a solid-state V_2O_5/Al_2O_3 bilayer gate stack; offering a pragmatic alternative to the ionic-liquid gate architectures proposed previously by Akghar et al. [216] which require continuous temperature cycling. In a subsequent study, Akhghar et al. also quantified the *g*-factor for carriers in the diamond 2DHG, a gyromagnetic parameter which characterises the coupling strength of hole spins to an external magnetic field [217]. They derived a hole *g*-factor of 2.6 ± 0.1, which is lower than that reported for other 2D hole systems [231,232]. Collectively, these studies demonstrate the ability to tune the spin-orbit interaction in H-diamond, which combined with the relatively mature nanofabrication technology for diamond FETs, warrants cautious optimism towards achieving spin-coherent transport devices.

It is evident from this section that both the induction of the sheet hole-accumulation and its transport properties exhibit complex quantum interactions, with most prevailing transport models falling short of explaining all experimental observations. The collective results from each of these independent studies suggest that variations in the chemistry and morphology of the diamond surface (gross or indeed subtle [233]) may play a crucial role in the transfer doping process and further complicate the simplified and currently widely accepted model.

5.2. Electrical contacts to diamond

A Schottky barrier is formed at the interface between a metal and semiconductor material. The Schottky barrier height (SBH, ϕ_B) is often considered to be governed by the Schottky-Mott relationship: $\phi_B = \phi_M - \chi$, coined in 1939 [234,235], which predicts a direct dependence of the SBH on the work-function ϕ_M of the contacting metal; this dependence is parametrically defined as $S = \frac{\partial \phi_B}{\partial \phi_M} = 1$. However, this is often unsupported by available experimental data which has repeatedly shown real contacts to have an S-parameter less than unity, i.e. $S = \frac{\partial \phi_B}{\partial \phi_M} \leq 1$. Experimental work has frequently shown that the SBH is varyingly insensitive to the work-function of the contact metal [94,236–241]; this effect is due to “Fermi level pinning” of a semiconductor surface, caused by surface states providing energy levels within the bandgap which “pin” the Fermi level. The disagreement of the Schottky-Mott relationship with empirical measurement is unsurprising, as it relies on assumptions which do not hold at a microscopic level. For instance, at the metal-semiconductor interface energy bands are assumed to have a discontinuous long-range order, however a more microscopic view shows that the rapidly varying short-range crystal potential remains continuous, to satisfy Poisson’s equation [237,242]. The band-structure at the interface does not abruptly change from metallic to semiconducting, rather, there is a finite distance over which this change evolves.

Two predominant strategies have emerged in forming low resistance ohmic metal contacts to the 2DHG of transfer-doped H-diamond. In 1994, Aoki et al. investigated the properties of as-grown CVD diamond surfaces in contact with various metals [243]. Their findings showed a strong correlation between interfacial SBH and the work-function of the deposited metal on H-diamond. This was attributed to the low density of states provided by H-termination, which allows a diamond surface sensitive to metal work-function by reducing Fermi level pinning. From this, the SBH can be modulated by the relative work-function of the contact metal following the traditional Schottky-Mott relationship. High work-function metals have thus demonstrated linear ohmic response on H-diamond, while low work-function metals have been used to produce contacts with large Schottky barriers [244].

Alternatively, carbide interfaces can also be formed on diamond in a similar fashion to silicide formation in Si MOS technology.

Greatly improved mechanical strength is a particular advantage of this approach, as well as suitability for higher temperature operation. However, a high thermal anneal step of 400–600 °C and above is required to form the carbide [245,246]. H-termination is also not a prerequisite for successful carbide formation, yet hydrogen plasma exposure at high temperatures has been shown as a means to simultaneously achieve both H-termination of the diamond surface and form a carbide beneath contacts [247]. Fig. 12 shows a cross section illustration of both contact types as described by [245].

Au has been the most commonly used ohmic contact on H-diamond due to its high work-function and ease of deposition, with reported contact resistances (R_c) varying from as low as 0.9 Ω.mm to an order of magnitude higher and above [177,178,248–250]. This variation is likely due to differences in surface conditions and coverage of hydrogen between diamond substrates, which will alter the barrier height and introduce trap states [243,244]. Ag, Cu, Ir, Pt and Pd have also been shown to produce an ohmic response on the H-diamond surface [251–255]. The most common carbide-based contact reported is TiC, with R_c values varying around 9 Ω.mm [245]. Jingu et al. also demonstrated a "hydrogen last" approach, by which TiC contacts are first formed on O-terminated diamond [245]. The active region between contacts was then H-terminated by hydrogen plasma, showing the TiC contacts could withstand the H-termination process [245]. Vardi et al. also communicated carbide contacts formed with tungsten (WC) showing a R_c of 2.6 Ω.mm and good mechanical stability [247]. Their results also demonstrated the WC contacts could survive hydrogen plasma exposure.

Table 2 shows a non-exhaustive, but representative, collation of contact resistances found in the literature for various metals and carbides [177,178,245,247–250,253,255,256]. It should be noted that much of the reported literature examining ohmic contacts on H-diamond uses specific contract resistance (Ω.cm^2), which makes comparison with values reported in Ω.mm challenging, as the information required for conversion between the two is often not available: specific contact resistance accounts for the so called 'transfer length' (L_t) of the contact (the region at the edge of the metal where current crowds) [257]. Contact resistance per unit width (Ω.mm) normalises resistance to the contact width without accounting for L_t and is more advantageous for comparison purposes, as extraction of L_t for H-diamond ohmic contacts through common transmission line model (TLM) measurements is likely to be inaccurate. This is due to the assumption that a uniform sheet resistance of the semiconductor exists (as normally achieved via impurity doping in materials such as Si [257]). In this instance, sheet resistance of the semiconductor is assumed to be near identical both between the ohmic contacts and beneath them. Under these conditions, L_t may therefore be determined through linear extraction of resistance vs gap size as R (Ω) trends to 0 for a gap size of <0. However, in transfer-doped H-diamond the surface conductivity induced by transfer doping is strongly dependant on species in contact with the H-diamond surface i.e. adsorbates or high EA oxide. For this reason, measured sheet resistance within the active regions between ohmic contacts will almost certainly differ to that of the H-diamond beneath the contact metal, rendering measurement of L_t via this method to be misleading. The same principle holds for carbide contacts (and indeed most alloyed metal/semiconductor ohmic contact systems), in which the sheet resistance of the H-diamond surface will almost certainly differ from the carbide formed regions under the metal. This effect was investigated by Kono et al. who devised an experiment to identify the sheet resistance beneath Au contacts on H-diamond [258]. Using a purpose made test circuit with an auto-sense resistor placed between current-source and voltage sense probes, they were able to estimate a quantitative ratio between sheet resistance of the gap between the ohmic contacts and that underneath the contacts. The reported results showed a 'beneath Au' sheet resistance roughly 200 times greater than that of the gap between contacts. A difference in sheet resistance of this magnitude would lead to a significant overestimation of L_t and thus introduce inaccuracy to associated specific contact resistance (Ω.cm^2) measurements extracted from traditional TLM structures.

Schottky contacts on diamond have been achieved for hydrogen, oxygen and fluorine-terminated surfaces. Tsugawa et al. found that Al, Pb, Zn, Ti, Co and Ni evaporated on the H-diamond surface formed large Schottky barriers, while Au, Cu, Pt and Ag formed contacts exhibiting ohmic behaviour [259]. They were able to explain their results using a modified 'metal-induced gap states' (MIGS) framework [260] and found the measured SBH correlated well with predicted trends for electronegativity. The SBH for Al, Pb, Zn, Ti, Co, Ni were extrapolated to be 0.58, 0.51, 0.36, 0.27 and 0.19 eV respectively; a general adherence to Mönch's correlation between interface charge transfer and electronegativity difference was observed [261,262]. As the electronegativity difference increased, the SBH magnitude decreased almost linearly; metals with relatively small electronegativities (<1.9 on the Pauling scale) showed Schottky characteristics with high SBH, whereas metals with high electronegativities showed ohmic characteristics.

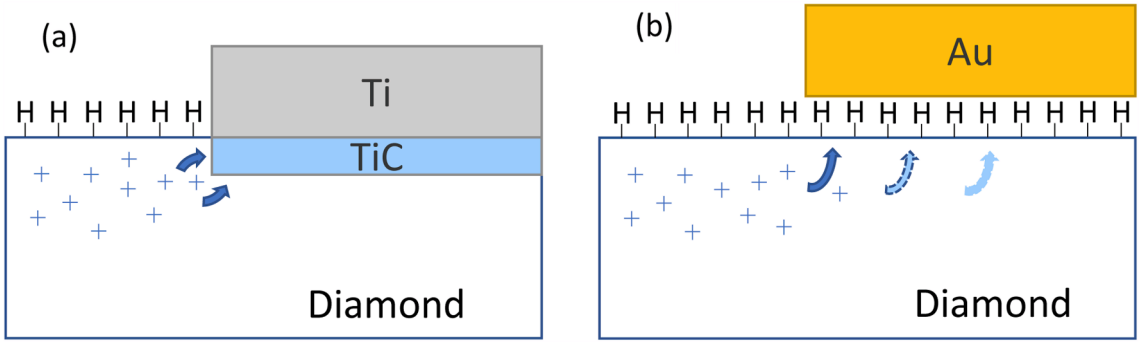

Fig. 12. Cross section illustration of ohmic contact formation to and carrier transport in hydrogen-terminated diamond (a) Carbide-based ohmic contact (b) High work-function metal-based ohmic contact.

Table 2
Compilation of reported contact resistances for various ohmic contact types on hydrogen-terminated diamond, including both carbide and high work-function metal-based contacts.

Metal	Resistance (ohm.mm)	Ref	Metal	Resistance (ohm.mm)	Ref
Au	0.90	[177]	Au	5.00	[250]
Au	1.84	[255]	Au	5.52	[248]
Au	3.00	[178]	Pd	0.42	[253]
Au	4.00	[256]	TiC	9.00	[245]
Au	4.00	[249]	WC	2.6	[247]

As expected, due to the inversion of the surface dipole, this trend is reversed for O-terminated diamond. A detailed study by Muret et al. examining barrier heights on O-diamond noted that metals with low electronegativity showed lower barrier heights on O-diamond, preserving the trend which correlates a larger electronegativity difference as the driver for a smaller SBH [94]. They used a bond-polarisation perspective to analyse their results [237,239,240], paying close attention to the surface preparation, adhesion and bond formation at the interface. The bond-polarisation model posits that wavefunctions originating in the metal interact with wavefunctions originating in the semiconductor in the interface-specific region (ISR), resulting in the formation of interface-specific electronic states which are not found in either the bulk semiconductor, nor the bulk metal. These interfacial states are the source of the (often undesirable) Fermi-level pinning effect observed in SBH measurements, such that both the extent of pinning and the pinning position (around mid-gap) follow as a result of the total energy minimisation of bonds at the interface. The higher the density of bonds in the ISR, the more insensitive the surface becomes to the overlaying material work-function (i.e. the lower the S-parameter); this contextualises why O-diamond typically exhibits a stronger Fermi-pinning effect than H-diamond, given its higher density of surface states. This model has been encapsulated succinctly by Tung in a rigorous energy-functional framework [239]. Muret et al. went further to explain the SBH lowering effect of annealing at $T \geq 350$ °C for a wide range of metals deposited on O-diamond [94]. Experimentally, they attributed the reduction in SBH of the Zr/O interface to the thermally induced evaporation of hydroxyl and carbonyl species from the O-diamond surface, leaving a well ordered O-termination with a lower density of surface states that is better able to electronically interact with overlaying metals. They found annealing led to stronger and shorter bonds between the Zr-lattice and terminating O-atoms. Bonding was “deeply modified” by annealing, transforming from physiosorbed metallic layer on the O-diamond surface (through weak interactions with hydroxyl species) to short, strong oxide bonds between Zr and O atoms, a result predicted from a bond polarisation perspective. The Fermi level for O-diamond can thus be “unpinned” by annealing the contacts; with barrier heights reduced from ~2 eV to 1.2 eV for gold [263,264], and from 1.93 eV to 0.93 eV for zirconium upon annealing [94].

XPS measurements have indicated that F-diamond surfaces form Schottky contacts with most commonly used contact metals, such as Au, Cu, and Pd. Li et al. compared Schottky barrier heights on F-diamond and O-terminated diamond for different metals [238]. Zhao et al. fabricated a dual-terminated Schottky barrier diode on O/F-terminated diamond and found a similar value for the SBH of Au on O/F-diamond, i.e. 2.0 eV and 2.39 eV respectively [265]. Studies have found that Schottky barrier heights on both F-diamond and O-diamond seem independent of the deposited metal work-function, which indicates Fermi level pinning for both surfaces [94,236,238].

The preceding discussion highlights the role of surface termination, uniformity, and overlaying metal characteristics on the nature of contacts to diamond. Once again, the attributes of the diamond surface and the interface dipole are a crucial determinant of device properties, underscoring a recurrent theme in our overview of diamond surface electronics.

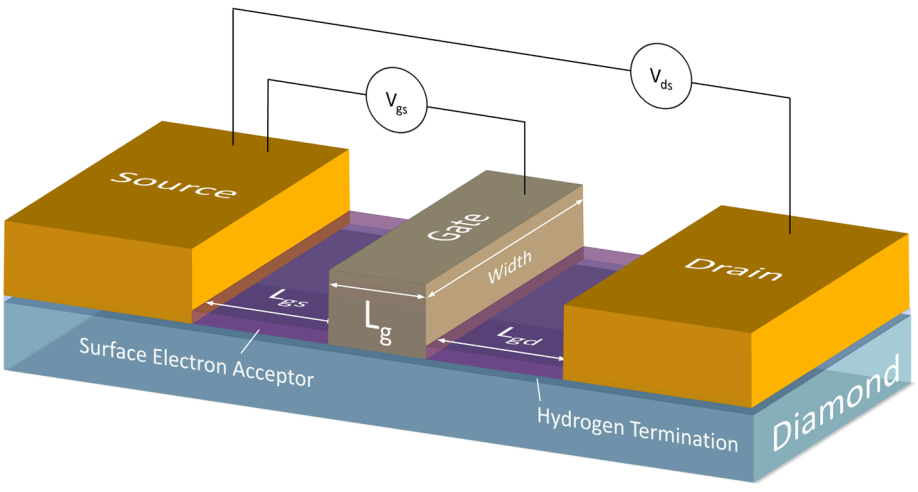

Fig. 13. Illustration of a 3-terminal hydrogen-terminated diamond-based field effect transistor device, consisting of a source, drain and gate. Notable dimensions are represented, such as gate length (L_g), gate-source separation (L_{gs}) and gate-drain separation (L_{gd}).

6. Applications of transfer doping in diamond

The sub-surface 2DHG formed through surface transfer doping within H-diamond provides a unique mechanism to access its attractive electronic properties, while avoiding the stringent limitations associated with more traditional substitutional doping. This phenomenon has been exploited in the development of various applications, the complete listing and discussion of which are beyond this review. Here follows a brief account of some of the more prevalent applications of surface transfer doping in diamond, providing some insight into the diversity of established and emergent technologies under development in this field.

6.1. Field effect transistors

The production of H-diamond FETs is an area where surface transfer doping of diamond has arguably been applied most extensively. The 2DHG generated by a transfer-doped H-diamond surface is well suited for the production of planar electronic devices, as originally demonstrated by Kawarada et al. in 1994 [266]. An illustrative example of their 3-terminal FET device is shown in Fig. 13, consisting of a CVD grown H-diamond substrate (1 0 0) transfer-doped by air exposure with an Al gate contact and Au source & drain ohmic contacts. In addition to facilitating the surface transfer doping process, termination of the diamond surface with hydrogen sufficiently reduces interface state density to allow an unpinned surface sensitive to metal work-function, as discussed in Section 5. Both Schottky and ohmic contacts may therefore be formed to the resultant 2DHG through appropriate selection of low and high work-function contact metals respectively, without the need for thermal treatment. This device had a gate length of 10 μm and operated in enhancement mode, demonstrating modest performance with a maximum drain current of 1.6 mA/mm and an extrinsic transconductance of up to 200 μS/mm [266]. The 10 μm gated FET could not be fully turned off; however, increasing gate length (L_g) to 40 μm resulted in the ability to fully turn off the device due to the increased depletion region of the larger gate. This in turn reduced transconductance to 20 μS/mm and maximum drain current to 0.14 mA/mm. The work was pioneering in that it verified the potential to exploit transfer-doped H-diamond for surface bound electronics. Since this early example, FET technology using H-diamond transfer-doped by air exposure has evolved substantially. Through improvement to synthetic diamond substrate quality, optimisation of FET geometry and surface contacts, greatly improved device performance and stability has been demonstrated as discussed below.

Since its original demonstration, optimisation of device geometry, and in particular reduction of L_g, has led to substantial enhancement in H-diamond FET performance. Reducing L_g can improve cut-off frequency (f_T) and maximum oscillation frequency (f_{max}), while decreasing the overall source-drain distance ($L_{gs} + L_g + L_{gd}$) will lower on-resistance (R_{on}) of the device. However, increasing L_{gd} can also result in a greater off-state breakdown voltage by reducing the electric field concentration between the gate and drain contacts. Likewise, a larger L_g can significantly improve off-state performance and power handling capability. Low resistance contacts to the 2DHG of H-diamond are critical in achieving high-performance FET devices, with particular impact on the R_{on} faced by current flowing from the source to the drain. Despite a number of studies looking into alternative metals, Au has been the most widely used ohmic contact material in H-diamond FETs to date, due to the ease with which it forms an effective ohmic contact on the H-diamond surface. Outlined in Section 5, carbide contacts such as TiC provide an alternative, albeit often higher resistance, approach. Devices with TiC contacts have demonstrated superior thermal and mechanical robustness, allowing high-voltage operation [267] and devices which survive high-temperatures [268].

In contrast to FET devices with Schottky based gate contacts (in which the gate interface is formed by a low work-function metal in direct contact with the H-diamond surface), substantial work has been dedicated to the development of metal-insulator-semiconductor FET (MISFET) H-diamond devices whereby various dielectric materials have been incorporated under the gate metal to increase both breakdown voltage potential and reduce current leakage through the gate contact. A non-exhaustive list of gate dielectric materials which have been demonstrated in H-diamond FETs, to-date, is shown in Table 3.

As discussed in Section 4, materials in contact with the H-diamond surface can act as an electron acceptor to induce transfer doping and form a 2DHG within H-diamond. The role of the materials presented in Table 3 as possible electron acceptors on H-diamond is complicated by the field effect process induced by a gate voltage applied across them in an actual FET device. Furthermore, the suitability of TMO electron acceptor materials such as V_2O_5 and MoO_3 as high performance, low leakage gate dielectric materials in H-diamond FET technology is still a point of investigation. For instance, larger gate leakage currents have been reported for H-diamond FETs that incorporate 10 nm MoO_3 as a gate dielectric, in comparison with 3 nm of Al_2O_3 and other similar thickness gate dielectric layers [248]. Further investigation is required in this area to fully understand the operation of TMO materials beneath the gate contact and the role of potential mobile charge within them. Residual atmospheric molecules, if not removed prior to material deposition e.g. by thermal *in-situ* annealing, may potentially become encapsulated at the H-diamond/gate dielectric interface and further contribute to the transfer doping process.

Table 3
Reported gate dielectric materials used in the fabrication of hydrogen-terminated diamond-based field effect transistor devices.

Gate dielectric material	Reference	Gate dielectric material	Reference
Al_2O_3	[269]	SiO_2	[270]
SiNx	[271]	HfO_2	[272]
Y_2O_3	[273]	LaB_6	[274]
V_2O_5	[275]	MoO_3	[276,248]

The most adopted and arguably most widely studied of the dielectric layers presented in Table 3 for use in H-diamond MISFETs is Al_2O_3, the application of which has led to substantial increases in performance and stability of operation, by both use as a gate dielectric and as a channel passivation layer. The highest maximum drain current reported thus far for a H-diamond FET is 1.35 A/mm, with L_g of 400 nm and Al_2O_3 passivation of the diamond surface after exposure to NO_2 [163]. Here, the Al_2O_3 layer also served as a gate dielectric to form a MISFET configuration. For comparison, the highest drain current achieved for a non-passivated air-doped device was 0.6 A/mm, measured from a 100 nm L_g FET reported by Ivanov et al. [277]. The highest extrinsic transconductance demonstrated for an air-doped H-diamond device was 143 mS/mm for a 100 nm L_g FET, reported by Ueda et al. [278].

The first reported demonstration of high-frequency performance of H-diamond FETs exhibited f_T of 2.2 GHz and f_{max} of 7 GHz for a 2 μm L_g device transfer-doped by air exposure [279]. Since this, an f_T of 70 GHz was achieved via reduction of L_g down to 100 nm and L_{gs} down to 350 nm for a MISFET with Al_2O_3 gate dielectric [255]. An f_{max} figure of 120 GHz has also been reported for an air-doped FET with a L_g of 100 nm [278]. Kubovic et al. were one of the first to report evaluation of RF power-density for H-diamond FETs with a L_g of 200 nm, transfer-doped by air exposure, and demonstrated a power output density of 0.35 W/mm at 1 GHz [280]. A 2019 study demonstrated a substantially higher maximum power density of 3.8 W/mm operating at 1 GHz, showing Class A operation for a H-diamond MISFET with a L_g of 500 nm and passivated by 100 nm of Al_2O_3 [281]. Due to the stability of the 100 nm Al_2O_3 film used, these FETs could be operated at drain-source voltages of up to 50 V, but demonstrated a relatively low transconductance of 15 mS/mm. The transfer doping mechanism between the H-diamond and Al_2O_3 in this device was reported to result from inclusion of H_2O as an oxidant in the ALD Al_2O_3 deposition process, discussed in Section 4. Gluche et al. reported the earliest assessment of H-diamond FET high-voltage performance, where an off-state breakdown voltage of up to 200 V was demonstrated for a FET with a L_g of 3 μm and a L_{gd} of 12 μm [282]. Room temperature off-state breakdown voltages up to 2 kV have been reported for a MISFET device passivated with 200 nm of ALD grown Al_2O_3 and a L_g of 5 μm, with a L_{gd} of 24 μm [267]. Partial oxygen termination of the diamond beneath the gate contact reportedly served to minimise off-state leakage current and also resulted in normally off (enhancement mode) FET characteristics, which is important for high-power applications due to safety concerns associated with normally-on devices.

The application of TMO electron acceptor materials MoO_3 [283], V_2O_5 [177,178,275], and WO_3 [284] in the previously air-exposed regions of H-diamond FETs has also led to varied improvements in device stability and performance. Of these, the highest drain currents (up to 700 mA/mm) and extrinsic transconductance (up to 153 mS/mm) were reported by Crawford et al. for V_2O_5 transfer-doped H-diamond FETs with L_g of 50–800 nm [177]. R_{on} was also comparatively low at 6 Ω.mm in these devices, due in part to a very low ohmic contact resistance of 0.9 Ω mm. However, at these dimensions the devices reportedly suffered from drain induced barrier lowering (DIBL) and thus poor off-state performance.

Beyond the conventional lateral FET device structure, more novel H-diamond FET designs have been demonstrated, such as a vertical-type "trench FET" for high-power operation [285]. In this configuration, a trench ~4.5 μm deep was etched into the diamond surface and then H-terminated. Al_2O_3 was then grown by ALD across the surface and trench sidewalls to act as a passivation layer. Utilising a nitrogen doped "blocking layer" formed by either ion implantation or epitaxial growth, the device could operate with low bulk leakage currents. An I_{on}/I_{off} ratio over eight orders of magnitude was demonstrated.

As discussed in Section 5, surface transfer doping of an ultra-wide bandgap material such as diamond is expected to be inherently independent of thermal conditions. This property, theoretically, could allow for stable conductivity over a wide range of temperatures with predictable device behaviour. H-diamond FETs with 200 nm of Al_2O_3 passivation and a L_g of 6 μm have been reported operating at temperatures from 10 to 700 K, with a decrease in maximum drain current of ~30% at 10 K [268]. This variation was reportedly due to low temperature effects on the device TiC ohmic contacts, rather than modulation of the H-diamond conductivity. The I_{on}/I_{off} ratio was also reduced from 10^8 at room temperature to 10^3 at 700 K, which was attributed to activation of deep donors in the substrate due to residual nitrogen. Despite this, the devices remained operational over a large temperature range.

The ability to "tune" the threshold voltage of H-diamond FETs due to the inherent unpinned Fermi level at the H-diamond surface using varied work-function gate materials has been exploited to produce normally-off FET technologies [286,287], an important feature for high-power applications as mentioned earlier. Diamond FETs have also been demonstrated in both enhancement mode and depletion mode operation on the same substrate to produce logic circuits in NOT, NOR and NAND configurations [288]. Diamond's intrinsic properties coupled with those of surface transfer doping may therefore allow production of simple logic circuits for operation in harsh environments (such as high-radiation and high-temperature) where other materials may suffer from environment-induced performance degradation.

6.2. *Surface & quantum applications*

Increasingly, the potential of diamond as a material for quantum computing, nanoscale sensing and spintronic applications is being recognised. The precise control of surface properties is imperative for the successful realisation of many optoelectronic applications. Surface transfer doping confers the unique ability to manipulate the conductivity and charge state of the H-diamond surface, using relatively simple and reversible chemical treatments. In addition, given the chemical inertness, low cytotoxicity, resilience and favourable tribological properties of diamond, a host of novel biomedical and metrological applications become plausible.

The nitrogen-vacancy (NV) centre in diamond is a paramagnetic point defect in the diamond lattice, which consists of a carbon vacancy in a lattice site adjacent to a nitrogen impurity atom. The defect exists in two charge states: the neutral NV^0 and the negative NV^-, of which the latter possesses desirable paramagnetic and optical properties. A nitrogen atom has five valence electrons; in the NV complex, three of these are covalently bonded to the neighbouring carbon atoms, while the remaining two unbonded electrons form a lone pair. The vacancy possesses three unpaired electrons from dangling bonds of the surrounding carbon atoms. Two of these form a quasi-covalent bond with one another, while the third one remains unpaired; together with the nitrogen lone pair, this results in five

electrons that are tied to the NV complex. The NV centre maintains axial symmetry, with the electron density distributed in a plane perpendicular to the central NV axis [289]. In the NV^- state, a sixth electron is captured from the lattice (typically from a nitrogen donor defect); this tends to be the prevalent state for centres buried deep in the crystal, however, it becomes unstable and transmutes to NV^0 for centres closer to the surface.

One of the most remarkable properties of the NV^- centre in diamond is that it enables optical readout for spin transitions in the defect, induced by proximal electromagnetic or mechanical perturbations. Using this property, sensors have been realised which can detect magnetic fields of a few nanotesla [290] or electric fields of 10 V/cm at kHz frequencies, which allows for the detection of an electromagnetic entity as minute as an electron, at a distance of tens of nanometres from the NV^- centre [291]. For nanoscale magnetometry, plasmonic devices, nano-biophotonic and quantum computing applications, the charge state of the NV centre is valuable, as defects with consistent spin properties located close to the surface are required. Stable NV centres have been observed at depths as shallow as 2 nm from the diamond surface [292] and in nanocrystals with a diameter of 4 nm [293]. The proximity to the surface acts as a double-edged sword, since the electronic stability and spin lifetime of the defects can deteriorate due to surface effects [292]. Surface transfer doping results in upward band bending – an effect which can be used to influence the electron occupancy probability (and therefore charge state) of these shallow NV centres by shifting the Fermi level such that it lies below the NV^- energy level, thereby discharging NV^- centres to NV^0. Since the photoluminescence and electronic paramagnetic resonance (EPR) spectra is suppressed for NV^0 centres, this allows for a way to engineer the optical and spin properties of shallow NV centres. The controllable switching of luminescence enables further possibilities for molecular imaging using nanodiamonds [294], and for use as bio-nanosensors that monitor DNA release in transfection experiments for nanoscale medical applications [295].

NV^- centres are also excellent candidates for room-temperature "qubits", owing to their long coherence times and compatibility with an optical interface [296]. The optical interfacing is key to achieving a scalable quantum system: when the NV^- centre is excited with a microwave frequency which is resonant with its spin transition, a sharp change in the fluorescence intensity occurs which serves as optical readout for the spin-state of the NV^- centre. This phenomenon is known as optically detected magnetic resonance (ODMR) and is only observed for a handful of other molecules and defect systems [297]. In a quantum computing context, transfer doping is being explored as a way to increase the conversion yield and coherence time of ion-implanted NV- centres [295,298–300]. A truly revolutionary opportunity is presented in the realisation of *n*-type transfer doping, which should in theory allow for an increased population of shallow NV^- centres, due to increased concentration of negative charge carriers in the vicinity of the defect.

As mentioned previously in Section 5.1, the asymmetric quantum well formed by the 2DHG in transfer-doped diamond also results in a strong spin-orbit interaction, due to the Rashba effect [216,217,225]. This makes transfer-doped diamond appealing for spintronic devices, including "spin-FETs". The term Spin-FET was coined by Dutta and Das in 1990 [301], and their proposed device has motivated much of the current prevailing interest in spintronics. In essence, their device relies on the giant magnetoresistance effect, which characterises a significant change in the electrical resistance of a material sandwiched between two ferromagnetic layers, depending on whether said ferromagnets are in a parallel or anti-parallel alignment [302,303]. Given that the magnetisation direction of the ferromagnetic layers can be controlled by an applied external magnetic field, this allows for the conceptualisation of a device with a hugely variable electrical resistance, in essence, a transistor. The device consists of ferromagnetic source and drain contacts, with a semiconductor channel to which the spin-direction of the charge carriers can be manipulated using a gate electrode. Since the current is injected into the device through the ferromagnetic source contact, the carriers are inherently spin-selected to be either spin-up or spin-down. Carriers migrating through the channel can then be uniformly spin-aligned by applying the appropriate gate bias, such that they are oriented either parallel or anti-parallel to the magnetisation direction of the ferromagnetic drain contact. Thus, the channel resistance is correspondingly manipulated to be in a relatively low or high state (i.e. 'on' or 'off'). As evident from this description, the coupling strength of the carrier spin to applied electromagnetic fields is critical to device operation. Akghar et al. reported a series of experiments which characterise the response of hole-spin in H-diamond, finding that the spin-orbit interaction in diamond supersedes 2D hole systems in other wide bandgap semiconductors [216,217]. Furthermore, by controlling the hole concentration using an ionic liquid gate, they were able to tune the strength of the spin-orbit interaction over a five-fold dynamic range, between 4.6 meV and 24.5 meV [216]. In early 2020, Xing et al. demonstrated a tuneable spin-orbit interaction using a bilayer dielectric gate stack, which circumvents many of the design issues that accompany a liquid gate architecture [230]. As before, the hole density was found to vary linearly with the gate bias, tuneable from 1.2×10^{13} cm^{-2} to 2.5×10^{13} cm^{-2}, with device characteristics that appear promising for low-temperature operation. The spin-orbit splitting also varied linearly between 3.5 and 8.4 meV, albeit a smaller dynamic range than that achieved in an earlier device by Akghar et al. [216].

While by no means exhaustive, this section previews some of the more promising capabilities of diamond, emphasising the utility of surface transfer doping out-with the purview of conventional electronics. As surface electronics and the science of transfer doping mature, the potentialities for diamond as a substrate material in diverse application spaces will continue to grow.

7. Conclusions

Here we have presented a review of progress in surface transfer doping of diamond, providing a detailed overview of this alternate route to procuring highly conductive diamond substrates that enable electronic device applications. This process draws upon many different aspects of the material system, predominantly bound to the surface conditions of diamond. Subtle variations in surface topology, construction, termination, and interface with an electron accepting medium will dramatically alter conductivity and behaviour of the resulting two-dimensional hole gas. To this end, we have discussed the history of early experimental work in diamond transfer doping, followed by an overview of the diamond surface and its construction. With this important understanding, the role of electron acceptors on the H-diamond surface was then explored. Examining the literature, it becomes clear that no single model of surface

transfer doping to-date is sufficient to provide a full explanation of all experimental results. Yet, the understanding and development of these models has rapidly progressed within the last decade alone. Today, sheet resistances well below 1 kΩ/□ at room temperature have been reported for hydrogen-terminated CVD grown diamond substrates, without any intentional impurity doping. Further development in this area, combined with continued advances in substrate-growth techniques, will likely deliver a range of diamond-based electronic, quantum and sensing device solutions in the near future.

Acknowledgements

This work was supported by the UK Engineering and Physical Sciences Research Council [grant number EP/E054668/1] and the UK Defence Science and Technology Laboratory. The authors wish to acknowledge the staff and facilities of the James Watt Nano-fabrication Centre. KGC wishes to thank colleagues at the US Army Research Laboratory for their support.

References

[1] C.J.H. Wort, R.S. Balmer, Diamond as an electronic material, Mater. Today 11 (2008) 22–28, https://doi.org/10.1016/S1369-7021(07)70349-8.
[2] F. Mohs, The characters of the classes, orders, genera, and species; or, The characteristic of the natural history system of mineralogy. Intended to enable students of discriminate minerals on principles similar to those of botany and zoology, W. and C. Tait, Edinburgh, (1820).
[3] E. Kohn, A. Denisenko, Concepts for diamond electronics, Thin Solid Films 515 (2007) 4333–4339, https://doi.org/10.1016/j.tsf.2006.07.179.
[4] H. Pierson, Handbook of Carbon, Graphite, and Fullerenes: Properties, Processing, and Applications, Elsevier Science, 1993.
[5] M. Kasu, K. Ueda, Y. Yamauchi, A. Tallaire, T. Makimoto, Diamond-based RF power transistors: fundamentals and applications, Diamond Related Mater. 16 (2007) 1010–1015, https://doi.org/10.1016/j.diamond.2006.12.046.
[6] S. Koizumi, H. Umezawa, J. Pernot, M. Suzuki, Power Electronics Device Applications of Diamond Semiconductors, Woodhead Publishing, 2018.
[7] H. Umezawa, Recent advances in diamond power semiconductor devices, Materials Science in Semiconductor Processing 78 (2018) 147–156, https://doi.org/10.1016/j.mssp.2018.01.007.
[8] M. Gabrysch, S. Majdi, D. Twitchen, J. Isberg, Electron and hole drift velocity in chemical vapor deposition diamond, J. Appl. Phys. 109 (2011), 063719, https://doi.org/10.1063/1.3554721.
[9] S. Baccaro, A. Cemmi, I.D. Sarcina, B. Esposito, G. Ferrara, A. Grossi, M. Montecchi, S. Podda, F. Pompili, L. Quintieri, M. Riva, Radiation damage tests on diamond and scintillation detector components for the ITER radial neutron camera, IEEE Trans. Nucl. Sci. 65 (2018) 2046–2053, https://doi.org/10.1109/TNS.2018.2807841.
[10] W.D. Boer, J. Bol, A. Furgeri, S. Müller, C. Sander, E. Berdermann, M. Pomorski, M. Huhtinen, Radiation hardness of diamond and silicon sensors compared, Phys. Status Solidi (a) 204 (2007) 3004–3010, https://doi.org/10.1002/pssa.200776327.
[11] W. Saslow, T.K. Bergstresser, M.L. Cohen, Band structure and optical properties of diamond, Phys. Rev. Lett. 16 (1966) 354–356, https://doi.org/10.1103/PhysRevLett.16.354.
[12] P. Koidl, C.P. Klages, Optical applications of polycrystalline diamond, Diam. Relat. Mater. 1 (1992) 1065–1074, https://doi.org/10.1016/0925-9635(92)90076-Z.
[13] A.M. Zaitsev, Optical Properties of Diamond, first ed., Springer Verlag Berlin-Heidelberg, 2001, ISBN 978-3-642-08585-7, https://doi.org/10.1007/978-3-662-04548-0.
[14] F.G. Brown, J. Gilland, R. Hassig, R.W. Boese, Pioneer-Venus Large Probe Infrared Radiometer (LIR) Optical System, in Proceedings Volume 0124, Modern Utilization of Infrared Technology III, 21st Annual Technical Symposium, San Diego, 1977, https://doi.org/10.1117/12.955851.
[15] K.K. de Groh, B.A. Banks, The Erosion of Diamond and Highly Oriented Pyrolytic Graphite After 1.5 Years of Space, Technical Memorandum, NASA, 2018, https://ntrs.nasa.gov/citations/20180001293 (accessed Oct 18th 2020).
[16] M.W. Geis, T.C. Wade, C.H. Wuorio, T.H. Fedynyshyn, B. Duncan, M.E. Plaut, J.O. Varghese, S.M. Warnock, S.A. Vitale, M.A. Hollis, Progress toward diamond power field-effect transistors, Phys. Status Solidi (a) 215 (2018) 1800681, https://doi.org/10.1002/pssa.201800681.
[17] R.S. Balmer, I. Friel, S.M. Woollard, C.J.H. Wort, G.A. Scarsbrook, S.E. Coe, H. El-Hajj, A. Kaiser, A. Denisenko, E. Kohn, J. Isberg, Unlocking diamond's potential as an electronic material, Philos. Trans. R. Soc. A: Math. Phys. Eng. Sci. 366 (2008), https://doi.org/10.1098/rsta.2007.2153.
[18] B.J. Baliga, Power semiconductor device figure of merit for high-frequency applications, IEEE Electron Dev. Lett. 10 (1989) 455–457, https://doi.org/10.1109/55.43098.
[19] M.E. Coltrin, R.J. Kaplar, Transport and breakdown analysis for improved figure-of-merit for AlGaN power devices, J. Appl. Phys. 121 (2017), 055706, https://doi.org/10.1063/1.4975346.
[20] A.Q. Huang, New unipolar switching power device figures of merit, IEEE Electron Dev. Lett. 25 (2004) 298–301, https://doi.org/10.1109/LED.2004.826533.
[21] R.M. Chrenko, Boron, the dominant acceptor in semiconducting diamond, Phys. Revi. B 7 (1973) 4560–4567, https://doi.org/10.1103/PhysRevB.7.4560.
[22] J.Y. Tsao, S. Chowdhury, M.A. Hollis, D. Jena, N.M. Johnson, K.A. Jones, R.J. Kaplar, S. Rajan, C.G. van de Walle, E. Bellotti, C.L. Chua, R. Collazo, M. E. Coltrin, J.A. Cooper, K.R. Evans, S. Graham, T.A. Grotjohn, E.R. Heller, M. Higashiwaki, M.S. Islam, P.W. Juodawlkis, M.A. Khan, A.D. Koehler, J.H. Leach, U.K. Mishra, R.J. Nemanich, R.C.N. Pilawa-Podgurski, J.B. Shealy, Z. Sitar, M.J. Tadjer, A.F. Witulski, M. Wraback, J.A. Simmons, Ultrawide-bandgap semiconductors: research opportunities and challenges, Adv. Electron. Mater. 4 (2018) 1600501, https://doi.org/10.1002/aelm.201600501.
[23] T. Inushima, T. Matsushita, S. Ohya, H. Shiomi, Hopping conduction via the excited states of boron in p-type diamond, Diam. Relat. Mater. 9 (2000) 1066–1070, https://doi.org/10.1016/S0925-9635(00)00226-0.
[24] T. Yokoya, T. Nakamura, T. Matsushita, T. Muro, Y. Takano, M. Nagao, T. Takenouchi, H. Kawarada, T. Oguchi, Origin of the metallic properties of heavily boron-doped superconducting diamond, Nature 438 (2005) 647–650, https://doi.org/10.1038/nature04278.
[25] F.J. Morin, J.P. Maita, Electrical properties of silicon containing arsenic and boron, Phys. Rev. 96 (1954) 28–35, https://doi.org/10.1103/PhysRev.96.28.
[26] J. Isberg, M. Gabrysch, A. Tajani, High-field electrical transport in single crystal CVD diamond diodes, Adv. Sci. Technol. 48 (2006) 73–76, https://doi.org/10.4028/www.scientific.net/AST.48.73.
[27] M. Nesladek, A. Bogdan, W. Deferme, N. Tranchant, P. Bergonzo, Charge transport in high mobility single crystal diamond, Diam. Relat. Mater. 17 (2008) 1235–1240, https://doi.org/10.1016/j.diamond.2008.03.015.
[28] I. Akimoto, Y. Handa, K. Fukai, N. Naka, High carrier mobility in ultrapure diamond measured by time-resolved cyclotron resonance, Appl. Phys. Lett. 105 (2014), 032102, https://doi.org/10.1063/1.4891039.
[29] L. Reggiani, S. Bosi, C. Canali, F. Nava, S.F. Kozlov, Hole-drift velocity in natural diamond, Phys. Rev. B 23 (1981) 3050–3057, https://doi.org/10.1103/PhysRevB.23.3050.
[30] J. Isberg, A. Lindblom, A. Tajani, D. Twitchen, Temperature dependence of hole drift mobility in high-purity single-crystal CVD diamond, Phys. Status Solidi A 202 (2005) 2194–2198, https://doi.org/10.1002/pssa.200561915.
[31] V.S. Bormashov, S.A. Tarelkin, S.G. Buga, M.S. Kuznetsov, S.A. Terentiev, A.N. Semenov, V.D. Blank, Electrical properties of the high quality boron-doped synthetic single crystal diamonds grown by the temperature gradient method, Diam. Relat. Mater. 35 (2013) 19–23, https://doi.org/10.1016/j.diamond.2013.02.011.
[32] K. Tsukioka, H. Okushi, Hall mobility and scattering mechanism of holes in boron doped homoepitaxial chemical vapor deposition diamond thin films, Jpn. J. Appl. Phys. 45 (2006) 8571, https://doi.org/10.1143/JJAP.45.8571.

[33] J. Isberg, J. Hammersberg, E. Johansson, T. Wikström, D.J. Twitchen, A.J. Whitehead, S.E. Coe, G.A. Scarsbrook, High carrier mobility in single-crystal plasma-deposited diamond, Science 297 (2002) 1670–1672, https://doi.org/10.1126/science.1074374.
[34] P.N. Volpe, J. Pernot, P. Muret, F. Omnès, High hole mobility in boron doped diamond for power device applications, Appl. Phys. Lett. 94 (2009), 092102, https://doi.org/10.1063/1.3086397.
[35] R. Peterson, M. Malakoutian, X. Xu, C. Chapin, S. Chowdhury, D.G. Senesky, Analysis of the mobility-limiting mechanisms of the two-dimensional hole gas on hydrogen-terminated diamond, Phys. Rev. B 102 (2020), 075303, https://doi.org/10.1103/PhysRevB.102.075303.
[36] J. Pernot, C. Tavares, E. Gheeraert, E. Bustarret, M. Katagiri, S. Koizumi, Hall electron mobility in diamond, Appl. Phys. Lett. 89 (2006), 122111, https://doi.org/10.1063/1.2355454.
[37] J. Pernot, P.N. Volpe, F. Omnès, P. Muret, V. Mortet, K. Haenen, T. Teraji, Hall hole mobility in boron-doped homoepitaxial diamond, Phys. Rev. B 81 (2010), 205203, https://doi.org/10.1103/PhysRevB.81.205203.
[38] G. Chicot, A. Fiori, P. Volpe, T.T. Thi, J. Gerbedoen, J. Bousquet, Electronic and physio-chemical properties of nanometric boron delta-doped diamond structures, J. Appl. Phys. 116 (2014), 083702, https://doi.org/10.1063/1.4893186.
[39] R.S. Balmer, I. Friel, S. Hepplestone, J. Isberg, M.J. Uren, M.L. Markham, Transport behavior of holes in boron delta-doped diamond structures, J. Appl. Phys. 113 (2013), 033702, https://doi.org/10.1063/1.4775814.
[40] N. Tsubouchi, M. Ogura, Y. Horino, Low-resistance p+ layer formation into diamond using heavily B ion implantation, Appl. Phys. Lett. 89 (2006), 012101, https://doi.org/10.1063/1.2219088.
[41] F. Agulló-Rueda, N. Gordillo, M.D. Ynsa, Lattice damage in 9-MeV-carbon irradiated diamond and its recovery after annealing, Carbon 123 (2017) 334–343, https://doi.org/10.1016/j.carbon.2017.07.076.
[42] J.B. Cui, J. Ristein, L. Ley, Electron affinity of the bare and hydrogen covered single crystal diamond (111) surface, Phys. Rev. Lett. 81 (1988) 429–432, https://doi.org/10.1103/PhysRevLett.81.429.
[43] R. Kalish, Doping of diamond, Carbon 37 (1999) 781–785, https://doi.org/10.1016/S0008-6223(98)00270-X.
[44] R. Kalish, Ion-implantation in diamond and diamond films: doping, damage effects and their applications, Appl. Surf. Sci. 117–118 (1997) 558–569, https://doi.org/10.1016/S0169-4332(97)80142-0.
[45] S. Koizumi, T. Teraji, H. Kanda, Phosphorus-doped chemical vapor deposition of diamond, Diam. Relat. Mater. 9 (2000) 935–940, https://doi.org/10.1016/S0925-9635(00)00217-X.
[46] J. Barjon, F. Jomard, S. Morata, Arsenic-bound excitons in diamond, Phys. Rev. B 89 (2014), 045201, https://doi.org/10.1103/PhysRevB.89.045201.
[47] M.I. Landstrass, K.V. Ravi, Resistivity of chemical vapor deposited diamond films, Appl. Phys. Lett. 55 (1989) 975, https://doi.org/10.1063/1.101694.
[48] J.I. Pankove, N.M. Johnson, Hydrogen in Semiconductors: Semiconductors and Semimetals, Elsevier, 34, 1991, pp. 1–629, ISBN: 978-0-12-752134-3, https://doi.org/10.1016/S0080-8784(08)62852-5.
[49] M.I. Landstrass, K.V. Ravi, Hydrogen passivation of electrically active defects in diamond, Appl. Phys. Lett. 55 (1989) 1391, https://doi.org/10.1063/1.101604.
[50] S. Albin, L. Watkins, Current-voltage characteristics of thin film and bulk diamond treated in hydrogen plasma, IEEE Electron Dev. Lett. 11 (1990) 159–161, https://doi.org/10.1109/55.61780.
[51] S.A. Grot, G.S. Gildenblat, C.W. Hatfield, C.R. Wronski, A.R. Badzian, R. Messier, The effect of surface treatment on the electrical properties of metal contacts to boron-doped - homoepitaxial diamond film, IEEE Electron Dev. Lett. 11 (1990) 100–102, https://doi.org/10.1109/55.46942.
[52] J. Shirafuji, T. Sugino, Electrical properties of diamond surfaces, Diam. Relat. Mater. 5 (1996) 706–713, https://doi.org/10.1016/0925-9635(95)00415-7.
[53] R.S. Gi, T. Mizumasa, Y. Akiba, Y. Hirose, T. Kurosu, M. Iida, Formation mechanism of p-type surface conductive layer on deposited diamond films, Jpn. J. Appl. Phys. 34 (1995) 5550, https://doi.org/10.1143/JJAP.34.5550.
[54] R.S. Gi, K. Tashiro, S. Tanaka, T. Fujisawa, H. Kimura, T. Kurosu, M. Iida, Hall effect measurements of surface conductive layer on undoped diamond films in NO2 and NH3 atmospheres, Jpn. J. Appl. Phys. 38 (1999) 3492, https://doi.org/10.1143/JJAP.38.3492.
[55] F. Maier, M. Riedel, B. Mantel, J. Ristein, L. Ley, Origin of surface conductivity in diamond, Phys. Rev. Lett. 85 (2000) 3472, https://doi.org/10.1103/PhysRevLett.85.3472.
[56] F.J. Himpsel, J.A. Knapp, J.A. VanVechten, D.E. Eastman, Quantum photoyield of diamond (111) – a stable negative-affinity emitter, Phys. Rev. B 20 (1979) 624–627, https://doi.org/10.1103/PhysRevB.20.624.
[57] F. Maier, J. Ristein, L. Ley, Electron affinity of plasma-hydrogenated and chemically oxidized diamond (100) surfaces, Phys. Rev. B 64 (2001), 165411, https://doi.org/10.1103/PhysRevB.64.165411.
[58] D. Takeuchi, M. Riedel, J. Ristein, L. Ley, Surface band bending and surface conductivity of hydrogenated diamond, Phys. Rev. B 68 (2003), 041304, https://doi.org/10.1103/PhysRevB.68.041304.
[59] J. Foord, C. Lau, M. Hiramatsu, R. Jackman, C.E. Nebel, P. Bergonzo, Influence of the environment on the surface conductivity of chemical vapor deposition diamond, Diam. Relat. Mater. 11 (2002) 856–860, https://doi.org/10.1016/S0925-9635(01)00689-6.
[60] M. Riedel, J. Ristein, L. Ley, The impact of ozone on the surface conductivity of single crystal diamond, Diam. Relat. Mater. 13 (2004) 746–750, https://doi.org/10.1016/j.diamond.2003.11.094.
[61] V. Chakrapani, S.C. Eaton, A.B. Anderson, M. Tabib-Azar, J.C. Angus, Studies of adsorbate-induced conductance of diamond surfaces, Electrochem. Solid-State Lett. 8 (2005) E4, https://doi.org/10.1149/1.1828351.
[62] V. Chakrapani, J.C. Angus, A.B. Anderson, S.D. Wolter, B.R. Stoner, G.U. Sumanasekera, Charge transfer equilibria between diamond and an aqueous oxygen electrochemical redox couple, Science 318 (2007) 1424–1430, https://doi.org/10.1126/science.1148841.
[63] M. Kubovic, M. Kasu, Enhancement and stabilization of hole concentration of hydrogen-terminated diamond surface using ozone adsorbates, Jpn. J. Appl. Phys. 49 (2010), 110208, https://doi.org/10.1143/JJAP.49.110208.
[64] M. Kubovic, M. Kasu, H. Kageshima, Sorption properties of NO2 gas and its strong influence on hole concentration of H-terminated diamond surfaces, Appl. Phys. Lett. 96 (2010), 052101, https://doi.org/10.1063/1.3291616.
[65] H. Sato, M. Kasu, Electronic properties of H-terminated diamond during NO2 and O3 adsorption and desorption, Diam. Relat. Mater. 24 (2012) 99–103, https://doi.org/10.1016/j.diamond.2011.12.004.
[66] H. Maeda, K. Ohtsubo, M. Irie, N. Ohya, K. Kusakabe, S. Morooka, Determination of diamond [100] and [111] growth rate and formation of highly oriented diamond film by microwave plasma-assisted chemical vapor deposition, J. Mater. Res. 10 (1995) 3115–3123, https://doi.org/10.1557/JMR.1995.3115.
[67] C.J. Chu, R.H. Hauge, J.L. Margrave, M.P. D'Evelyn, Growth kinetics of (100), (110) and (111) homoepitaxial diamond films, Appl. Phys. Lett. 61 (1992) 1393, https://doi.org/10.1063/1.107548.
[68] B. El-Dasher, J.J. Gray, J.W. Tringe, J. Biener, A.V. Hamza, Crystallographic anisotropy of wear on a polycrystalline diamond surface, Appl. Phys. Lett. 88 (2006), 241915, https://doi.org/10.1063/1.2213180.
[69] K.C. Pandey, New dimerized-chain model for the reconstruction of the diamond (111)-(2 × 1) surface, Phys. Rev. B 25 (1982) 4338–4341, https://doi.org/10.1103/PhysRevB.25.4338.
[70] R. Graupner, M. Hollering, A. Ziegler, J. Ristein, L. Ley, A. Stampfl, Dispersions of surface states on diamond (100) and (111), Phys. Rev. B 55 (1997) 10841, https://doi.org/10.1103/PhysRevB.55.10841.
[71] L.S. Pan, D.R. Kania, Diamond: Electronic Properties and Applications, Springer, Boston MA, 1995.
[72] J. Ristein, The Physics of Hydrogen-Terminated Diamond Surfaces, in: AIP Conference Proceedings, 772, 2005, 377, https://doi.org/10.1063/1.1994145.
[73] S.J. Sque, R. Jones, P.R. Briddon, Structure, electronics, and interaction of hydrogen and oxygen on diamond surfaces, Phys. Rev. Lett. B 73 (2006), 085313, https://doi.org/10.1103/PhysRevB.73.085313.
[74] F.-B. Liu, J.-D. Wang, D.-R. Chen, D.-Y. Yan, Electronic properties of hydrogen- and oxygen-terminated diamond surfaces exposed to the air, Chin. Phys. B 18 (2009) 2041, https://doi.org/10.1088/1674-1056/18/5/052.

[75] D. Petrini, K. Larsson, A theoretical study of the energetic stability and geometry of hydrogen- and oxygen-terminated diamond (100) surfaces, J. Phys. Chem. C 111 (2007) 795–801, https://doi.org/10.1021/jp063383h.
[76] M.M. Hassan, K. Larsson, Effect of surface termination on diamond (100) surface electrochemistry, J. Phys. Chem. C 118 (2014) 22995–23002, https://doi.org/10.1021/jp500685q.
[77] K. Larsson, Simulation of diamond surface chemistry: reactivity and properties, in: E. Lipatov, Some Aspects of Diamonds in Scientific Research and High Technology, IntechOpen, 2019, https://doi.org/10.5772/intechopen.86865.
[78] S.H. Yang, D.A. Drabold, J.B. Adams, Ab initio study of diamond C(100) surfaces, Phys. Rev. B 48 (1993) 5261, https://doi.org/10.1103/PhysRevB.48.5261.
[79] X.M. Zheng, P.V. Smith, The topologies of the clean and hydrogen-terminated C(100) surfaces, Surf. Sci. 256 (1991) 1–8, https://doi.org/10.1016/0039-6028(91)91194-3.
[80] B.D. Thoms, J.E. Butler, HREELS and LEED of H/C(100): The 2 × 1 monohydride dimer row reconstruction, Surf. Sci. 328 (1995) 291–301, https://doi.org/10.1016/0039-6028(95)00039-9.
[81] P.G. Lurie, J.M. Wilson, The diamond surface: I The structure of the clean surface and the interaction with gases and metals, Surf. Sci. 65 (1977) 453–475, https://doi.org/10.1016/0039-6028(77)90459-9.
[82] P.G. Lurie, J.M. Wilson, The diamond surface: II Secondary electron emission, Surf. Sci. 65 (1977) 476–498, https://doi.org/10.1016/0039-6028(77)90460-5.
[83] A.V. Hamza, G.D. Kubiak, R.H. Stulen, Hydrogen chemisorption and the structure of the diamond C(100)-(2 × 1) surface, Surf. Sci. 237 (1990) 35–52, https://doi.org/10.1016/0039-6028(90)90517-C.
[84] R.E. Thomas, R.A. Rudder, R.J. Markunas, Thermal desorption from hydrogenated and oxygenated diamond (100) surfaces, J. Vac. Sci. Technol., A 10 (1992) 2451, https://doi.org/10.1116/1.577983.
[85] J.B. Marsh, H.E. Farnsworth, Low-energy electron diffraction studies of (100) and (111) surfaces of semiconducting diamond, Surf. Sci. 1 (1964) 3–21, https://doi.org/10.1016/0039-6028(64)90014-7.
[86] B.B. Pate, The diamond surface: atomic and electronic structure, Surf. Sci. 165 (1986) 83–142, https://doi.org/10.1016/0039-6028(86)90665-5.
[87] T.E. Derry, L. Smit, J.F. van der Veen, Ion scattering determination of the atomic arrangement at polished diamond (111) surfaces before and after reconstruction, Surf. Sci. Lett. 167 (1986) 502–518, https://doi.org/10.1016/0039-6028(86)90720-X.
[88] T. Aizawa, T. Ando, M. Kamo, Y. Sato, High-resolution electron-energy-loss spectroscopic study of epitaxially grown diamond (111) and (100) surfaces, Phys. Rev. B 48 (1993) 18348–18351, https://doi.org/10.1103/PhysRevB.48.18348.
[89] J.E. Butler, R.L. Woodin, Thin film diamond growth mechanisms, Philos. Trans. R. Soc. Lond. Series A: Phys. Eng. Sci. 342 (1993) 209–224, https://doi.org/10.1098/rsta.1993.0015.
[90] T.W. Mercer, P.E. Pehrsson, Surface state transitions on the reconstructed diamond C(100) surface, Surf. Sci. 399 (1998) L327–L331, https://doi.org/10.1016/S0039-6028(97)00877-7.
[91] P.E. Pehrsson, T.W. Mercer, Oxidation of the hydrogenated diamond (100) surface, Surf. Sci. 460 (2000) 49–66, https://doi.org/10.1016/S0039-6028(00)00494-5.
[92] P.E. Pehrsson, T.W. Mercer, Oxidation of heated diamond C (100): H surface, Surf. Sci. 460 (2000) 74–90, https://doi.org/10.1016/S0039-6028(00)00495-7.
[93] P. Muret, C. Saby, Band bending, electronic affinity and density of states at several (100) surfaces of boron-doped homoepitaxial diamond thin films, Semicond. Sci. Technol. 19 (2004) 1, https://doi.org/10.1088/0268-1242/19/1/001.
[94] P. Muret, A. Traoré, A. Maréchal, D. Eon, J. Pernot, J.C. Pinero, M.P. Villar, D. Araujo, Potential barrier heights at metal on oxygen-terminated diamond interfaces, J. Appl. Phys. 118 (2015), 204505, https://doi.org/10.1063/1.4936317.
[95] T. Tsuno, T. Tomikawa, S. Shikata, Diamond(001) single-domain 2 × 1 surface grown by chemical vapor deposition, Appl. Phys. Lett. 64 (1994) 572, https://doi.org/10.1063/1.111107.
[96] M.W. Leksono, Diamond thin films grown by microwave plasma assisted chemical vapor deposition, Retrospective Theses and Dissertations, 11961, Digital Repository @, Iowa State University, 1991.
[97] J. Ristein, M. Riedel, L. Ley, Electrochemical surface transfer doping: the mechanism behind the surface conductivity of hydrogen-terminated diamond, J. Electrochem. Soc. 151 (2004) E315, https://doi.org/10.1149/1.1785797.
[98] P. Strobel, M. Riedel, J. Ristein, L. Ley, Surface transfer doping of diamond, Nature 430 (2004) 439–441, https://doi.org/10.1038/nature02751.
[99] I.L. Krainsky, V.M. Asnin, G.T. Mearini, J.A. Dayton, Negative-electron-affinity effect on the surface of chemical-vapor-deposited diamond polycrystalline films, Phys. Rev. B 53 (1996) R7650–R7653, https://doi.org/10.1103/PhysRevB.53.R7650.
[100] Y. Takagi, K. Shiraishi, M. Kasu, H. Sato, Mechanism of hole doping into hydrogen terminated diamond by the adsorption of inorganic molecule, Surf. Sci. 609 (2013) 203–206, https://doi.org/10.1016/j.susc.2012.12.015.
[101] N. Eimori, Y. Mori, A. Hatta, Electron affinity of single-crystalline chemical-vapor-deposited diamond studied by ultraviolet synchrotron radiation, Jpn. J. Appl. Phys. 33 (1994) 6312, https://doi.org/10.1143/JJAP.33.6312.
[102] D. Takeuchi, H. Kato, G.S. Ri, T. Yamada, P.R. Vinod, D. Hwang, C.E. Nebel, H. Okushi, S. Yamasaki, Direct observation of negative electron affinity in hydrogen-terminated diamond surfaces, Appl. Phys. Lett. 86 (2005), 152103, https://doi.org/10.1063/1.1900925.
[103] L. Diederich, P. Aebi, O.M. Küttel, L. Schlapbach, NEA peak of the differently terminated and oriented diamond surfaces, Surf. Sci. 424 (1999) L314–L320, https://doi.org/10.1016/S0039-6028(99)00210-1.
[104] H. Emanuel, Diamonds and Precious Stones: Their History, Value, and Distinguishing Characteristics, second ed., John Camden Hotten, 1867.
[105] E.C. Sowa, G.D. Kubiak, R.H. Stulen, Structural analysis of the diamond C(111)-(2×1) reconstructed surface by low-energy electron diffraction, J. Vac. Sci. Technol., A 6 (1988) 832, https://doi.org/10.1116/1.575078.
[106] J.P. Goss, R. Jones, M.I. Heggie, C.P. Ewels, P.R. Briddon, S.O. Berg, Theory of hydrogen in diamond, Phys. Rev. B 15 (2002) R551, https://doi.org/10.1088/0953-8984/15/17/201.
[107] J.C. Angus, A. Argoitia, R. Gat, Z. Li, M. Sunkara, L. Wang, Y. Wang, Chemical vapour deposition of diamond, in: A.H. Lettington, J.W. Steeds, Thin Film Diamond. Springer, Dordrecht, 1994, https://doi.org/10.1007/978-94-011-0725-9_1.
[108] H. Kawarada, Hydrogen-terminated diamond surfaces and interfaces, Surf. Sci. Rep. 26 (1996) 205–206, https://doi.org/10.1016/S0167-5729(97)80002-7.
[109] S. Koizumi, C. Nebel, M. Nesladek, Physics and Applications of CVD Diamond, Wiley-VCH Verlag GmbH & Co, KGaA, 2008.
[110] M. Kamo, S. Matsumoto, Y. Sato, N. Setaka, Method for synthesizing diamond, National Institute for Research in Inorganic Material, United States Patent US4434188A, 1984.
[111] P.K. Bachmann, D. Leers, H. Lydtin, Towards a general concept of diamond chemical vapour deposition, Diam. Relat. Mater. 1 (1991) 1–12, https://doi.org/10.1016/0925-9635(91)90005-U.
[112] B. Koslowski, S. Strobel, M.J. Wenig, P. Ziemann, Roughness transitions of diamond(100) induced by hydrogen-plasma treatment, Appl. Phys. A 66 (1998) 1159–1163, https://doi.org/10.1007/s003390051318.
[113] A. Gaisinskaya, R. Edrei, A. Hoffman, Y. Feldheim, Morphological evolution of polished single crystal (100) diamond surface exposed to microwave hydrogen plasma, Diam. Relat. Mater. 18 (2009) 1466–1473, https://doi.org/10.1016/j.diamond.2009.09.014.
[114] K.G. Crawford, A. Tallaire, X. Li, D.A. Macdonald, D. Qi, D.A.J. Moran, The role of hydrogen plasma power on surface roughness and carrier transport in transfer-doped H-diamond, Diam. Relat. Mater. 84 (2018) 48–54, https://doi.org/10.1016/j.diamond.2018.03.005.
[115] A. Tallaire, T. Ouisse, A. Lantreibecq, R. Cours, M. Legros, H. Bensalah, J. Barjon, V. Mille, J.A.O. Brinza, J. Barjon, Identification of dislocations in synthetic chemically vapor deposited diamond single crystals, Crystal Growth Des. 16 (2016) 2741–2746, https://doi.org/10.1021/acs.cgd.6b00053.
[116] B. Baral, S.S.M. Chan, R.B. Jackman, Cleaning thin-film diamond surfaces for device fabrication: an auger electron spectroscopic study, J. Vac. Sci. Technol., A 14 (1996) 2303, https://doi.org/10.1116/1.580063.
[117] J.J. Lander, J. Morrison, Low energy electron diffraction study of the (111) diamond surface, Surf. Sci. 4 (1966) 241–246, https://doi.org/10.1016/0039-6028(66)90004-5.

[118] W. Chen, D. Qi, X. Gao, A.T.S. Wee, Surface transfer doping of semiconductors, Prog. Surf. Sci. 84 (2009) 729–1321, https://doi.org/10.1016/j.progsurf.2009.06.002.
[119] S. Sangtawesin, B.L. Dwyer, S. Srinivasan, J.J. Allred, L.V.H. Rodgers, K.D. Greve, A. Stacey, N. Dontschuk, K.M. O'Donnell, D. Hu, D.A. Evans, C. Jaye, D. A. Fischer, M.L. Markham, D.J. Twitchen, H. Park, M.D. Lukin, N.P. de Leon, Origins of diamond surface noise probed by correlating single-spin measurements with surface spectroscopy, Phys. Rev. X 9 (2019) 03152, https://doi.org/10.1103/PhysRevX.9.031052.
[120] S. Skokov, C.S. Carmer, B. Weiner, M. Frenklach, Reconstruction of (100) diamond surfaces using molecular diamond with combined quantum and empirical forces, Phys. Rev. B 49 (1994) 5662–5671, https://doi.org/10.1103/PhysRevB.49.5662.
[121] J. Navas, D. Araujob, J. Pinero, A. Sánchez-Coronillac, E. Blanco, P. Villar, R. Alcántaraa, J. Montserrat, M. Florentin, D. Eon, J. Pernot, Oxygen termination of homoepitaxial diamond surface by ozone and chemical methods: an experimental and theoretical perspective, Appl. Surf. Sci. 422 (2018) 408–418, https://doi.org/10.1016/j.apsusc.2017.10.065.
[122] M.J. Rutter, J. Robertson, Ab initio calculation of electron affinities of diamond surfaces, Phys. Rev. B 10 (1998) 330–333, https://doi.org/10.1016/S0927-0256(97)00104-3.
[123] J. Ristein, Surface transfer doping of diamond, J. Phys. D Appl. Phys. 39 (2006) R71, https://doi.org/10.1088/0022-3727/39/4/R01.
[124] P. John, N. Polwart, C.E. Troupe, J.I. Wilson, The oxidation of diamond: the geometry and stretching frequency of carbonyl on the (100) surface, J. Am. Chem. Soc. 125 (2003) 6600–6601, https://doi.org/10.1021/ja029586a.
[125] M. Jiang, H. Yu, X. Li, S. Lu, X. Hu, Thermal oxidation induced high electrochemical activity of boron-doped nanocrystalline diamond electrodes, Electrochim. Acta 258 (2017) 61–70, https://doi.org/10.1016/j.electacta.2017.10.008.
[126] K. Ueda, K. Kawamoto, H. Asano, High-temperature and high-voltage characteristics of Cu/diamond Schottky diodes, Diam. Relat. Mater. 57 (2015) 28–31, https://doi.org/10.1016/j.diamond.2015.03.006.
[127] S. Ghodbane, T. Haensel, Y. Coffinier, S. Szunerits, D. Steinmuller-Nethl, R. Boukherroub, S.I. Ahmed, J.A. Schaefer, HREELS investigation of the surfaces of nanocrystalline diamond films oxidized by different processes, Langmuir 26 (2010) 18798–18805, https://doi.org/10.1021/la1032652.
[128] K. O'Donnell, M. Edmonds, J. Ristein, A. Tadich, L. Thomsen, Q.-H. Wu, C. Pakes, L. Ley, Diamond surfaces with air-stable negative electron affinity and giant electron yield enhancement, Adv. Funct. Mater. 23 (2013) 5608–5614, https://doi.org/10.1002/adfm.201301424.
[129] P. Baumann, R. Nemanich, Surface cleaning, electronic states and electron affinity of diamond (100), (111) and (110) surfaces, Surf. Sci. 409 (1998) 320–335, https://doi.org/10.1016/S0039-6028(98)00259-3.
[130] A. Denisenko, C. Pietzka, A. Romanyuk, H. El-Hajj, E. Kohn, The electronic surface barrier of boron-doped diamond by anodic oxidation, J. Appl. Phys. 103 (2008), 014904, https://doi.org/10.1063/1.2827481.
[131] H. Notsu, I. Yagi, T. Tatsuma, D.A. Tryk, A. Fujishima, Surface carbonyl groups on oxidized diamond electrodes, J. Electroanal. Chem. 492 (2000) 31–37, https://doi.org/10.1016/S0022-0728(00)00254-0.
[132] P. Pehrsson, The acid-cleaned CVD diamond surface, in: Proceedings of Third International Symposium of Diamond Materials, 183rd Meeting of the Electrochemical Society, Honolulu, 1993.
[133] J. Raymakers, K. Haenen, W. Maes, Diamond surface functionalization: from gemstone to photoelectrochemical applications, J. Mater. Chem. C 7 (2019) 10134–10165, https://doi.org/10.1039/C9TC03381E.
[134] M.C. James, P.W. May, N.L. Allan, Ab initio study of negative electron affinity from light metals on the oxygen-terminated diamond (1 1 1) surface, J. Phys.: Condens. Matter 31 (2019), 295002, https://doi.org/10.1088/1361-648X/ab18ef.
[135] K.M. O'Donnell, T.L. Martin, N.A. Fox, D. Cherns, Ab initio investigation of lithium on the diamond C(100) surface, Phys. Rev. B 82 (2010), 115303, https://doi.org/10.1103/PhysRevB.82.115303.
[136] K.M. O'Donnell, T.L. Martin, N.L. Allan, Light metals on oxygen-terminated diamond (100): structure and electronic properties, Chem. Mater. 27 (2015) 1306–1315, https://doi.org/10.1021/cm5043155.
[137] K.M. O'Donnell, M.T. Edmonds, A. Tadich, L. Thomsen, A. Stacey, A. Schenk, C.I. Pakes, L. Ley, Extremely high negative electron affinity of diamond via magnesium adsorption, Phys. Rev. B 92 (2015), 035303, https://doi.org/10.1103/PhysRevB.92.035303.
[138] K.J. Rietwyk, S.L. Wong, L. Cao, K.M. O'Donnell, L. Ley, A.T.S. Wee, C.I. Pakes, Work function and electron affinity of the fluorine-terminated (100) diamond surface, Appl. Phys. Lett. 102 (2013), 091604, https://doi.org/10.1063/1.4793999.
[139] A. Freedman, C.D. Stinespring, Fluorination of diamond (100) by atomic and molecular beams, Appl. Phys. Lett. 57 (1990) 1194, https://doi.org/10.1063/1.104097.
[140] A. Freedman, Halogenation of diamond (100) and (111) surfaces by atomic beams, J. Appl. Phys. 75 (1994) 3112, https://doi.org/10.1063/1.356163.
[141] J.S. Foord, N.K. Singh, R.B. Jackman, Reactions of xenon difluoride and atomic hydrogen at chemical vapour deposited diamond surfaces, Surf. Sci. 488 (2001) 335–345, https://doi.org/10.1016/S0039-6028(01)01142-6.
[142] S. Durrant, V. Baranauskas, A.C. Peterlevitz, S.G. Castro, R. Landers, M.A. Bica de Moraes, Characterization of diamond fluorinated by glow discharge plasma treatment, Diam. Relat. Mater. 10 (2001) 490–495, https://doi.org/10.1016/S0925-9635(00)00534-3.
[143] S. Ferro, A.D. Battisti, The 5-V window of polarizability of fluorinated diamond electrodes in aqueous solutions, Anal. Chem. 75 (2003) 7040–7042, https://doi.org/10.1021/ac034717r.
[144] G. Siné, L. Ouattara, M. Panizza, Ch. Comninellis, Electrochemical behavior of fluorinated boron-doped diamond, Electrochem. Solid-State Lett. 6 (2003) D9, https://doi.org/10.1149/1.1592914.
[145] H. Shiomi, Reactive ion etching of diamond in O2 and CF4 plasma, and fabrication of porous diamond for field emitter cathodes, Jpn. J. Appl. Phys. 36 (1997) 7745, https://doi.org/10.1143/JJAP.36.7745.
[146] T. Kondo, H. Ito, K. Kusakabe, K. Ohkawa, K. Honda, Y. Einaga, A. Fujishima, T. Kawai, Characterization and electrochemical properties of CF4 plasma-treated boron-doped diamond surfaces, Diam. Relat. Mater. 17 (2008) 48–54, https://doi.org/10.1016/j.diamond.2007.10.009.
[147] T. Nakamura, T. Ohana, M. Hasegawa, K. Tsugawa, M. Suzuki, M. Ishihara, A. Tanaka, Y. Koga, Chemical modification of diamond surfaces with fluorine-containing functionalities, New Diamond Front. Carbon Technol. 15 (2005).
[148] S. Cui, E.L. Hu, Increased negatively charged nitrogen-vacancy centres in fluorinated diamond, Appl. Phys. Lett. 103 (2013), 051603, https://doi.org/10.1063/1.4817651.
[149] C. Popov, W. Kulisch, S. Bliznakov, G. Ceccone, D. Gilliland, L. Sirghi, F. Rossi, Surface modification of nanocrystalline diamond/amorphous carbon composite films, Diam. Relat. Mater. 17 (2008) 1229–1234, https://doi.org/10.1016/j.diamond.2008.01.078.
[150] W. Kulisch, A. Voss, D. Merker, J.P. Reithmaier, R. Merz, M. Kopnarski, C. Popov, Plasma surface fluorination of ultrananocrystalline diamond films, Surf. Coat. Technol. 302 (2016) 448–453, https://doi.org/10.1016/j.surfcoat.2016.06.029.
[151] A. Krueger, Fluorination of diamond materials for the control of surface properties, in: MRS Fall Meeting, Boston, 2019.
[152] L. Mayrhofer, G. Moras, N. Mulakaluri, S. Rajagopalan, P.A. Stevens, M. Moseler, Fluorine-terminated diamond surfaces as dense dipole lattices: the electrostatic origin of polar hydrophobicity, J. Am. Chem. Soc. 138 (2016) 4018–4028, https://doi.org/10.1021/jacs.5b04073.
[153] F.G. Sen, Y. Qi, A.T. Alpas, Surface stability and electronic structure of hydrogen and fluorine terminated diamond surfaces: a first principles investigation, J. Mater. Res. 24 (2009) 2461–2470, https://doi.org/10.1557/jmr.2009.0309.
[154] M. Mertens, M. Mohr, K. Brühne, H.J. Fecht, M. Lojkowski, W. Swieszkowski, W. Lojkowski, Patterned hydrophobic and hydrophilic surfaces of ultra-smooth nanocrystalline diamond layers, Appl. Surf. Sci. 390 (2016) 526–530, https://doi.org/10.1016/j.apsusc.2016.08.130.
[155] C. Yamaguchi, K. Natsui, S. Iizuka, Y. Tateyama, Y. Einaga, Electrochemical properties of fluorinated boron-doped diamond electrodes via fluorine-containing plasma treatment, Phys. Chem. Chem. Phys. 21 (2019) 13788–13794, https://doi.org/10.1039/C8CP07402J.
[156] S. Ferro, A. de Battisti, Physicochemical properties of fluorinated diamond electrodes, J. Phys. Chem. B 107 (2003) 7567–7573, https://doi.org/10.1021/jp0274280.
[157] K.G. Crawford, D. Qi, J. McGlynn, T.G. Ivanov, P.B. Shah, J. Weil, A. Tallaire, A.Y. Ganin, D.A.J. Moran, Thermally stable high performance transfer doping of diamond using transition metal oxides, Sci. Rep. 8 (2018) 3342, https://doi.org/10.1038/s41598-018-21579-4.

[158] O.A. Williams, R.B. Jackman, Surface conductivity on hydrogen terminated diamond, Semicond. Sci. Technol. 18 (2003) S34, https://doi.org/10.1088/0268-1242/18/3/305.

[159] P. Strobel, M. Riedel, J. Ristein, L. Ley, O. Boltalina, Surface transfer doping of diamond by fullerene, Diam. Relat. Mater. 14 (2005) 451–458, https://doi.org/10.1016/j.diamond.2004.12.051.

[160] P. Strobel, J. Ristein, L. Ley, K. Seppelt, I.V. Goldt, O. Boltalina, Surface conductivity induced by fullerenes on diamond: passivation and thermal stability, Diam. Relat. Mater. 15 (2006) 720–724, https://doi.org/10.1016/j.diamond.2005.10.034.

[161] D. Qi, W. Chen, X. Gao, L. Wang, S. Chen, K.P. Loh, A.T.S. Wee, Surface transfer doping of diamond (100) by tetrafluoro-tetracyanoquinodimethane, J. Am. Chem. Soc. 129 (2007) 8084–8085, https://doi.org/10.1021/ja072133r.

[162] H. Sato, M. Kasu, Maximum hole concentration for Hydrogen-terminated diamond surfaces with various surface orientations obtained by exposure to highly concentrated NO_2, Diam. Relat. Mater. 31 (2013) 47–49, https://doi.org/10.1016/j.diamond.2012.10.007.

[163] K. Hirama, H. Sato, Y. Harada, H. Yamamoto, M. Kasu, Diamond field-effect transistors with 1.3 A/mm drain current density by Al2O3 passivation layer, Jpn. J. Appl. Phys. 51 (2012) 090112, https://doi.org/10.1143/JJAP.51.090112.

[164] M. Kasu, Diamond field-effect transistors for RF power electronics: novel NO2 hole doping and low temperature deposited Al2O3 passivation, J. Appl. Phys. 56 (2017) 01AA01, https://doi.org/10.7567/JJAP.56.01AA01.

[165] K. Hirama, H. Takayanagi, S. Yamauchi, J.H. Yang, H. Kawarada, H. Umezawa, Spontaneous polarization model for surface orientation dependence of diamond hole accumulation layer and its transistor performance, Appl. Phys. Lett. 92 (2008), 112107, https://doi.org/10.1063/1.2889947.

[166] H. Kawarada, High-current metal oxide semiconductor field-effect transistors on H-terminated diamond surfaces and their high-frequency operation, Jpn. J. Appl. Phys. 51 (2012), 090111, https://doi.org/10.1143/JJAP.51.090111.

[167] M.W. Geis, T.H. Fedynyshyn, M.E. Plaut, T.C. Wade, C.H. Wuorio, S.A. Vitale, J.O. Varghese, T.A. Grotjohn, R.J. Nemanich, M.A. Hollis, Chemical and semiconducting properties of NO_2-activated H-terminated diamond, Diam. Relat. Mater. 84 (2018) 86–94, https://doi.org/10.1016/j.diamond.2018.03.002.

[168] M. Kasu, H. Sato, K. Hirama, Thermal stabilization of hole channel on H-terminated diamond surface by using atomic-layer-deposited Al_2O_3 overlayer and its electric properties, Appl. Phys Express 5 (2012), 025701, https://doi.org/10.1143/APEX.5.025701.

[169] S.A.O. Russell, L. Cao, D. Qi, A. Tallaire, K.G. Crawford, A.T.S. Wee, D.A.J. Moran, Surface transfer doping of diamond by MoO_3: a combined spectroscopic and Hall measurement study, Appl. Phys. Lett. 103 (2013), 202112, https://doi.org/10.1063/1.4832455.

[170] M. Tordjman, C. Saguy, A. Bolker, R. Kalish, Superior surface transfer doping of diamond with MoO_3, Adv. Mater. Interfaces 1 (2014) 1300155, https://doi.org/10.1002/admi.201300155.

[171] C. Verona, W. Ciccognani, S. Colangeli, E. Limiti, M. Marinelli, G. Verona-Rinati, Comparative investigation of surface transfer doping of hydrogen terminated diamondby high electron affinity insulators, J. Appl. Phys. 120 (2016), 025104, https://doi.org/10.1063/1.4955469.

[172] K.G. Crawford, L. Cao, D. Qi, A. Tallaire, E. Limiti, C. Verona, A.T.S. Wee, D.A.J. Moran, Enhanced surface transfer doping of diamond by V_2O_5 with improved thermal stability, Appl. Phys. Lett. 108 (2016), 042103, https://doi.org/10.1063/1.4940749.

[173] M. Tordjman, K. Weinfeld, R. Kalish, Boosting surface charge-transfer doping efficiency and robustness of diamond with WO_3 and ReO_3, Appl. Phys. Lett. 111 (2017), 111601, https://doi.org/10.1063/1.4986339.

[174] Y. Xiang, M. Jiang, H. Xiao, K. Xing, X. Peng, S. Zhang, D. Qi, A DFT study of the surface charge transfer doping of diamond by chromium trioxide, Appl. Surf. Sci. 496 (2019), 143604, https://doi.org/10.1016/j.apsusc.2019.143604.

[175] H. Irfan, Y. Ding, D.Y. Gao, J. Kim, F. Subbiah, So, Energy level evolution of molybdenum trioxide interlayer between indium tin oxide and organic semiconductor, Appl. Phys. Lett. 96 (2010), 073304, https://doi.org/10.1063/1.3309600.

[176] J. McGhee, V.P. Georgiev, Simulation study of surface transfer doping of hydrogenated diamond by MoO_3 and V_2O_5 metal oxides, Micromachines 11 (2020) 433, https://doi.org/10.3390/mi11040433.

[177] K.G. Crawford, J.D. Weil, P.B. Shah, D.A. Ruzmetov, M.R. Neupane, K. Kingkeo, A.G. Birdwell, T.G. Ivanov, Diamond field-effect transistors with V_2O_5-induced transfer doping: scaling to 50-nm gate length, IEEE Trans. Electron Devices 67 (2020) 2270–2275, https://doi.org/10.1109/TED.2020.2989736.

[178] D.A. Macdonald, K.G. Crawford, A. Tallaire, R. Issaoui, D.A.J. Moran, Performance enhancement of Al_2O_3/H-diamond MOSFETs utilizing vacuum annealing and V_2O_5 as a surface electron acceptor, IEEE Electron Dev. Lett. 39 (2018) 1354–1357, https://doi.org/10.1109/LED.2018.2856920.

[179] M.W. Geis, J.O. Varghese, M.A. Hollis, Y. Yichen, R.J. Nemanich, C.H. Wuorio, X. Zhang, G.W. Turner, S.M. Warnock, S.A. Vitale, R.J. Molnar, T. Osadchy, B. Zhang, Stable, low-resistance, 1.5 to 3.5 kΩ sq-1, diamond surface conduction with a mixed metal-oxide protective film, Diamond Related Mater. 106 (2020) 107819, https://doi.org/10.1016/j.diamond.2020.107819.

[180] D. Oing, M. Geller, A. Lorke, N. Wöhrl, Tunable carrier density and high mobility of two-dimensional hole gases on diamond: the role of oxygen adsorption and surface roughness, Diam. Relat. Mater. 97 (2019), 107450, https://doi.org/10.1016/j.diamond.2019.107450.

[181] K. Xing, D.L. Creedon, S.A. Yianni, G. Akhgar, L. Zhang, L. Ley, J.C. McCallum, D. Qi, C.I. Pakes, Strong spin-orbit interaction induced by transition metal oxides at the surface of hydrogen-terminated diamond, Carbon 164 (2020) 244–250, https://doi.org/10.1016/j.carbon.2020.03.047.

[182] M. Meenakshi, R. Sivakumar, P. Perumal, C. Sanjeeviraja, Studies on electrochromic properties of RF sputtered vanadium oxide: tungsten oxide thin films, Mater. Today:. Proc. 3 (2016) S30–S39, https://doi.org/10.1016/j.matpr.2016.01.005.

[183] C. Verona, M. Benetti, D. Cannatà, W. Ciccognani, S. Colangeli, F.D. Pietrantonio, E. Limiti, M. Marinelli, G. Verona-Rinati, Stability of H-terminated diamond MOSFETs with V_2O_5/Al_2O_3 as gate insulator, IEEE Electron Device Lett. 40 (2019) 765–768, https://doi.org/10.1109/LED.2019.2903578.

[184] A. Hiraiwa, A. Daicho, S. Kurihara, Y. Yokoyama, H. Kawarada, Refractory two-dimensional hole gas on hydrogenated diamond surface, J. Appl. Phys. 112 (2012), 124504, https://doi.org/10.1063/1.4769404.

[185] A. Daicho, T. Saito, S. Kurihara, A. Hiraiwa, H. Kawarada, High-reliability passivation of hydrogen-terminated diamond surface by atomic layerdeposition of Al_2O_3, J. Appl. Phys. 115 (2014), 223711, https://doi.org/10.1063/1.4881524.

[186] A. Hiraiwa, T. Saito, D. Matsumura, H. Kawarada, Isotope analysis of diamond-surface passivation effect of high-temperature H2O-grownatomic layer deposition-Al2O3 films, J. Appl. Phys. 117 (2015), 215304, https://doi.org/10.1063/1.4921824.

[187] Y. Yang, F.A. Koeck, M. Dutta, X. Wang, S. Chowdhury, R.J. Nemanich, Al_2O_3 dielectric layers on H-terminated diamond: controlling surface conductivity, J. Appl. Phys. 122 (2017), 155304, https://doi.org/10.1063/1.4985808.

[188] H. Kawarada, T. Yamada, D. Xu, Y. Kitabayashi, M. Shibata, D. Matsumura, M. Kobayashi, T. Saito, T. Kudo, M. Inaba, A. Hiraiwa, Diamond MOSFETs using 2D hole gas with 1700V breakdown voltage, in: Proceedings of the 2016 28th International Symposium on Power Semiconductor Devices and ICs, Prague, Czech Republic, 2016, https://doi.org/10.1109/ISPSD.2016.7520883.

[189] K. Matsunaga, T. Tanaka, T. Yamamoto, Y. Ikuhara, First-principles calculations of intrinsic defects in Al_2O_3, Phys. Rev. B 68 (2003), 085110, https://doi.org/10.1103/PhysRevB.68.085110.

[190] Z. Ren, D. Lv, J. Xu, J. Zhang, J. Zhang, K. Su, C. Zhang, Y. Hao, High temperature (300 °C) ALD grown Al_2O_3 on hydrogen terminated diamond: band offset and electrical properties of the MOSFETs, Appl. Phys. Lett. 116 (2019), 013503, https://doi.org/10.1063/1.5126359.

[191] Y. Yang, T. Sun, J. Shammas, M. Kaur, M. Hao, R.J. Nemanich, Electron affinity of cubic boron nitride terminated with vanadium oxide, J. Appl. Phys. 118 (2015), 165310, https://doi.org/10.1063/1.4934508.

[192] J. Yang, B.S. Eller, M. Kaur, R.J. Nemanich, Characterization of plasma-enhanced atomic layer deposition of Al_2O_3 using dimethylaluminum isopropoxide, J. Vac. Sci. Technol., A 32 (2014), 021514, https://doi.org/10.1116/1.4866378.

[193] K. Wu, Y. Zhang, J. Ma, Z. Fu, C. Chen, Two-dimensional hole gas formed at diamond surface by Al_2O_3/diamond interface engineering, Diam. Relat. Mater. 105 (2020), 107807, https://doi.org/10.1016/j.diamond.2020.107807.

[194] S.K.R. Pillai, C.R.K. Vijayachandra, N.C.G. Ramachandran, A comparative study on the acidic properties and catalytic activities of TiO2, SiO2, Al2O3, SiO2–Al2O3, SiO2–TiO2, Al2O3–TiO2, and TiO2–SiO2–Al2O3, Bull. Chem. Soc. Jpn. 64 (1991) 1920–1925, https://doi.org/10.1246/bcsj.64.1920.

[195] S. Atsushi, W. Yenni, K. Yuichi, H. Tadashi, M. Yuichi, Determination of the acid strength of binary oxide catalysts using temperature-programmed desorption of pyridine, Bull. Chem. Soc. Jpn. 70 (1997) 1311–1317, https://doi.org/10.1246/bcsj.70.1311.

[196] H. Kawakami, S. Yoshida, T. Yonezawa, A quantum chemical approach to the generation of solid acidity in composite metal oxides, J. Chem. Soc., Faraday Trans. 2 80 (1984) 205–217, https://doi.org/10.1039/F29848000205.
[197] H.J. Looi, R.B. Jackman, J.S. Foord, High carrier mobility in polycrystalline thin film diamond, Appl. Phys. Lett. 72 (1998) 353, https://doi.org/10.1063/1.120734.
[198] B. Rezek, H. Watanabe, C.E. Nebel, High carrier mobility on hydrogen terminated [100] diamond surfaces, Appl. Phys. Lett. 88 (2006), 042110, https://doi.org/10.1063/1.2168497.
[199] C.E. Nebel, B. Rezek, A. Zrenner, 2D-hole accumulation layer in hydrogen terminated diamond, Phys. Status Solidi (a) 201 (2004) 2432–2438, https://doi.org/10.1002/pssa.200405185.
[200] P.W. Anderson, Absence of diffusion in certain random lattices, Phys. Rev. 109 (1958) 1492, https://doi.org/10.1103/PhysRev.109.1492.
[201] N.F. Mott, Electrons in disordered structures, Adv. Phys. 16 (1967) 49–144, https://doi.org/10.1080/00018736700101265.
[202] N.F. Mott, M. Pepper, S. Pollitt, R.H. Wallis, C.J. Adkins, The Anderson transition, Proc. R. Soc. A 345 (1975) 169–205, https://doi.org/10.1098/rspa.1975.0131.
[203] N. Mott, The mobility edge since 1967, J. Phys. C: Solid State Phys. 20 (1987) 3075, https://doi.org/10.1088/0022-3719/20/21/008.
[204] J.A. Garrido, T. Heimbeck, M. Stutzmann, Temperature-dependent transport properties of hydrogen-induced diamond surface conductive channels, Phys. Rev. B 71 (2005), 245310, https://doi.org/10.1103/PhysRevB.71.245310.
[205] E. Arnold, Disorder-induced carrier localization in silicon surface inversion layers, Appl. Phys. Lett. 25 (1974) 705, https://doi.org/10.1063/1.1655369.
[206] E. Arnold, Conduction mechanisms in bandtails at the Si-SiO_2 interface, Surf. Sci. 58 (1976) 60–70, https://doi.org/10.1016/0039-6028(76)90113-8.
[207] E. Arnold, Comment on the frequency dependence of electron conductivity in the silicon inversion layer in the metallic and localized regimes, Phys. Rev. B 17 (1978) 4111–4113, https://doi.org/10.1103/PhysRevB.17.4111.
[208] M. Willatzen, M. Cardona, N.E. Christensen, Linear muffin-tin-orbital and k·p calculations of effective masses and band structure of semiconducting diamond, Phys. Rev. B 50 (1994) 18054, https://doi.org/10.1103/PhysRevB.50.18054.
[209] G. Daligou, J. Pernot, 2D hole gas mobility at diamond/insulator interface, Appl. Phys. Lett. 116 (2020), 162105, https://doi.org/10.1063/5.0002768.
[210] Y. Li, J.-F. Zhang, G.-P. Liu, Z.-Y. Ren, J.-C. Zhang, Y. Hao, Mobility of two-dimensional hole gas in H-terminated diamond, Phys. Status Solidi RRL 12 (2018) 1700401, https://doi.org/10.1002/pssr.201700401.
[211] Y. Sasama, K. Komatsu, S. Moriyama, M. Imura, T. Teraji, K. Watanabe, T. Taniguchi, T. Uchihashi, Y. Takahide, High-mobility diamond field effect transistor with a monocrystalline h-BN gate dielectric, APL Mater. 6 (2018), 111105, https://doi.org/10.1063/1.5055812.
[212] Y. Sasama, T. Kageura, K. Komatsu, S. Moriyama, J. Inoue, M. Imura, K. Watanabe, T. Taniguchi, T. Uchihashi, Y. Takahide, Charge-carrier mobility in hydrogen-terminated diamond field-effect transistors, J. Appl. Phys. 127 (2020), 185707, https://doi.org/10.1063/5.0001868.
[213] K. Xing, Y. Xiang, M. Jiang, D.L. Creedon, G. Akhgar, S.A. Yianni, H. Xiao, L. Ley, A. Stacey, J.C. McCallum, S. Zhuiykov, C.I. Pakes, D. Qi, MoO_3 induces p-type surface conductivity by surface transfer doping in diamond, Appl. Surf. Sci. 509 (2020), 144890, https://doi.org/10.1016/j.apsusc.2019.144890.
[214] K. Xing, S. Zhang, A. Tsai, H. Xiao, D.L. Creedon, S.A. Yianni, J.C. McCallum, C.I. Pakes, D. Qi, High-electron-affinity oxide V_2O_5 enhances surface transfer doping on hydrogen-terminated diamond, Diam. Relat. Mater. 108 (2020), 107865, https://doi.org/10.1016/j.diamond.2020.107865.
[215] T. Wade, M.W. Geis, T.H. Fedynyshyn, S.A. Vitale, J.O. Varghese, D.M. Lennon, T.A. Grotjohn, R.J. Nemanich, M.A. Hollis, Effect of surface roughness and H–termination chemistry on diamond's semiconducting surface conductance, Diam. Relat. Mater. 76 (2017) 79–85, https://doi.org/10.1016/j.diamond.2017.04.012.
[216] G. Akhgar, O. Klochan, L.H. Willems van Beveren, M.T. Edmonds, F. Maier, B.J. Spencer, J.C. McCallum, L. Ley, A.R. Hamilton, C.I. Pakes, Strong and tunable spin-orbit coupling in a two-dimensional hole gas in ionic-liquid gated diamond devices, Nano Lett. 16 (2016) 3768–3773, https://doi.org/10.1021/acs.nanolett.6b01155.
[217] G. Akhgar, D.L. Creedon, L.H. Willems van Beveren, A. Stacey, D.I. Hoxley, J.C. McCallum, L. Ley, A.R. Hamilton, C.I. Pakes, G-factor and well width variations for the two-dimensional hole gas in surface conducting diamond, Appl. Phys. Lett. 112 (2018), 042102, https://doi.org/10.1063/1.5010800.
[218] M.T. Edmonds, C.I. Pakes, L. Ley, Self-consistent solution of the Schrödinger-Poisson equations for hydrogen-terminated diamond, Phys. Rev. B 81 (2010), 085314, https://doi.org/10.1103/PhysRevB.81.085314.
[219] L. Gan, E. Baskin, C. Saguy, R. Kalish, Quantization of 2D hole gas in conductive hydrogenated diamond surfaces observed by electron field emission, Phys. Rev. Lett. 96 (2006), 196808, https://doi.org/10.1103/PhysRevLett.96.196808.
[220] T. Yamada, S. Shikata, C.E. Nebel, Resonant field emission from two dimensional intrinsic diamond, J. Appl. Phys. 107 (2010), 013705, https://doi.org/10.1063/1.3277010.
[221] C.E. Nebel, B. Rezek, A. Zrenner, Electronic properties of the 2D-hole accumulation layer on hydrogen terminated diamond, Diam. Relat. Mater. 13 (2004) 2031–2036, https://doi.org/10.1016/j.diamond.2004.06.028.
[222] F. Herman, C.D. Kuglin, K.F. Cuff, R.L. Kortum, Relativistic corrections to the band structure of tetrahedrally bonded semiconductors, Phys. Rev. Lett. 11 (1963) 541, https://doi.org/10.1103/PhysRevLett.11.541.
[223] G. Dresselhaus, Spin-orbit coupling effects in zinc blende structures, Phys. Rev. J. Arch. 100 (1955) 580, https://doi.org/10.1103/PhysRev.100.580.
[224] G. Bihlmayer, O. Rader, R. Winkler, Focus on the Rashba effect, New J. Phys. 17 (2015), 050202, https://doi.org/10.1088/1367-2630/17/5/050202.
[225] M.T. Edmonds, L.H. Willems van Beveren, O. Klochan, J. Cervenka, K. Ganesan, S. Prawer, L. Ley, A.R. Hamilton, C.I. Pakes, Spin-orbit interaction in a two-dimensional hole gas at the surface of hydrogenated diamond, Nano Lett. 15 (2015) 16–20, https://doi.org/10.1021/nl502081y.
[226] S. Hikami, A.I. Larkin, Y. Nagaoka, Spin-orbit interaction and magnetoresistance in the two dimensional random system, Progr. Theoret. Phys. 63 (1980) 707–710, https://doi.org/10.1143/PTP.63.707.
[227] R. Winkler, D. Culcer, S. Papadakis, B. Habib, M. Shayegan, Semicond. Sci. Technol. 23 (2008), 114017, https://doi.org/10.1088/0268-1242/23/11/114017.
[228] R. Moriya, K. Sawano, Y. Hoshi, S. Masubuchi, Y. Shiraki, A. Wild, C. Neumann, G. Abstreiter, D. Bougeard, T. Koga, T. Machida, Cubic Rashba spin-orbit interaction of a two-dimensional hole gas in a strained-Ge/SiGe quantum well, Phys. Rev. Lett. 113 (2014), 086601, https://doi.org/10.1103/PhysRevLett.113.086601.
[229] C. Morrison, P. Wiśniewski, S.D. Rhead, J. Foronda, D.R. Leadley, M. Myronov, Appl. Phys. Lett. 105 (2014), 182401, https://doi.org/10.1063/1.4901107.
[230] K. Xing, A. Tsai, D.L. Creedon, S.A. Yianni, J.C. McCallum, L. Ley, D. Qi, C.I. Pakes, Engineering the spin–orbit interaction in surface conducting diamond with a solid-state gate dielectric, Appl. Phys. Lett. 116 (2020), 174002, https://doi.org/10.1063/5.0005690.
[231] T.M. Lu, C.T. Harris, S.-H. Huang, Y. Chuang, J.-Y. Li, C.W. Liu, Effective g factor of low-density two-dimensional holes in a Ge quantum well, Appl. Phys. Lett. 111 (2017), 102108, https://doi.org/10.1063/1.4990569.
[232] I.L. Drichko, A.A. Dmitriev, V.A. Malysh, I. Yu. Smirnov, H. von Känel, M. Kummer, D. Chrastina, G. Isella, Effective g factor of 2D holes in strained Ge quantum wells, 123 (2018) 165703, https://doi.org/10.1063/1.5025413.
[233] T.A. Goodwin, P. Mark, The influence of chemisorption on the electrical conductivity of thin semiconductors, Prog. Surf. Sci. 1 (1971) 1–64, https://doi.org/10.1016/0079-6816(71)90002-5.
[234] W. Schottky, Zur Halbleitertheorie der Sperrschicht- und Spitzengleichrichter, Z. Angew. Phys. 113 (1939) 367–414, https://doi.org/10.1007/BF01340116.
[235] N.F. Mott, The theory of crystal rectifiers, Proc. R. Soc. Lond. Ser. A 171 (1939) 27–38, https://doi.org/10.1098/rspa.1939.0051.
[236] P. Volpe, P. Muret, J. Pernot, F. Omnès, T. Teraji, F. Jomard, D. Planson, P. Brosselard, N. Dheilly, B. Vergne, S. Scharnholtz, High breakdown voltage Schottky diodes synthesized on p-type CVD diamond layer, Phys. Status Solidi A 207 (2010) 2088–2092, https://doi.org/10.1002/pssa.201000055.
[237] R.T. Tung, Recent advances in Schottky barrier concepts, Mater. Sci. Eng.: R: Reports 35 (2001) 1–138, https://doi.org/10.1016/S0927-796X(01)00037-7.
[238] F. Li, J. Zhang, X. Wang, Z. Liu, W. Wang, S. Li, H. Wang, X-ray photoelectron spectroscopy study of Schottky junctions based on oxygen-/fluorine-terminated (100) diamond, Diam. Relat. Mater. 63 (2016) 180–185, https://doi.org/10.1016/j.diamond.2015.12.007.
[239] R.T. Tung, The physics and chemistry of the Schottky barrier height, Appl. Phys. Rev. 1 (2014), 011304, https://doi.org/10.1063/1.4858400.
[240] R.T. Tung, Schottky-barrier formation at single-crystal metal-semiconductor interfaces, in: W. Mönch, Electronic Structure of Metal-Semiconductor Contacts. Perspectives in Condensed Matter Physics, vol. 4, 1990, Springer, Dordrecht. https://doi.org/10.1007/978-94-009-0657-0_22.

[241] S.G. Louie, J.R. Chelikowsky, M.L. Cohen, Ionicity and the theory of Schottky barriers, Phys. Rev. B 15 (1977) 2154–2162, https://doi.org/10.1103/PhysRevB.15.2154.

[242] R.T. Tung, Chemical bonding and fermi level pinning at metal-semiconductor interfaces, Phys. Rev. Lett. 84 (2000) 6078–6081, https://doi.org/10.1103/PhysRevLett.84.6078.

[243] M. Aoki, H. Kawarada, Electric properties of metal/diamond interfaces utilizing hydrogen-terminated surfaces of homoepitaxial diamonds, Jpn. J. Appl. Phys. 33 (1994) L708, https://doi.org/10.1143/JJAP.33.L708.

[244] H. Kawarada, M. Aoki, H. Sasaki, K. Tsugawa, Characterization of hydrogen-terminated CVD diamond surfaces and their contact properties, Diam. Relat. Mater. 3 (1994) 961–965, https://doi.org/10.1016/0925-9635(94)90309-3.

[245] Y. Jingu, K. Hirama, H. Kawarada, Ultrashallow TiC source/drain contacts in diamond MOSFETs formed by hydrogenation-last approach, IEEE Trans. Electron. Dev. 57 (2010) 966–972, https://doi.org/10.1109/TED.2010.2043311.

[246] H.J. Looi, L.Y.S. Pang, M.D. Whitfield, J.S. Foord, R.B. Jackman, Engineering low resistance contacts on p-type hydrogenated diamond surfaces, Diam. Relat. Mater. 9 (2000) 975–981, https://doi.org/10.1016/S0925-9635(00)00240-5.

[247] A. Vardi, M. Tordjman, R. Kalish, J.A. del Alamo, Refractory W ohmic contacts to H-terminated diamond, IEEE Trans. Electron Devices 67 (2020) 3516–3521, https://doi.org/10.1109/TED.2020.3009174.

[248] Z. Ren, J. Zhang, J. Zhang, C. Zhang, D. Chen, R. Quan, J. Yang, Z. Lin, Y. Hao, Polycrystalline diamond RF MOSFET with MoO_3 gate dielectric, AIP Adv. 7 (2017), 125302, https://doi.org/10.1063/1.5004475.

[249] C. Verona, W. Ciccognani, S. Colangeli, F.D. Pietrantonio, E. Giovine, E. Limiti, M. Marinelli, G. Verona-Rinati, Gate-source distance scaling effects in H-terminated diamond MESFETs, IEEE Trans. Electron. Dev. 62 (2015) 1150–1156, https://doi.org/10.1109/TED.2015.2398891.

[250] S.A.O. Russell, S. Sharabi, A. Tallaire, D.A.J. Moran, Hydrogen-terminated diamond field-effect transistors with cutoff frequency of 53 GHz, IEEE Electron Dev. Lett. 33 (2012) 1471–1473, https://doi.org/10.1109/LED.2012.2210020.

[251] Y. Wang, X. Chang, S. Li, D. Zhao, G. Shao, T. Zhu, J. Fu, P. Zhang, X. Chen, F. Li, Z. Liu, S. Fan, R. Bu, F. Wen, J. Zhang, W. Wang, H.-X. Wang, Ohmic contact between iridium film and hydrogen-terminated single crystal diamond, Sci. Rep. 7 (2017) 12157, https://doi.org/10.1038/s41598-017-09380-1.

[252] X. Yuan, J. Liu, S. Shao, J. Liu, J. Wei, B. Da, C. Li, Y. Koide, Thermal stability investigation for Ohmic contact properties of Pt, Au, and Pd electrodes on the same hydrogen-terminated diamond, AIP Adv. 10 (2020), 055114, https://doi.org/10.1063/5.0008167.

[253] W. Wang, C. Hu, F.N. Li, S.Y. Li, Z.C. Liu, F. Wang, J. Fu, H.X. Wang, Palladium Ohmic contact on hydrogen-terminated single crystal diamond film, Diam. Relat. Mater. 59 (2015) 90–94, https://doi.org/10.1016/j.diamond.2015.09.012.

[254] K. Xing, A. Tsai, S. Rubanov, D.L. Creedon, S.A. Yianni, L. Zhang, W. Hao, J. Zhuang, J.C. McCallum, C.I. Pakes, D. Qi, Palladium forms Ohmic contact on hydrogen-terminated diamond down to 4 K, Appl. Phys. Lett. 116 (2019), 111601, https://doi.org/10.1063/1.5141775.

[255] X. Yu, J. Zhou, C. Qi, Z. Cao, Y. Kong, T. Chen, A high frequency hydrogen-terminated diamond MISFET with fT/fmax of 70/80 GHz, IEEE Electron Dev. Lett. 39 (2018) 1373–1376, https://doi.org/10.1109/LED.2018.2862158.

[256] D.A.J. Moran, O.J.L. Fox, H. McLelland, S. Russell, P.W. May, Scaling of hydrogen-terminated diamond FETs to Sub-100-nm gate dimensions, IEEE Electron Dev. Lett. 32 (2011) 599–601, https://doi.org/10.1109/LED.2011.2114871.

[257] H.H. Berger, Models for contacts to planar devices, Solid-State Electron. 15 (1972) 145–158, https://doi.org/10.1016/0038-1101(72)90048-2.

[258] S. Kono, T. Sasaki, M. Inaba, A. Hiraiwa, H. Kawarada, Sheet resistance underneath the Au ohmic-electrode on hydrogen- terminated surface-conductive diamond (001), Diam. Relat. Mater. 80 (2017) 93–98, https://doi.org/10.1016/j.diamond.2017.09.020.

[259] K. Tsugawa, H. Noda, K. Hirose, H. Kawarada, Schottky barrier heights, carrier density, and negative electron affinity of hydrogen-terminated diamond, Phys. Rev. B 81 (2010), 045303, https://doi.org/10.1103/PhysRevB.81.045303.

[260] J.F. Wager, K. Kuhn, Device physics modeling of surfaces and interfaces from an induced gap state perspective, Crit. Rev. Solid State Mater. Sci. 42 (2017) 373–415, https://doi.org/10.1080/10408436.2016.1223013.

[261] W. Mönch, Chemical trends of barrier heights in metal-semiconductor contacts: on the theory of the slope parameter, Appl. Surf. Sci. 92 (1996) 367–371, https://doi.org/10.1016/0169-4332(95)00257-X.

[262] W. Mönch, Slope parameters of the barrier heights of metal-organic contacts, Appl. Phys. Lett. 88 (2006), 112116, https://doi.org/10.1063/1.2178473.

[263] M. Werner, Diamond metallization for device applications, Semicond. Sci. Technol. 18 (2003) S41, https://doi.org/10.1088/0268-1242/18/3/306.

[264] S. Kumaragurubaran, T. Yamada, S. Shikata, Annealing effects in H- and O-terminated P-doped diamond (111) surfaces, Diam. Relat. Mater. 17 (2008) 472–475, https://doi.org/10.1016/j.diamond.2007.12.068.

[265] D. Zhao, Z. Liu, J. Wang, Y. Liang, M. Nauman, J. Fu, Y. Wang, S. Fan, W. Wang, H.-X. Wang, Fabrication of dual-termination Schottky barrier diode by using oxygen-/fluorine-terminated diamond, Appl. Surf. Sci. 457 (2018) 411–416, https://doi.org/10.1016/j.apsusc.2018.06.270.

[266] H. Kawarada, M. Aoki, M. Ito, Enhancement mode metal-semiconductor field effect transistors using homoepitaxial diamonds, Appl. Phys. Lett. 65 (1994) 1563, https://doi.org/10.1063/1.112915.

[267] Y. Kitabayashi, T. Kudo, H. Tsuboi, T. Yamada, D. Xu, M. Shibata, D. Matsumura, Y. Hayashi, M. Syamsul, M. Inaba, A. Hiraiwa, H. Kawarada, Normally-Off C-H diamond MOSFETs With partial C–O channel achieving 2-kV breakdown voltage, IEEE Electron Dev. Lett. 38 (2017) 363–366, https://doi.org/10.1109/LED.2017.2661340.

[268] H. Kawarada, T. Yamada, D. Xu, H. Tsuboi, T. Saito, A. Hiraiwa, Wide temperature (10K–700K) and high voltage (~1000V) operation of C-H diamond MOSFETs for power electronics application, in: IEEE International Electron Devices Meeting, San Francisco, CA, 2014, https://doi.org/10.1109/IEDM.2014.7047030.

[269] K. Hirama, S. Miyamoto, H. Matsudaira, K. Yamada, H. Kawarada, Characterization of diamond metal-insulator-semiconductor field-effect transistors with aluminum oxide gate insulator, Appl. Phys. Lett. 88 (2006), 112117, https://doi.org/10.1063/1.2186072.

[270] T. Saito, K.H. Park, K. Hirama, H. Umezawa, M. Satoh, H. Kawarada, Z. Liu, K. Mitsuishi, K. Furuya, H. Okushi, Fabrication of metal–oxide–diamond field-effect transistors with submicron-sized gate length on boron-doped (111) H-terminated surfaces using electron beam evaporated SiO_2 and Al_2O_3, J. Electron. Mater. 40 (2011) 247–252, https://doi.org/10.1007/S11664-010-1500-1.

[271] W. Wang, C. Hu, S.Y. Li, F.N. Li, Z.C. Liu, F. Wang, J. Fu, H.X. Wang, Diamond based field-effect transistors of Zr gate with SiN_x dielectric layers, J. Nanomater. 2015 (2015), https://doi.org/10.1155/2015/124640.

[272] J.W. Liu, M.Y. Liao, M. Imura, H. Oosato, E. Watanabe, Y. Koide, Electrical characteristics of hydrogen-terminated diamond metal-oxide-semiconductor with atomic layer deposited HfO_2 as gate dielectric, Appl. Phys. Lett. 102 (2013), 112910, https://doi.org/10.1063/1.4798289.

[273] J.W. Liu, H. Oosato, M.Y. Liao, Y. Koide, Enhancement-mode hydrogenated diamond metal-oxide-semiconductor field-effect transistors with Y_2O_3 oxide insulator grown by electron beam evaporator, Appl. Phys. Lett. 110 (2017), 203502, https://doi.org/10.1063/1.4983091.

[274] W. Wang, Y. Wang, M. Zhang, R. Wang, G. Chen, X. Chang, F. Lin, F. Wen, K. Jia, H. Wang, An enhancement-mode hydrogen-terminated diamond field-effect transistor with lanthanum hexaboride gate material, IEEE Electron Device Lett. 41 (2020) 585–588, https://doi.org/10.1109/LED.2020.2972330.

[275] C. Verona, W. Ciccognani, S. Colangeli, E. Limiti, M. Marinelli, G. Verona-Rinati, D. Cannatà, M. Benetti, F. Pietrantonio, V_2O_5 MISFETs on H-terminated diamond, IEEE Trans. Electron Devices 63 (2016) 4647–4653, https://doi.org/10.1109/TED.2016.2617362.

[276] Z. Ren, J. Zhang, J. Zhang, C. Zhang, S. Xu, Y. Li, Y. Hao, Diamond field effect transistors with MoO_3 gate dielectric, IEEE Electron Device Lett. 38 (2017) 786–789, https://doi.org/10.1109/LED.2017.2695495.

[277] T.G. Ivanov, J. Weil, P.B. Shah, A.G. Birdwell, K. Kingkeo, E.A. Viveiros, Diamond RF Transistor Technology with ft=41 GHz and fmax=44 GHz, in: IEEE/MTT-S International Microwave Symposium - IMS, Philadelphia, PA, 2018, https://doi.org/10.1109/MWSYM.2018.8439521.

[278] K. Ueda, M. Kasu, Y. Yamauchi, T. Makimoto, M. Schwitters, D.J. Twitchen, G.A. Scarsbrook, S.E. Coe, Diamond FET using high-quality polycrystalline diamond with fT of 45 GHz and fmax of 120 GHz, IEEE Electron Device Lett. 27 (2006) 570–572, https://doi.org/10.1109/LED.2006.876325.

[279] H. Taniuchi, H. Umezawa, T. Arima, M. Tachiki, H. Kawarada, High-frequency performance of diamond field-effect transistor, IEEE Electron Device Lett. 22 (2001) 390–392, https://doi.org/10.1109/55.936353.

[280] M. Kubovic, M. Kasu, I. Kallfass, M. Neuburger, A. Aleksov, G. Koley, M.G. Spencer, E. Kohn, Microwave performance evaluation of diamond surface channel FETs, Diam. Relat. Mater. 13 (2004) 802–807, https://doi.org/10.1016/j.diamond.2003.11.089.
[281] S. Imanishi, K. Horikawa, N. Oi, S. Okubo, T. Kageura, A. Hiraiwa, H. Kawarada, 3.8 W/mm power density for ALD Al_2O_3-based two-dimensional hole gas diamond MOSFET operating at saturation velocity, IEEE Electron Device Lett. 40 (2019) 279–282, https://doi.org/10.1109/LED.2018.2886596.
[282] P. Gluche, A. Aleksov, A. Vescan, W. Ebert, E. Kohn, Diamond surface-channel FET structure with 200 V breakdown voltage, IEEE Electron Devices Lett. 18 (1997) 547–549, https://doi.org/10.1109/55.641441.
[283] A. Vardi, M. Tordjman, J.A. del Alamo, R. Kalish, A diamond:H/MoO_3 MOSFET, IEEE Electron Devices Lett. 35 (2014) 1320–1322, https://doi.org/10.1109/LED.2014.2364832.
[284] Z. Yin, M. Tordjman, A. Vardi, R. Kalish, J.A.D. Alamo, A Diamond:H/WO_3 Metal–Oxide–Semiconductor, IEEE Electron Device Lett. 39 (2018) 540–543, https://doi.org/10.1109/LED.2018.2808463.
[285] N. Oi, M. Inaba, S. Okubo, I. Tsuyuzaki, T. Kageura, S. Onoda, A. Hiraiwa, H. Kawarada, Vertical-type two-dimensional hole gas diamond metal oxide semiconductor field-effect transistors, Sci. Rep. 8 (2018), https://doi.org/10.1038/s41598-018-28837-5.
[286] F. Wang, X. Chang, X. Zhang, J. Fu, S. Fan, R. Bu, J. Zhang, W. Wang, H.X. Wang, J. Wang, Normally-off hydrogen-terminated diamond field-effect transistor with Al2O3 dielectric layer formed by thermal oxidation of Al, Diam. Relat. Mater. 81 (2018) 113–117, https://doi.org/10.1016/j.diamond.2017.11.016.
[287] C. Sun, T. Hao, J. Li, H.T. Ye, C. Gu, The design and performance of hydrogen-terminated diamond metal-oxide-semiconductor field-effect transistors with high k oxide HfO_2, Micro Nano Eng. 6 (2020), 100046, https://doi.org/10.1016/j.mne.2020.100046.
[288] A. Hokazono, T. Ishikura, K. Nakamura, S. Yamashita, H. Kawarada, Enhancement/depletion MESFETs of diamond and their logic circuits, Diam. Relat. Mater. 6 (1997) 339–343, https://doi.org/10.1016/S0925-9635(96)00726-1.
[289] A. Gali, M. Fyta, E. Kaxiras, Ab initio supercell calculations on nitrogen-vacancy center in diamond: electronic structure and hyperfine tensors, Phys. Rev. B 77 (2008), 155206, https://doi.org/10.1103/PhysRevB.77.155206.
[290] J.R. Maze, P.L. Stanwix, J.S. Hodges, S. Hong, J.M. Taylor, P. Cappellaro, L. Jiang, M.V.G. Dutt, E. Togan, A.S. Zibrov, A. Yacoby, R.L. Walsworth, M.D. Lukin, Nanoscale magnetic sensing with an individual electronic spin in diamond, Nature 455 (2008) 644–647, https://doi.org/10.1038/nature07279.
[291] F. Dolde, H. Fedder, M.W. Doherty, T. Nöbauer, F. Rempp, G. Balasubramanian, T. Wolf, F. Reinhard, L.C.L. Hollenberg, F. Jelezko, J. Wrachtrup, Electric-field sensing using single diamond spins, Nat. Phys. 7 (2011) 459–463, https://doi.org/10.1038/nphys1969.
[292] R. Schirhagl, K. Chang, M. Loretz, C.L. Degen, Nitrogen-vacancy centers in diamond: nanoscale sensors for physics and biology, Annu. Rev. Phys. Chem. 65 (2014) 83–105, https://doi.org/10.1146/annurev-physchem-040513-103659.
[293] T. Rosskopf, A. Dussaux, K. Ohashi, M. Loretz, R. Schirhagl, H. Watanabe, S. Shikata, K. Itoh, C. Degen, Investigation of surface magnetic noise by shallow spins in diamond, Phys. Rev. Lett. 112 (2014), 147602, https://doi.org/10.1103/PhysRevLett.112.147602.
[294] C. Fu, H. Lee, K. Chen, T. Lim, H. Wu, P. Lin, P. Wei, P. Tsao, H. Chang, W. Fann, Characterization and application of single fluorescent nanodiamonds as cellular biomarkers, Proc. Natl. Acad. Sci. 104 (2007) 727–732, https://doi.org/10.1073/pnas.0605409104.
[295] V. Petrakova, M. Ledvina, M. Nesladek, Surface doping of diamond and induced optical effects, in: R.P. Mildren, J.R. Rabeau (Eds.), Optical Engineering of Diamond, 2013, pp. 209–238, https://doi.org/10.1002/9783527648603.ch7.
[296] J. Wrachtrup, S.Y. Kilin, A.P. Nizovtsev, Quantum computation using the ^{13}C nuclear spins near the single NV defect center in diamond, Opt. Spectrosc. 91 (2001) 429–437, https://doi.org/10.1134/1.1405224.
[297] J. Köhler, J.A.J.M. Disselhorst, M.C.J.M. Donckers, E.J.J. Groenen, J. Schmidt, W.E. Moerner, Magnetic resonance of a single molecular spin, Nature 363 (1993) 242–244, https://doi.org/10.1038/363242a0.
[298] N.J. Glaser, G. Braunbeck, O. Bienek, I.D. Sharp, F. Reinhard, Can surface-transfer doping and UV irradiation during annealing improve shallow implanted nitrogen-vacancy centers in diamond? Appl. Phys. Lett. 117 (2020), 054003 https://doi.org/10.1063/5.0012375.
[299] M.V. Hauf, B. Grotz, B. Naydenov, M. Dankerl, S. Pezzagna, J. Meijer, F. Jelezko, J. Wrachtrup, M. Stutzmann, F. Reinhard, J.A. Garrido, Chemical control of the charge state of nitrogen-vacancy centers in diamond, Phys. Rev. B 83 (2011), 081304, https://doi.org/10.1103/PhysRevB.83.081304.
[300] B. Grotz, M.V. Hauf, M. Dankerl, B. Naydenov, S. Pezzagna, J. Meijer, F. Jelezko, J. Wrachtrup, M. Stutzmann, F. Reinhard, J.A. Garrido, Charge state manipulation of qubits in diamond, Nat. Commun. 3 (2012) 729, https://doi.org/10.1038/ncomms1729.
[301] S. Datta, B. Das, Electronic analog of the electro-optic modulator, Appl. Phys. Lett. 56 (1990) 665, https://doi.org/10.1063/1.102730.
[302] M.N. Baibich, J.M. Broto, A. Fert, F.N.V. Dau, F. Petroff, P. Etienne, G. Creuzet, A. Friederich, J. Chazelas, Giant magnetoresistance of (001)Fe/(001)Cr magnetic superlattices, Phys. Rev. Lett. 61 (1988) 2472, https://doi.org/10.1103/PhysRevLett.61.2472.
[303] G. Binasch, P. Grünberg, F. Saurenbach, W. Zinn, Enhanced magnetoresistance in layered magnetic structures with antiferromagnetic interlayer exchange, Phys. Rev. B 39 (1989) 4828–4830, https://doi.org/10.1103/PhysRevB.39.4828.